



UNIVERSIDADE DE BRASÍLIA
INSTITUTO DE GEOCIÊNCIAS
PROGRAMA DE PÓS-GRADUAÇÃO EM GEOLOGIA
ÁREA DE CONCENTRAÇÃO: GEOLOGIA REGIONAL

DISSERTAÇÃO DE MESTRADO N° 360

**“GEOCRONOLOGIA E ISOTOPIA DO MAGMATISMO
PALEOZOICO NA ZONA DE DIABLILLOS, BORDA
ORIENTAL DA PUNA AUSTRAL (NW DA ARGENTINA):
EVOLUÇÃO CRUSTAL DO ORÓGENO PALEOZOICO
INFERIOR NA MARGEM OCIDENTAL DE GONDWANA”**

AGUSTÍN ORTIZ YAÑEZ

Brasília –Abril de 2016



UNIVERSIDADE DE BRASÍLIA
INSTITUTO DE GEOCIÊNCIAS
PROGRAMA DE PÓS-GRADUAÇÃO EM GEOLOGIA
ÁREA DE CONCENTRAÇÃO: GEOLOGIA REGIONAL

DISSERTAÇÃO DE MESTRADO N° 360

**“GEOCRONOLOGIA E ISOTOPIA DO MAGMATISMO
PALEOZOICO NA ZONA DE DIABLILLOS, BORDA
ORIENTAL DA PUNA AUSTRAL (NW DA ARGENTINA):
EVOLUÇÃO CRUSTAL DO ORÓGENO PALEOZOICO
INFERIOR NA MARGEM OCIDENTAL DE GONDWANA”¹**

AGUSTÍN ORTIZ YAÑEZ

Dissertação apresentada à banca
examinadora do Instituto de Geociências
da Universidade de Brasília como
exigência final para a obtenção do Título
de Mestre em Geologia

Banca examinadora:

Orientadora: Profa. Dra. Natalia
Hauser - UnB
Examinador interno: Prof. Dr. Valmir
Souza da Silva - UnB
Examinador externo: Prof. Dr. Miguel
Angelo Stipp Basei - USP

Brasília –Abril de 2016

¹ Este trabalho foi desenvolvido com apoio financeiro do Conselho Nacional de Desenvolvimento Científico e Tecnológico (CNPq).

“O mundo está nas mãos daqueles que têm a coragem de sonhar e tomar o risco de viver o seu sonho”

Anônimo

Geocronologia e isotopia do magmatismo paleozoico na zona de Diablillos, borda oriental da Puna austral (NW da Argentina): Evolução crustal do orôgeno paleozoico inferior na margem ocidental de Gondwana

INDICE

Lista de Figuras	8
Lista de Tabelas	13
Resumo	14
Abstract	15
Capítulo 1	16
 1. Introdução	17
1.1. Objetivos	21
1.2. Marco geológico	21
1.3. Etapas de trabalho	26
1.4. Vias de acesso.....	27
Capítulo 2	28
 1. Procedimentos analíticos	29
2.1. Analises Geoquímicas.....	29
2.2. Procedimentos analíticos de U-Pb e isótopos de Lu-Hf	29
2.3. Analises na Microssonda	33
2.4. Geoquímica isotópica Sr-Nd	33
Capítulo 3	34
Artigo científico: “ Zircon U-Pb ages and Hf isotopes for the Diablillos Intrusive Complex, Southern Puna, Argentina: crustal evolution of the Lower Paleozoic orogen, Southwestern Gondwana margin”	35

Abstract	36
1.1.Introduction	37
1.2.Geological setting	41
2.1. Local Geology and Petrography	42
3. Analytical Procedures	53
3.1.Geochemical analyses	53
3.2.U-Pb and Lu-Hf isotope analytical procedures	53
3.3.Microprobe analysis	56
3.4.Sr-Nd isotopes analytical procedures	56
4. Results	57
4.1.Geochemistry	57
4.1.1.Major, trace and rare earth elements	57
4.2.Zircon U-Pb geochronology	64
4.3.Lu-Hf isotope data for zircons	70
4.4.Sr-Nd isotope data	72
5. Discussion	74
5.1.Emplacement age of the Diablillos Intrusive Complex	74
5.2. Magma sources for the Diablillos Intrusive Complex	76
5.2.1. Geochemistry and Sr-Nd isotopes	76
5.2.2. Crustal evolution evidences from Hf isotopes	77
5.3. Eastern Magmatic Belt, Lower Paleozoic Arc, SW Gondwana margin: A long-lived magmatic event?	79
6. Conclusions	83

Geocronologia e isotopia do magmatismo paleozoico na zona de Diablillos, borda oriental da Puna austral (NW da Argentina): Evolução crustal do orôgeno paleozoico inferior na margem ocidental de Gondwana

7. Acknowledgements84

Capítulo 485

4. Conclusões finais..........86

5. Referências bibliográficas87

6. Agradecimentos100

7. Anexo..........101

Table 1. Whole rock geochemical analyses for major and trace, including rare earth element data for the CID and CEO, Eastern Magmatic Belt, Southern Puna101

Table 2. Results of in situ U-Pb isotope analysis of zircon from rocks of the Diablillos Intrusive Complex, Eastern Magmatic Belt, Southern Puna103

Table 3. Results of in situ Lu-Hf isotope analysis of zircon from rocks of the Diablillos Intrusive Complex, Eastern Magmatic Belt, Southern Puna109

Table 4. Microprobe analyses for zircon crystals from rocks of the Diablillos Intrusive Complex, Eastern Magmatic Belt, Southern Puna110

Table 5. Whole rock Sr and Nd isotope analyses on rocks of the CID and CEO, Eastern Magmatic Belt, Southern Puna111

Email de confirmação do artigo submetido ao Periódico Gondwana Research.....112

LISTA DE FIGURAS

CAPÍTULO I

1. Introdução

Fig. 1: Mapa regional mostrando as principais unidades geológicas no NW Argentina. CN: Salar Centenario. DB: Salar Diablillos. RT: Salar Ratones. CB: Cerro Blanco. TA: Tajamar. AC: Acazoque. Requadro interno mostra um mapa geotectônico esquemático do embasamento da América do Sul. Modificado de **Viramonte et al. (2007)** e **Hauser et al. (2011)**.

Fig. 2: Mapa geológico de semi-detalhe onde se observam as principais unidades do Complexo Intrusivo Diablillos. Modificado de **Nieves (2014)**.

Fig. 3: Vias de acesso na área de estudo. A mesma é marcada no retângulo com linhas ponteadas pretas.

CAPÍTULO II

2. Procedimentos analíticos

Fig. 4: Relações medias ponderadas $^{206}\text{Pb}/^{238}\text{U}$ do zircão estándar GJ, feitas durante as sessões analíticas das amostras (a) Monzogranito (b) Diorito (c) Granodiorito (d) Exemplos de mounts para as análises de U-Pb. Os mounts foram polidos, para que de essa forma, as superfícies dos minerais de zircão ficaram expostas.

Fig. 5: Diagrama da concordia (**Wetherill, 1956**) com as idades concordantes U-Pb do zircão estándar TEMORA, feitas durante as sessões analíticas das amostras. (a) Monzogranito (b) Diorito (c) Granodiorito

CAPÍTULO III

Zircon U-Pb ages and Hf isotopes for the Diablillos Intrusive Complex, Southern Puna, Argentina: crustal evolution of the Lower Paleozoic orogen, Southwestern Gondwana margin

Geocronologia e isotopia do magmatismo paleozoico na zona de Diablillos, borda oriental da Puna austral (NW da Argentina): Evolução crustal do orôgeno paleozoico inferior na margem ocidental de Gondwana

1. Introduction

Fig. 1: Regional map, showing the main geological units in the geological provinces of NW Argentina. CN: Salar Centenario. DB: Salar Diablillos. RT: Salar Ratones. CB: Cerro Blanco. TA: Tajamar. AC: Acazoque. Inset shows a geotectonic sketch map of the South American basement. Modified after **Viramonte et al. (2007)** and **Hauser et al. (2011)**.

2. Geological setting

2.1. Local Geology and Petrography

Fig. 2: Detailed geological map showing the main units in the Diablillos Intrusive Complex. Modified after **Nieves (2014)**. The positions of the sampling sites for this study are also shown.

Fig. 3: (a) Panoramic view of the Diablillos salar and the Inca Viejo Range. (b) Contact relationship between a porphyritic monzogranite and parts of a mafic dismembered body. Hammer is 40 cm long. (c) Contact relationships between a porphyritic monzogranite, a granodiorite enclave, and a mafic dismembered body. White dotted lines delimit granodiorite enclave with K-feldspar phenocrysts. Black cover lens is 4 cm in diameter. (d) Field image showing the transitional contact between the monzogranite and the granodiorite facies, and a contact with a tonalite enclave. Black arrows show K-feldspar phenocrysts that migrated from the monzogranite to the granodiorite. Note the MME included into the tonalite enclave. (e) Intrusive contact, delimited with a white dotted line, between the monzogranite and slates from the Rio Blanco Metamorphic Complex. Hammer is 40 cm long. Dt: Diorite. Gr: Monzogranite. Gd: Granodiorite. Tn: Tonalite.

Fig. 4: Q-A-P diagram showing the modal classification of the analyzed samples from the CID, in comparison with the samples from **Suzano et al. (2015)**. The modal classification was made by counting approximately 800 points in a thin section, for the four analyzed samples.

Fig. 5: Microphotographs of the facies of the Diablillos Intrusive Complex. (a) Monzogranite facies (sample D-13-01) with holocrystalline porphyritic texture. It is composed mainly of K-feldspar (Kfs) and plagioclase (Pl) phenocrysts, and the matrix is composed of Kfs, quartz (Qz), and Pl. (b) Granodiorite facies (sample D-13-02). Holocrystalline porphyritic texture with Pl, Kfs and Qz phenocrysts. The matrix is formed by fine- to medium-grained Qz, Pl, Kfs. Biotite (Bt) is abundant. The microcline phenocrysts have Bt inclusions (Inc) along the rims. (c) Tonalite facies (sample D-13-15) showing porphyritic to equigranular textures. Some Pl phenocrysts have a rim of Bt as well as Bt inclusions (Inc). Poikilitic Qz with inclusions of Bt (Inc) is shown. (d) Porphyritic diorite with Pl phenocrysts (sample D-13-40). The fine-grained matrix is formed by Pl,

amphibole (Amp), Bt and Qz. All images taken in cross-polarized light. Mineral abbreviations after **Whitney and Evans (2010)**. Kfs: K-feldspar. Pl: Plagioclase. Qz: Quartz. Bt: Biotite. Ms: Muscovite. Amp: Amphibole.

4. Results

4.1. Geochemistry

4.1.1. Major, trace and rare elements

Fig. 6: (a) Granitoid TAS diagram (**Middlemost, 1994**) for the various facies of the CID. Rocks are classified as granites, granodiorites, tonalities, and quartz diorites. (b) In the A/CNK vs A/NK plot (**Shand, 1943**) diorites fall into the metaluminous field, whereas the tonalites, granodiorites and monzogranites fall into the peraluminous field. (c) In the AFM diagram (**Irvine and Baragar 1971**), the CID rocks show a calk-alkaline trend. The diorites show a slight tendency towards tholeiitic characteristics. (d) Geotectonic Rb vs Y+Nb diagram (**Pearce et al., 1984**). The CID and CEO rocks plot in the VAG field, with a minor tendency towards the WPG field.

Fig. 7: Harker diagrams for the basic plutonic rocks and, the intermediate plutonic rocks. With increasing values of SiO₂, a negative correlation trend is evidenced, for MgO, FeOt, TiO₂ and CaO, whereas the Na₂O and K₂O values show a positive correlation trend with increasing SiO₂. Data in wt.%.

Fig. 8: Harker-style trace element variation diagrams, showing decreasing Sr with increasing SiO₂. Rb and Ba show positive correlation trends with increasing SiO₂. The intermediate rocks show increasing values of Zr with increasing SiO₂. Trace element data in ppm, SiO₂ contents in wt.%.

Fig. 9: (a) Chondrite-normalized trace element spider diagram (**Thompson, 1982**). Intermediate-felsic rocks show enrichment in the LILE compared to the basic rocks. Also, note in the more evolved group depletion in the HFSE. The basic rocks show a slight depletion in the LILE and illustrate a stronger depletion in the HFSE than the intermediate rocks. (b) REE abundances normalized to chondrite (**Boynton, 1984**). The intermediate rocks show enrichment of the LREE and a decreasing HREE pattern, compared to the basic rocks. Note the similarities between the CID and CEO rocks with those from the Ojo de Colorados Complex, Western Magmatic Belt (**Zimmermann et al., 2014**), Guasayán Pluton, Northern Sierras Pampeanas (**Dahlquist et al., 2016**), a Metadacite from Niño Muerto, Northeastern Magmatic Belt (**Hauser et al., 2011**) and the Tastil batholith, Cordillera Oriental (**Hauser et al., 2011**). (c) Upper crust-normalized trace element abundances (normalization after **Taylor and McLennan, 1985**). The mafic rocks display slightly negative patterns of the LILE and illustrate a stronger depletion in the HFSE than observed for the intermediate rocks.

Geocronologia e isotopia do magmatismo paleozoico na zona de Diablillos, borda oriental da Puna austral (NW da Argentina): Evolução crustal do orôgeno paleozoico inferior na margem ocidental de Gondwana

4.2. Zircon U-Pb geochronology

Fig. 10: (a) U-Pb isotope data. (a) Concordia diagram (Wetherill, 1956) displaying the scatter of concordant U-Pb ages for zircon from monzogranite sample D-13-01. Errors are shown as ellipses at the 1σ level. Upper left inset shows the Concordia diagram for U-Pb ratios of all zircon grains analyzed. Lower right inset shows the weighted average age diagram (data in Ma) for the monzogranite facies. (b) CL images of representative zircon crystals from the monzogranite sample. Age results are shown for the spots analyzed. (c) Concordia diagram displaying the scatter of concordant U-Pb ages for zircon from diorite sample D-13-40. Errors are shown as ellipses at the 1σ level. Upper left inset shows the Concordia diagram for U-Pb ratios of all zircon grains analyzed. Lower right inset shows the weighted average age diagram (data in Ma) for the diorite facies. (d) CL images of representative zircon crystals from the diorite sample. (e) Concordia diagram displaying the concordant U-Pb ages for zircon from granodiorite sample D-13-02. Errors are shown as ellipses at the 2σ level. Upper left inset shows the Concordia diagram for U-Pb ratios of all zircon analyses. (f) CL images of representative zircon crystals from the granodiorite sample. Note: In (b), (d), and (f), yellow circles mark the spots of U-Pb analyses. r: rim; c: core. Red circles mark the locations of Hf analyses.

Fig. 11: Probability Density Plots. Ages for the various peak populations are given in black letters. (a) Monzogranite facies, (b) Diorite facies, and (c) Granodiorite facies, and (d) the combined data set from all three samples from the Diablillos Intrusive Complex. For explanation see text.

4.3. Lu-Hf isotope data for zircon

Fig. 12: Plot of $\epsilon\text{Hf}_{(t)}$ vs. U-Pb ages for zircon from the CID facies. Black dotted ellipse shows that most of the analyzed samples with ages between ~490-540 Ma are plotting near the CHUR line. The majority of the T_{DM} ages are constrained between the red dotted lines, denoting T_{DM} ages from 1.2 to 1.55 Ga. The red solid line indicates the most frequent T_{DM} observed is 1.4 Ga. For comparison, the Ordovician metadacite $\epsilon\text{Hf}(t)$ data from the Northern Eastern Magmatic Belt, the Cambrian Tastil batolith $\epsilon\text{Hf}(t)$ data from the Cordillera Oriental (Hauser et al., 2011), and the data by Dahlquist et al. (2016) for the Cambrian Guasayán Pluton in the Sierras Pampeanas are also shown. Inset (a) Hf(t) histogram: The Hf(t) values for the selected samples range from + 2.0 to -2.0, whereby the latter value is observed more frequently. Inset (b) shows a T_{DM} age histogram for the analyzed samples. The most frequent T_{DM} age for the ~490-540 Ma zircon U/Pb ages is ~1.4 Ga.

4.4. Sr-Nd isotope data

Fig. 13: (a) Nd isotope evolution diagram for the CID and CEO rocks. T_{DM} ages vary from ~ 1.3 to ~ 1.6 Ga (black dotted lines); the most frequent T_{DM} age is ~ 1.4 Ga. Note that the samples show similar $Nd(t)$ values and T_{DM} ages to the results from **Viramonte et al. (2007)** for the Centenario salar area, Southeastern Magmatic Belt, Puna, and to the data by **Hauser et al. (2011)** for the Northeastern Magmatic Belt, Puna and the Tastil batholith, Cordillera Oriental. (b) Nd isotopic ratios plotted versus Sr isotopic ratios for the CID and CEO rocks. There is a negative correlation trend from the basic rocks towards the felsic rocks (black dotted line). Felsic facies display similar Nd and Sr ratios to the rocks from the Cordillera Oriental and Eastern Magmatic Belt, Northern Puna (**Hauser et al., 2011**).

5. Discussion

5.3. Eastern Magmatic Belt, Lower Paleozoic Arc, SW Gondwana margin: A long-lived magmatic event?

Fig. 14: Schematic map showing the main geological provinces, and sampling positions and related ages of some Lower Paleozoic granitoids in NW Argentina: the Complejo Ojo de Colorados (**Zimmermann et al., 2014**) in the Western Magmatic Belt (Puna); the Tastil batholith (**Hauser et al., 2011**), the granitic dykes in Mojotoro (**Aparicio González et al., 2011**), and the Nevado de Chañi and Cañañi granitoids (**Zapettini et al., 2008; Escayola et al., 2011**, respectively) in the Cordillera Oriental. Also shown is the Guasayán pluton in the Northern Sierras Pampeanas (**Dahlquist et al., 2016**). Inset (a) shows the Probability Density Plot illustrating zircon U-Pb ages for the Eastern Magmatic Belt (Puna), from the CID, and the North and Southeastern Magmatic Belt; data from **Viramonte et al. (2007); Hauser et al. (2011)**, and **Bahlburg et al. (2014)**. Inset (b) shows the Probability Density Plot for zircon U-Pb ages for the Cordillera Oriental and Northern Sierras Pampeanas from **Hauser et al. (2011)**, **Aparicio González et al. (2011)**, and **Dahlquist et al. (2016)**. CID: Diablillos Intrusive Complex. COC: Complejo Ojo de Colorados. CO: Cordillera Oriental. SP: Sierras Pampeanas. SS: Sierras Subandinas. Modified from **Aparicio González et al. (2011)**.

LISTA DE TABELAS

ANEXO

Table 1. Whole rock geochemical analyses for major and trace, including rare earth element data for the CID and CEO, Eastern Magmatic Belt, Southern Puna.

Table 2. Results of in situ U-Pb isotope analysis of zircon from rocks of the Diablillos Intrusive Complex, Eastern Magmatic Belt, Southern Puna.

Table 3. Results of in situ Lu-Hf isotope analysis of zircon from rocks of the Diablillos Intrusive Complex, Eastern Magmatic Belt, Southern Puna.

Table 4. Microprobe analyses for zircon crystals from rocks of the Diablillos Intrusive Complex, Eastern Magmatic Belt, Southern Puna.

Table 5. Whole rock Sr and Nd isotope analyses on rocks of the CID and CEO, Eastern Magmatic Belt, Southern Puna.

RESUMO

Para melhorar o entendimento da evolução crustal do Orógeno do Paleozoico Inferior no Noroeste argentino, são apresentados novos dados U–Pb e isótopos de Hf combinados em zircão das facies de monzogranito, granodiorito e diorito do Complexo Intrusivo Diablillos, Faixa Magmática Oriental, Puna na margem Suloriental de Gondwana. Idades meias ponderadas $^{206}\text{Pb}/^{238}\text{U}$ de 517 ± 3 Ma para as facies monzogranito e 515 ± 6 Ma para o diorito e uma idade concordante de 521 ± 4 Ma para as facies de granodiorito foram obtidas durante este trabalho. Foi definida uma idade de emprazamento para o Complexo Intrusivo de Diablillos entre 540 e 490 Ma; com um máximo na atividade magmática aos ~ 515 -520 Ma. As análises de geoquímica indicaram que tanto as fácieis de monzogranito e granodiorito são de natureza peraluminosa e as fácieis de diorito são de natureza metaluminosa. Além disso, junto com os valores iniciais de $^{87}\text{Sr}/^{86}\text{Sr}$ entre 0.70446 a 0.71278, valores de Nd(t) entre +2 e -4 em rocha total, e valores Hf(t) em zircão entre +2.0 e -2.0 indicam que as amostras analisadas representam magmas contaminados, mesmo as fácieis de diorito. Os dados de Hf(t) em zircão – os primeiros apresentados neste Complexo e na Puna Sul – e os dados de Nd(t) em rocha total indicam que as rochas do Complexo Intrusivo Diablillos derivaram de uma interação entre uma fonte crustal dominante Mesopróterozoica e magmas juvenis, com idades modelo T_{DM} entre ~ 1.2 - 1.5 Ga, que foi retrabalhada durante o Paleozoico Inferior. As semelhanças nas fontes dos magmas e as idades U-Pb em zircão apresentadas nesta contribuição e em diferentes estudos tanto na Puna Norte e Sul, permitiram sugerir que a Faixa Magmática Oriental na Puna foi um evento de larga duração, suportando o modelo para o embasamento dos Andes Centrais, definindo uma evolução em uma faixa móvel. Neste contexto, os ciclos Pampeanos e Famatinianos não puderam ser individualizados e poderiam formar parte de um único evento desde os ~ 600 até os 400 Ma.

Palavras chaves: Gondwana Ocidental; Puna Argentina; Arco do Paleozoico Inferior; Geocronologia U-Pb em zircão; isótopos de Hf.

Geocronologia e isotopia do magmatismo paleozoico na zona de Diablillos, borda oriental da Puna austral (NW da Argentina): Evolução crustal do orôgeno paleozoico inferior na margem ocidental de Gondwana

ABSTRACT

To better comprehend the crustal evolution of the Lower Paleozoic Orogen at the Southwestern Gondwana margin, we present new combined U–Pb and Hf isotope analyses on zircon by LA-MC-ICP-MS from monzogranite, granodiorite and diorite facies of the Diablillos Intrusive Complex, Eastern Magmatic Belt, Southern Puna. We display $^{206}\text{Pb}/^{238}\text{U}$ concordant weighted average ages of 517 ± 3 Ma and 515 ± 6 Ma for the monzogranite and diorite facies of the complex respectively, and a concordant age of 521 ± 4 Ma for the granodiorite facies. These ages permit to constrain the magmatic activity climax in the Diablillos Complex around ~ 515 - 520 Ma. Major and trace element data, initial $^{87}\text{Sr}/^{86}\text{Sr}$ values varying from 0.70446 to 0.71278, positive and negative Nd(t) values between +2.5 and -4, as well as Hf(t) for zircon data between + 3 and -3 indicate that the analyzed samples represent contaminated magmas. The Hf(t) and the Nd(t) values for this complex specify that the rocks from the Diablillos Intrusive Complex are derived from an interaction of a dominant Mesoproterozoic crustal source and juvenile mantle-derived magmas, with a T_{DM} model age range of ~ 1.2 - 1.5 Ga, that were reworked during lower Paleozoic times. The combined data obtained in this contribution allow us to suggest that the Eastern Magmatic Belt in the Puna represents a long-lived magmatic event. Supporting the model for the evolution of the Central Andean basement involving the formation of a mobile belt, whereby the Pampean and Famatinian cycles do not represent distinct events but comprise a single, non-differentiable event from Neoproterozoic to Lower Paleozoic times.

Key words: Western Gondwana; Puna Argentina; Lower Paleozoic Arc; Zircon U-Pb geochronology; Hf isotopes.

Agustín Ortiz Yañez

CAPITULO I

Geocronologia e isotopia do magmatismo paleozoico na zona de Diablillos, borda oriental da Puna austral (NW da Argentina): Evolução crustal do orôgeno paleozoico inferior na margem ocidental de Gondwana

1. INTRODUCÇÃO

A evolução do supercontinente Gondwana tem sido objeto de vários trabalhos de pesquisa nos últimos anos (**por ex., Pimentel et al., 2000; Ramos, 2008; Rapela et al., 2007; Cordani et al., 2009; Piper, 2007; Rapela et al., 2015**). Os principais modelos para explicar a formação deste supercontinente são: a amalgamaçao de dois blocos, Gondwana Oeste formado por África e América do Sul e Gondwana Leste formado por India, Antártica leste, Madagascar, Austrália e Sri Lanka (**Squire et al., 2006; Yoshida and Upreti, 2006; Yoshida, 2007**); e a existência de um supercontinente de larga duração desde tempos paleoproterozóicos (**Piper, 2000; Piper, 2007**). Existe um consenso geral em que o bloco Oeste de Gondwana representa os descendentes de Rodinia –primeiro supercontinente- ocorrendo desde tempos Mesoproterozóicos até tempos Cambrianos (**Pimentel and Fuck, 1992; Pimentel et al., 2000; Alkmim et al., 2001; Escayola et al., 2007; Rapela et al., 2007; Fuck et al., 2007; Ramos, 2008; Cordani et al., 2009**)

Nos Andes Centrais, a evolução do embasamento de Cordilheira Oriental e altiplano da Puna, do NW Argentina (**Fig. 1**), que faz parte da margem Sul oriental de Gondwana ainda é muito discutida. Diferentes autores (e. g. **Cordani et al., 2009; Collo et al., 2009; Drobe et al., 2009; Loewy et al., 2004; Ramos et al., 1986; Ramos, 1988; Ramos, 2008; Rapela et al., 2007; Hauser et al., 2011; Escayola et al., 2011; entre outros**) reconhecem dois eventos orogênicos tradicionais: o Pampeano (Precambriano Superior–Cambriano Inferior) e o evento Famatiniano (Cambriano Superior- Siluriano inferior). Esses eventos seriam relacionados com processos de subducção com a formação de arcos magmáticos, seguidos por sucessivas colisões de terrenos peri-Gondwânicos ou de tipo exóticos. Devido à falta de evidência e indicadores destes processos de colisão, tais como, zonas de sutura e ausência de ofiolitos relacionados à crosta oceânica; outros autores (**Becchio et al., 1999; Bock et al., 2000; Lucassen et al. (2000); Buttner et al., 2005**) propuseram um modelo alternativo, sugerindo uma evolução geodinâmica dominada pelo reciclagem intracrustal com menores contribuições de material juvenil. **Lucassen et al. (2000)** postularam que o embasamento dos Andes Centrais teria evoluído numa faixa móvel de larga duração. Por

tanto os ciclos Pampeanos e Famatinianos não seriam eventos diferenciáveis, e sim um só evento que teria acontecido desde os 600 Ma até os 400 Ma. A faixa móvel culminou num metamorfismo de *low-P/ high-T* aproximadamente aos 525-500 Ma. Seguidamente, um regime de larga duração de alto gradiente termal foi seguido até tempos silurianos (**Lucassen et al., 2000**). A faixa móvel cambriana seria similar aos atuais Andes Centrais, com construção de uma espessa crosta continental e desenvolvimento de atividade magmática silícica, sendo esse magmatismo, na sua maioria produto de reciclagem de crosta mais antiga (**Lucassen et al., 2000**).

A província geológica Puna é um plateau de altura de 4.000 metros sobre o nível do mar. No noroeste argentino, essa região constitui a parte oeste das províncias de Salta, Jujuy e parte noroeste da província de Catamarca (**Fig. 1**). O registro magmático neste setor é associado à orogenia Famatiniana, magmatismo que iniciou-se no Tremadociano Inferior, chegando ao seu máximo no Arenigiano. Esse registro magmático está dividido em duas faixas magmáticas N-S, com uma extensão a cada uma de ~200 km; definindo uma Faixa Eruptiva Oriental (**Méndez et al., 1973**), representada por granitoides, metadacitos e metariolitos calcálicos, peraluminosos; e a Faixa Eruptiva Ocidental (**Palma et al., 1986**), caracterizada por granitoides metaluminosos de tipo I (**Fig. 1**). Neste trabalho, essas faixas serão renomeadas como Faixas Magmáticas, pois estão compostas não só por rochas vulcânicas, mas também rochas plutónicas e subvulcânicas.

Na Puna Sul, na Faixa Magmática Oriental, **Becchio et al. (2011)** definiram o Complexo Intrusivo Diablillos (CID); formado principalmente por granitoides, dioritos e diques básicos. Recentemente, **Suáñez et al. (2015)** apresentaram um trabalho de petrografia e processos de diferenciação magmática neste Complexo. Estes autores interpretaram que o principal processo que atuou na origem e evolução do Complexo foi a mistura de magmas.

Nos anos passados, a evolução da ciência e tecnologia deu como resultado aproveitar-se das características particulares que o mineral zircão possui. Como por exemplo, datar eventos magmáticos e metamórficos, a partir do U-Pb geocronologia (**Hoskin and Schaltegger, 2003**); também, o zircão foi utilizado com sucesso para

Geocronologia e isotopia do magmatismo paleozoico na zona de Diablillos, borda oriental da Puna austral (NW da Argentina): Evolução crustal do orógeno paleozoico inferior na margem ocidental de Gondwana

identificar processos petrogenéticos em rochas magmáticas e metamórficas (**Hawkesworth and Kemp, 2006; Castiñeiras et al., 2011**). Recentemente, pesquisas das composições do zircão não foram dirigidas na geocronologia, mas foram dirigidas na habilidade do mineral zircão possuir em registrar os processos petrogenéticos em sistemas ígneos (**Huan Li et al. 2014**), através das medições de isótopos de Hf (**Zeh et al. 2007, Dong et al. 2013, Li et al. 2014**). Esse isótopo é uma ferramenta útil na discriminação da origem das rochas em geral, consequentemente, revelando a fonte e natureza dos protólitos (**Claiborne et al., 2010; Guo et al., 2007; Liu et al., 2009; Nardi et al., 2012**), oferecendo parâmetros importantes para a modelagem da evolução crustal das rochas (**Hawkesworth and Kemp, 2006**).

Sobre o complexo intrusivo Diablillos, localizado no sul da Faixa Magmática Oriental, a ausência de dados geocronológicos no CID- uma Weighted Average U-Pb idade de 501 Ma com um erro de 17 Ma (**Suzaño et al., 2015**)- e insuficiência de dados geológicos neste setor Sul da Puna motivou parte deste trabalho. Assim resulta uma tarefa essencial datar e determinar a idade de emprazamento do Complexo Intrusivo Diablillos. Além disso, as poucas quantidades de dados geológicos neste setor Sul da Puna, o complexo seletivo um lugar essencial para estudar e prover novas evidências na história de desenvolvimento da Faixa Magmática Oriental, na margem SW de Gondwana.

Aproveitando as mencionadas características únicas que o mineral zircão pode prover, nesta dissertação apresentada em forma de artigo científico, apresentamos três novas idades U-Pb em zircão pelo método Laser Ablation Inductively Coupled Plasma Mass Spectrometry (LA-ICP-MS) no Complexo Intrusivo Diablillos de amostras que representam as facies do complexo. Ao mesmo tempo, apresentamos os primeiros dados de isótopos de Lu-Hf neste complexo e na Puna Sul, também, apresentamos novos dados geoquímicos e isótopos de Sr-Nd para as rochas do CID. Consequentemente, essa dissertação contribui com novos dados geológicos para a Faixa Magmática Oriental na Puna Sul, e contribuímos para melhorar o conhecimento que se tem sobre a evolução crustal do Orógeno do Paleozoico Inferior na margem Sudoeste de Gondwana.

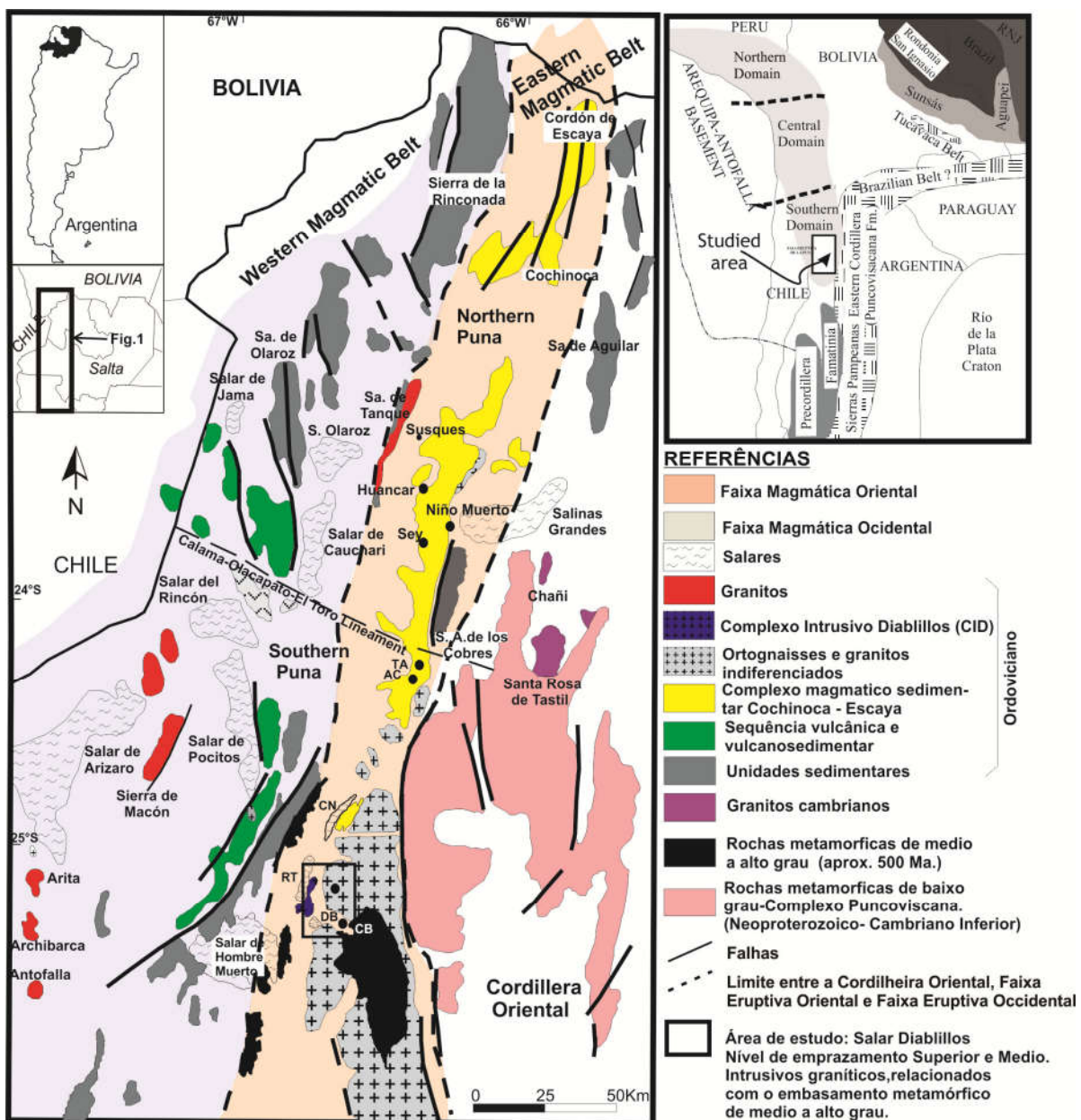


Fig. 1: Mapa regional mostrando as principais unidades geológicas no NW Argentina. CN: Salar Centenario. DB: Salar Diablillos. RT: Salar Ratones. CB: Cerro Blanco. TA: Tajamar. AC: Acazoque. Requadro interno mostra um mapa geotectônico esquemático do embasamento da América do Sul. Modificado de Viramonte et al. (2007) e Hauser et al. (2011).

Geocronologia e isotopia do magmatismo paleozoico na zona de Diablillos, borda oriental da Puna austral (NW da Argentina): Evolução crustal do orógeno paleozoico inferior na margem ocidental de Gondwana

1.1. OBJETIVOS

O objetivo central do tema de pesquisa consiste no estudo da geoquímica isotópica (Sr-Nd em rocha total e Lu-Hf em zircão) e geocronologia (U-Pb zircão) das rochas plutônicas que representam o magmatismo do Complexo Intrusivo Diablillos, localizado na parte oeste do Salar de Diablillos, na borda Oriental da Puna Austral. Os dados obtidos permitirão propôr um modelo petrogenético e de evolução dos magmas e assim melhorar a compreensão das relações entre o magmatismo e os diferentes níveis crustais. Cumprindo com este objetivo, procura-se avançar no conhecimento dos processos atuantes na crosta média a superior, durante a construção de um orógeno em zona de subducção, e contribuir na elaboração de um modelo sobre a arquitetura desse orógeno.

Para alcançar o objetivo geral são propostos os seguintes objetivos específicos:

- 1) Realização de um mapa geológico de semi-detalhe (escala 1:25.000) dos corpos ígneos estudados para estabelecer relações espaciais entre os corpos e as rochas encaixantes.
- 2) Caracterização petrográfica e geoquímica (elementos maiores, traços e elementos de terras raras) das unidades litológicas reconhecidas.
- 3) Datação dos corpos ígneos através de Análises U-Pb em zircão pelo LA-MC-ICP-MS para estabelecer uma geocronologia dos corpos.
- 4) Análises isotópicas Sr-Nd em rocha total e Lu-Hf em zircão para a caracterização das fontes magmáticas e dos processos de evolução dos magmas.
- 5) Contribuir para a reconstrução da história evolutiva do orógeno Paleozoico para o noroeste argentino.

A pesquisa será apresentada em forma de artigo científico.

1.2. MARCO GEOLÓGICO

A origem das faixas magmática oriental e ocidental, localizadas na Puna, Província de Salta, Argentina, apresentam várias interpretações tais como: colisão de terrenos alloctonos, para-autoctonos ou autocronos com a margem sudoeste de Gondwana foram propostos por vários autores (**Coira et al., 1982; Ramos, 1986; Conti et al., 1996**). Outros

autores (**Dalziel and Forsythe, 1985; Ramos 1988; Rapela et al., 1992**) interpretaram essas duas faixas magmáticas como dois arcos magmáticos, relacionados aos processos de subducção. Em contraste, para **Aceñolaza and Toselli (1981)**, a faixa magmática oriental foi originada por um regime ensialico tensional, desenvolvido entre o craton de Arequipa no oeste e o craton Brasiliense no leste. **Coira et al. (1999)**, propuseram um modelo onde a faixa magmática ocidental (Cambriano Superior-Arenigiano Inferior) ocorreu progressivamente num arco ativo até um arco em diminuição. Entretanto, a faixa oriental, ocorreu num regime de convergência obliqua, gerando importantes falhas, produzindo no norte, fusão parcial da crosta, e criando uma zona de subducção no sul.

O embasamento da Puna Sul, está representado por rochas Neoproterozoicas de médio a alto grau metamórfico da Formação Pachamama (**Hongn and Seggiaro, 2001**), que compreende micaxistas, gnaisses (orto e para) com intercalações de rochas calciosilicáticas e anfibolitos (Fig. 1). Da mesma forma, também afloram rochas metamórficas de baixo a méio grau do Complexo Metamórfico Neoproterozoico-Cambriano de Rio Blanco (**Hongn and Seggiaro, 2001**) (Fig. 1); esse embasamento consiste em ardósias, filitos, metaquartzcitos e xistos silimaníticos. **Becchio et al. (1999)** e **Lucassen and Becchio (2003)**, indicaram um pico metamórfico de alta T e baixa a meia P aprox. aos 510 Ma (isócrona Sm-Nd em minerais, e U-Pb em titatinas das capas calciosilicáticas). Além disso, essas rochas são intrudidas por granitoides ordovicianos do Complexo Eruptivo Oire (**CEO; Hongn and Seggiaro, 2001**) da Faixa Magmática Leste. Os granitoides do CEO são conformados por granitos e granodioritos de grãos finos a grossos, equigranulares a porfiríticos, ocorrendo numa extensa (~100 km) faixa com direccao N-S, na margem oriental do salar de Centenario, Ratones e Diablillos (Fig. 1). Mais para o leste, esses granitoides gradualmente cambiam a ortognaisses com diferentes graus de milonitzacao. O CEO foi interpretado como um episódio magmático syn-kinematic – post-kinematic, associado às fases de deformação Guandacol e Ocloyica, em tempos do Ordoviciano inicial e tardio, respectivamente (**Mon and Hongn, 1996; Hongn and Seggiaro, 2001**).

As rochas do embasamento Ordoviciano são representados por rochas metassedimentares marinas de baixo grau e ardósias com intercalações de rochas

Geocronologia e isotopia do magmatismo paleozoico na zona de Diablillos, borda oriental da Puna austral (NW da Argentina): Evolução crustal do orôgeno paleozoico inferior na margem ocidental de Gondwana

vulcânicas da Formação Falda Ciénega (Llanvirn-Llandeilian, **Aceñolaza et al., 1976**) aflorando na borda oeste do salar Centenario (Filo Copalayo, **Fig. 1**), e no Filo de Oire Grande. Em contato tectônico, no Filo Copalayo (**Mon and Hongn, 1996**), afloram unidades metamórficas de médio a alto grau, compreendem micaxistos, granito-granodiorita-tonalito ortognaisse (**Fig. 1**), com uma idade de cristalização de 467 ± 10 Ma (idade U-Pb em zircão, **Domínguez et al., 2006**). Na borda oriental do salar Centenário, aflora uma unidade volcano-sedimentar (Cochinoca- Escaya Magmatic- Sedimentary Complex, **Coira et al., 2004**), formada por ardósias, metapsamitos e micaxistos de baixo à medio grau (**Fig. 1**). Essa sequência é intercalada por um magmatismo bimodal representado por metariolitos, metadacitos e metabasaltos (**Fig. 1**). Essas últimas rochas estão intrudidas por sieno e leucogranitos do Complexo Eruptivo Oire, gerando hornfels e xistos mosqueados. **Viramonte et al. (2007)** definiram uma idade U-Pb de cristalização para os metariolitos entre 472-485 Ma, e uma idade de emprazamento para as unidades plutónicas do CEO de 462-475 Ma.

O Complexo Intrusivo Diablillos (CID), definido por **Becchio et al. (2011)** foi emprazado na Serra de Inca Viejo, na faixa Magmática suloriental. A serra Inca Viejo, oeste do Filo de Oire Grande, é uma montanha que divide o salar Ratones e Centenario no noroeste, com o salar Diablillos no sudeste (**Fig. 2**).

Além de novos dados geoquímicos e isotópicos apresentados nesta dissertação, e baseado na localização geográfica e por características macroscópicas (por exemplo, a ocorrência de quartzo azul, **Seifert et al., 2011**) **Becchio et al. (2011)** associaram as fácies graníticas do CID com os granitoides ordovicianos do Complexo Eruptivo Oire (CEO) (**Fig. 2**).

Recentemente, **Suzaño et al. (2015)** presentaram um artigo detalhado de campo no Complexo Intrusivo Diablillos. Esses autores reconheceram e descreveram nesse Complexo, fácies de Mozogranitos, Granodioritos e Tonalitos, fácies de Dioritos e fácies de diques básicos.

Na borda oriental da serra Inca Viejo, as mencionada fácies do CID, em contato intrusivo neto, intrudem rochas metamórficas de baixo grau do Complexo Metamórfico Rio Blanco (**Hongn and Seggiaro, 2001**) (**Fig. 2**). Na borda ocidental, as fácies de monzogranitos, em contato intrusivo, intrudem rochas metamórficas de medio grau, como ser, micaxistas, para e ortognaisses, incluídos na Formação Pachamama (**Hongn and Seggiaro, 2001**) (**Fig. 2**). Além disso, afloram corpos subvolcanicos da Andesita Ratones e a Formação Inca Viejo de idades Miocenas (**González, 1984**), para o norte e sul da serra respectivamente. Esses corpos presentam alterações hidrotermais e concentrações minerais de interesse económico. Finalmente, as rochas do embasamento e os intrusivos subvolcánicos Neógenos estão cobertos por vulcanitas Quaternárias da Formação Incahuasi (**Aceñolaza et al., 1976**) (**Fig. 2**), e por materiais aluviais/fluviais e salares com interesse económico pelas concentrações de sais de borato e lítio.

Geocronologia e isotopia do magmatismo paleozoico na zona de Diablillos, borda oriental da Puna austral (NW da Argentina): Evolução crustal do orôgeno paleozoico inferior na margem ocidental de Gondwana

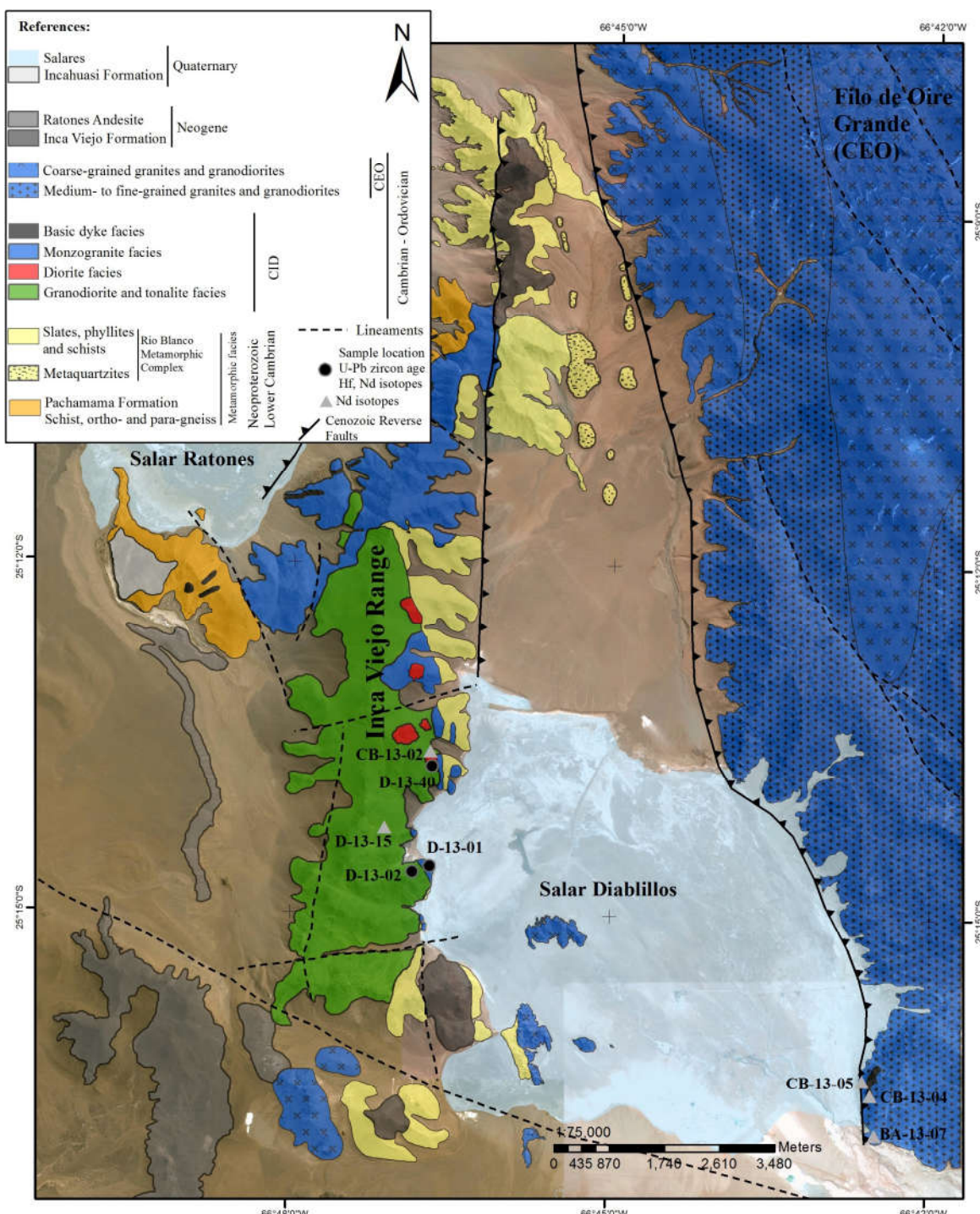


Fig. 2: Mapa geológico de semi-detalhe onde se observam as principais unidades do Complexo Intrusivo Diablillos. Modificado de Nieves (2014).

1.3. ETAPAS DE TRABALHO

Com a finalidade de alcançar os objetivos propostos neste projeto, utilizaram-se as seguintes etapas e métodos de trabalho:

- *Pesquisa Bibliográfica* – Leitura de publicações relacionadas à geologia da área de estudo e aos métodos que foram utilizados.
- Realização de um mapa geológico de semi-detalhe (escala 1:25.000) dos corpos ígneos estudados.
- *Trabalho de Campo – identificação das diversas litologias aflorantes*. Realizaram-se uma campanha de campo de dez dias. Coletaram-se amostras representativas das unidades estudadas e verificação das relações estructurais e estratigráficas entre as diferentes unidades.
- *Análise Petrográfica* – Descrição petrográfica das unidades estudadas visando à caracterização dos protólitos e dos eventos termo-tectônicos que afetaram a região.
- *Análises Geoquímicas dos Elementos Maioritários, Traços e Terras Raras*. Realizaram-se oito análises geoquímicas em amostras seletadas. A preparação de amostras para análises de elementos maioritários e traços foram feitas no Laboratório de Geoquímica, Instituto Geonorte, Universidade Nacional de Salta. As análises foram realizadas nos laboratórios ACME, em Canadá.
- *Análises Isotópicas* – As análises U-Pb, Lu-Hf (3 amostras) e Sr-Nd (8 amostras), das amostras representativas foram realizadas no Laboratório de Geocronologia da Universidade de Brasília, seguindo as respectivas rotinas adotadas, segundo Buhn *et al.*, (2009), Matteini *et al.*, (2010) e Gioia e Pimentel (2000).
- *Integração dos Resultados* – A interpretação dos dados produzidos e aplicação destes na evolução geológica serão expostas na dissertação de mestrado que será apresentada em forma de artigo científico, submetido ao Periódico Gondwana Research. Além disso, um segundo artigo científico onde inclui as rochas encaixantes dos corpos magmáticos será realizado e submetido no ano próximo.

1.4.VIAS DE ACESSO

A zona de estudo, delimitada pelos paralelos 25°09' e 25°18' S e os meridianos 66°50'- 66°42' W, encontra-se localizada na Província de Salta, Argentina (Fig. 3). Desde a cidade de Salta pela estrada N°51, depois de percorrer uns 170 km se chega até San Antonio de los Cobres, no altiplano da Puna. Dessa localidade se segue pela estrada provincial N°129, para o sul, até Santa Rosa de los Pastos Grandes. A partir desse ponto até a Mineira Maggi, no Salar Centenario recorrem-se pelo Sul, uns 40 km aproximadamente. Finalmente, e por caminho minero, segue uns 50 km pelo Sul até arribar ao Salar Diablillos e a zona de estudo.

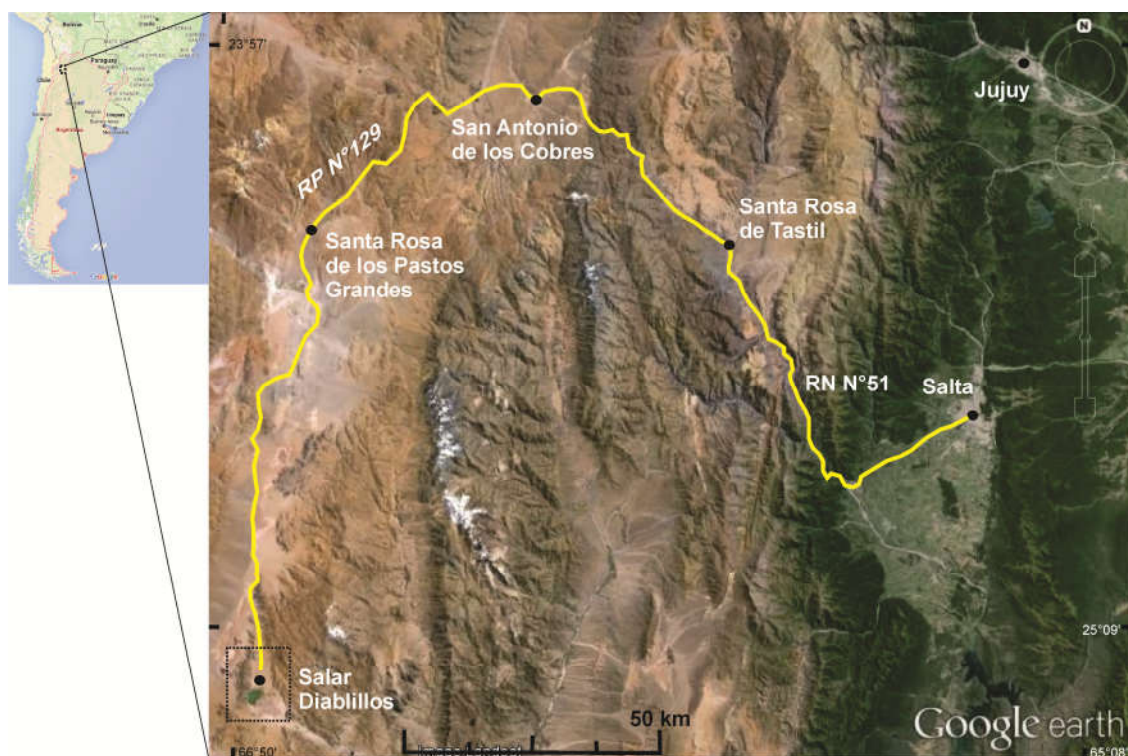


Fig. 3: Vias de acesso na área de estudo. A mesma é marcada no retângulo com linhas ponteadas pretas.

Agustín Ortiz Yáñez

CAPITULO II

2. PROCEDIMENTOS ANALITICOS

2.1. Análises Geoquímicas

A preparação de amostras para os análises de elementos maioritários e traços foram feitas no Laboratório de Geoquímica, Instituto Geonorte, Universidade Nacional de Salta. Os procedimentos consistiram em moer as amostras em britador a mandíbula e uma vez quarteadas, foram pulverizadas em moinho tipo Herzog, com anéis oscilatórios de carbono de tungstênio. As amostras foram enviadas nos laboratórios ACME, em Canadá. As Análises de elementos maioritários mais Ni e Sc (ppm) foram analisados pelo ICP-OES (Inductively Coupled Plasma Emission Spectrometer) e os elementos traços foram analisados pelo ICP-MS (Inductively Coupled Plasma Mass Spectrometer) (**Table 1**).

1.2. Procedimentos analíticos de U-Pb e isótopos de Lu-Hf

Depois de moer 5 kg de cada amostra selecionadas, os concentrados de zircão foram extraídos pelo separador magnético Frantz, no Laboratório de Geoquímica, Instituto Geonorte, Universidade Nacional de Salta, a purificação final dos concentrados foi alcançada pela seleção manual usando uma lupa binocular. Os minerais de zircão foram escolhidos a mão com uma agulha de acupuntura e montados numa pastilha de vidro, onde estava grudada uma fita de dupla faz para segurar os grãos. Logo, um anel plástico de 9 mm foi posicionado em torno aos minerais, e recheado com epoxy mais endurecedor. Depois de um dia, uma vez que a resina estiver seca, a fita e a pastilha foram removidas dos *mounts*. Finalmente, os *mounts* foram polidos, para que de essa forma, as superfícies dos minerais de zircão ficaram expostas (**Fig. 4d**). Para selecionar os spots nos minerais, foram realizados imageamento de Cathodoluminiscência (CL) dos zircões com um Microscópio Electrónico de Varredura (MEV) JEOL Quantas 450 no Laboratório de Geocronologia da Universidade de Brasília.

As análises de U-Pb (**Table 2**) e Lu-Hf (**Table 3**) foram realizadas em zircões de três amostras selectadas pelo Thermo-Fisher Neptune MC-ICP-MS acoplado com um sistema de ablação laser Nd:YAG UP213 New Wave, no Laboratório de Geocronologia da Universidade de Brasília. Para as Análises de U-Pb o diâmetro do furo foi 30 μ m. Uma

frequência de 7 Hz com 80% de energia foi usado, e 40cps. O padrão GJ-1 foi utilizado para normalizar as frequências isotópicas durante as Análises. O chumbo comum ^{204}Pb foi monitorado com as massas de ^{202}Hg e ($^{204}\text{Hg}+^{204}\text{Pb}$). Em todos os Análises nos grãos de zircão a correção de Pb comum, calculada segundo **Stacey and Kramers (1975)**, não foi necessária devido a baixa sinal da massa ^{204}Pb (< 30 cps) e alta relação $^{206}\text{Pb}/^{204}\text{Pb}$. Os erros são propagados pela adição quadrática $[(2SD^2+2SE^2)^{1/2}]$ de reprodução externa. A reprodução externa é representada pela deviação standard (SD) obtida por repetidas análises ($n=20$, ~1.1 % para $^{207}\text{Pb}/^{206}\text{Pb}$ e até ~2 % for $^{206}\text{Pb}/^{238}\text{U}$) do zircão standard GJ-1, feito durante a sessão analítica, e dentro da precisão no erro estándard (SE) calculado para cada análises (**Fig. 4 a, b, c**). Além disso, durante a sessão analítica o zircão estándard TEMORA foi analisado como um mineral desconhecido para obter melhores parâmetros de medição e certeza (**Fig. 5**). Diagramas da concórdia (2σ erro elipses), idades concordantes e idades de intercepção superior foram calculados pelo Isoplot/Ex software (**Ludwig, 2003**). As análises de U-Pb nos grãos de zircão foram realizados com o método de estándard-amostra bracketing (**Albarède et al., 2004**), usando o zircão standard GJ-1 para quantificar a quantidade de fraccionamento do ICP-MS. Entre dois e quatro desconhecidos foram analisados entre análises de GJ-1, e as relações $^{206}\text{Pb}/^{207}\text{Pb}$ e $^{206}\text{Pb}/^{238}\text{U}$ foram corregidas pelo tempo. Em grãos de zircão pequeno fraccionamento da relação $^{206}\text{Pb}/^{238}\text{U}$ foi induzido pelo laser spot, e foi corrigido usando o método de regressão lineal (**Kosler et al., 2002**). Os dados brutos foram processados off-line e reduzidos usando uma folha de Excel (**Buhn et al., 2009**). A descrição completa dos métodos e procedimentos foram apresentadas por **Buhn et al. (2009)**.

Os isótopos de Lu-Hf foram analisados em grãos de zircão previamente analisados pelo método U-Pb. Os dados dos isótopos de Lu-Hf foram coletados durante um tempo de ablação de 40-50 segundos, usando um diâmetro de furo de 40 μm e 85% de energia. Os sinais de interferência de isótopos livres ^{171}Yb , ^{173}Yb e ^{175}Lu foram monitoradas durante as análises para corrigir as interferências isobáricas dos sinais de ^{176}Yb e ^{176}Lu no ^{176}Hf . A contribuição de ^{176}Yb e ^{176}Lu foram calculadas usando as abundâncias isotópicas de Lu e Hf, propostas por **Chu et al. (2002)**. As medições contemporâneas de ^{171}Yb , ^{173}Yb proveem um método para corrigir o *mass-bias* do Yb usando o fator de normalização para a relação $^{173}\text{Yb}/^{171}\text{Yb}$ de 1.132685 (**Chu et al., 2002**). As relações isotópicas de Hf, $^{179}\text{Hf}/^{177}\text{Hf}$

Geocronologia e isotopia do magmatismo paleozoico na zona de Diablillos, borda oriental da Puna austral (NW da Argentina): Evolução crustal do orôgeno paleozoico inferior na margem ocidental de Gondwana

foram normalizadas com um valor de 0.7325 (**Patchett, 1983**). Quando foi possível, os furos de Pb e Hf foram realizados o mais próximo possível, para analisar porções de grãos de zircão com as mesmas características isotópicas de U e Pb. Uma detalhada descrição dos métodos e procedimentos foi descrevida por **Matteini et al. (2010)**.

Os valores de $\epsilon_{\text{Hf}}(t)$ foram calculados pela constante de decaimento $\lambda=1.865 \times 10^{-11}$, proposta por **Scherer et al. (2006)**, e os valores de $^{176}\text{Lu}/^{177}\text{Hf}$ e $^{176}\text{Hf}/^{177}\text{Hf}$ CHUR de 0.0332 e 0.282772 proposto por **Blichert-Toft and Albarède (1997)**. A idade T_{DM} em dois estágios foi calculada pela composição inicial de Hf no zircão, usando uma meia crustal da relação de Lu/Hf (**Gerdes and Zeh, 2009; Nebel et al., 2007**). A composição inicial de Hf no zircão representa o valor de $^{176}\text{Hf}/^{177}\text{Hf}$ calculado no tempo de cristalização do zircão, o seja, a idade U-Pb, possivelmente concordante, obtida previamente no mesmo cristal. A idade modelo de Hf do manto depletado ($T_{\text{DM}} \text{ Hf}$) foi calculada usando $^{176}\text{Lu}/^{177}\text{Hf}=0.0384$ e $^{176}\text{Hf}/^{177}\text{Hf}=0.28325$ para o manto depletado (**Chauvel and Blichert-Toft, 2001**) e valores $^{176}\text{Lu}/^{177}\text{Hf}$ de 0.0113 para a crosta meia (**Taylor and McLennan, 1985; Wedepohl, 1995**). Antes das medidas dos isótopos de Hf nos zircões, análises réplicas de solução standard 200 ppb Hf JMC 475 adicionada com Yb (Yb/Hf=0.02) foram realizadas ($^{176}\text{Hf}/^{177}\text{Hf}=0.282162 \pm 13 \text{ 2s, } n=4$). Durante as sessões de réplicas, análises do zircão standard GJ-1 foram executadas obtendo relações $^{176}\text{Hf}/^{177}\text{Hf}$ de $0.282006 \pm 16 \text{ 2}\sigma$ ($n=25$), em acordo com os valores de referência do zircão standard GJ obtidos por **Morel et al. (2008)**. Os valores de ϵ_{Hf} para cada grão foi calculada com a idade U-Pb previamente obtida no mesmo grão de zircão. Para as análises levemente discordantes as idades $^{206}\text{Pb}/^{238}\text{U}$ e $^{207}\text{Pb}/^{206}\text{Pb}$ foram usadas para grãos jovens ($<1 \text{ Ga}$) e velhos ($>1 \text{ Ga}$) respectivamente.

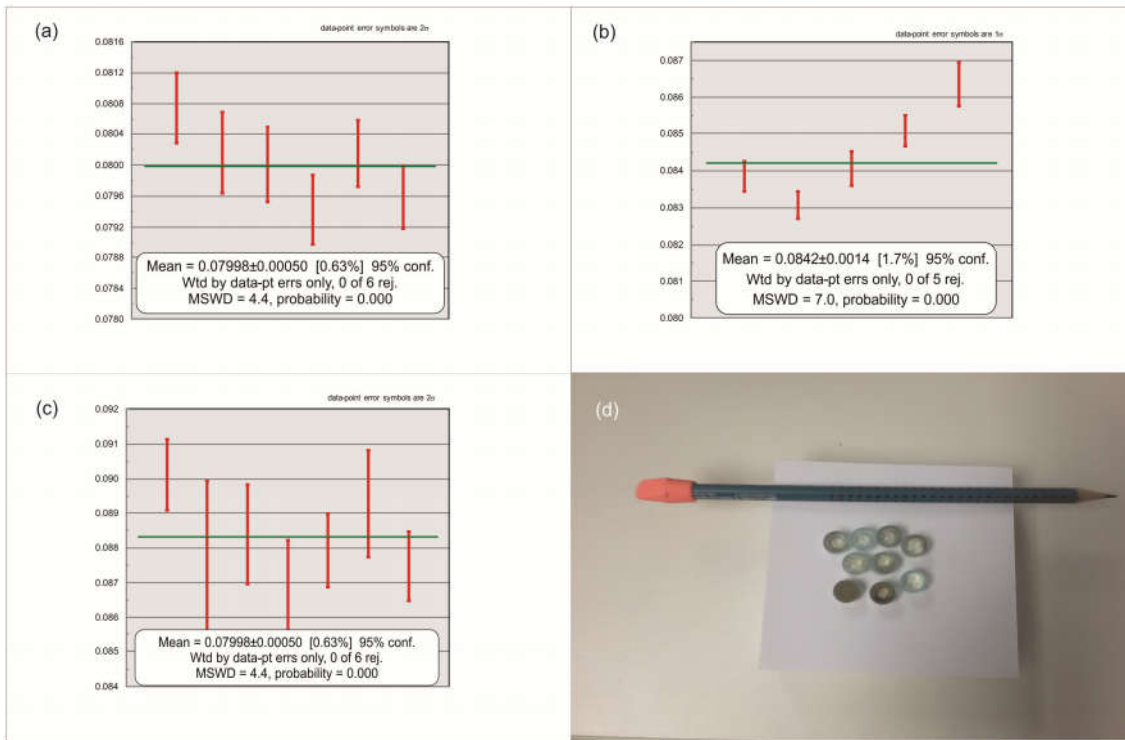


Fig. 4: Relações medias ponderadas $^{206}\text{Pb}/^{238}\text{U}$ do zircão estándar GJ, feitas durante as sessões analíticas das amostras (a) Monzogranito (b) Diorito (c) Granodiorito (d) Exemplos de mounts para as análises de U-Pb. Os mounts foram polidos, para que de essa forma, as superfícies dos minerais de zircão ficaram expostas.

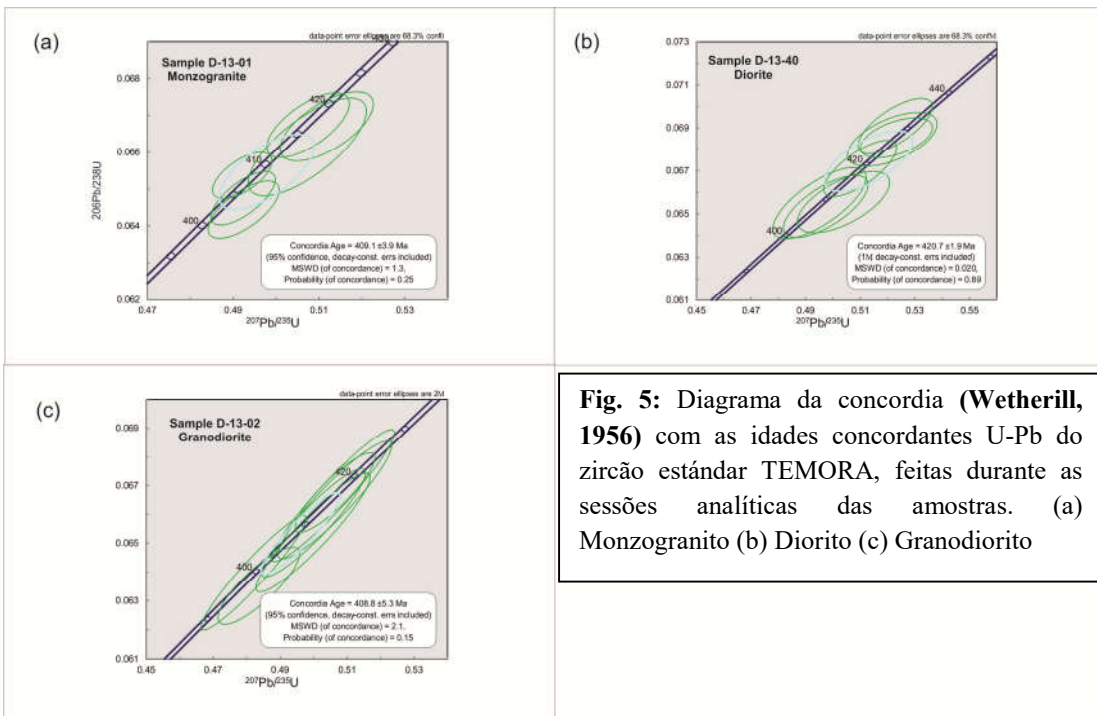


Fig. 5: Diagrama da concordia (Wetherill, 1956) com as idades concordantes U-Pb do zircão estándar TEMORA, feitas durante as sessões analíticas das amostras. (a) Monzogranito (b) Diorito (c) Granodiorito

2.3. Analises na Microsonda

Análises na microssonda foram realizadas em zircões analisados previamente pelo método laser ablation U-Pb, usando o equipamento JEOL JXA-8230 Superprobe na Universidade de Brasília. Dez diferentes zircões das amostras selecionadas foram analisados. Os elementos analisados foram HfO₂, SiO₂, ZrO₂, Y₂O₃, UO₂ e ThO₂ (**Table 4**). As condições das análises foram 20kV energia, 10 nA de corrente para Si, Zr e Hf; 100 nA para Ti, U, Th e Y. Contagem spike 10s para Si e Zr; 60s para os demais elementos.

2.4. Geoquímica isotópica Sr-Nd

Análises de Sr-Nd (**Table 5**) foram realizadas em oito amostras de rocha total do CID no Laboratório de Geocronologia da UnB. As análises Sm-Nd foram feitas segundo o método descrito por **Gioia e Pimentel (2000)**. Entre 70 e 100mg de pó de amostra foram misturados com uma solução traçadora mista (spike) de 149 Sm-150Nd e dissolvidos em cápsulas Savillex. A extração dos elementos lantanídeos foi feita através de técnicas convencionais de troca iônica em colunas de quartzo, usando resina BIO-RAD AG-50W-X8. As extrações de Sm e Nd foram realizadas em colunas de teflon empacotadas com resina LN-Spec (resina líquida HDEHP-ácido di-ethylhexil fosfórico impregnada em pó de teflon). As frações de Sr, Sm e Nd foram depositadas em arranjos duplos de filamentos de rênio. As razões isotópicas foram determinadas em espectrômetro de massa multi-coletor Finnigan MAT 262 em modo estático. As incertezas para ⁸⁷Sr/⁸⁶Sr são menores do que 0.01% (2σ) e para as razões ¹⁴⁷Sm/¹⁴⁴Nd e ¹⁴³Nd/¹⁴⁴Nd são melhores do que ±0.2% (1σ) e ±0.005% (1σ) respectivamente, baseadas em análises repetidas dos padrões BHVO-1 e BCR-1. As razões ¹⁴³Nd/¹⁴⁴Nd são normalizadas para o valor de ¹⁴⁶Nd/¹⁴⁴Nd de 0.7219 e a constante de desintegração (λ) usada é 6.54 x 10-12 a-1. Os resultados foram processados utilizando-se o programa ISOPLOT/Ex 3 (**Ludwig, 2003**).

Agustín Ortiz Yañez

CAPITULO III

Geocronologia e isotopia do magmatismo paleozoico na zona de Diablillos, borda oriental da Puna austral (NW da Argentina): Evolução crustal do orôgeno paleozoico inferior na margem ocidental de Gondwana

**Zircon U-Pb ages and Hf isotopes for the Diablillos Intrusive Complex,
Southern Puna, Argentina: crustal evolution of the Lower Paleozoic
orogen, Southwestern Gondwana margin**

**A. Ortiz^{1,2*}, N. Hauser¹, R. Becchio², A. Nieves², N. Suzaño², A. Sola², M. Pimentel¹,
W.U. Reimold^{1,3,4}**

¹ Geochronology Laboratory, Instituto de Geociências, Universidade de Brasília, 70910 900 Brasília, DF.

² GEONORTE - INENCO (Universidad Nacional de Salta – CONICET), Av. Bolivia 5150, A4400FVY, Salta, Argentina.

³Museum für Naturkunde – Leibniz-Institute for Evolution and Biodiversity Research, Invalidenstrasse 43, 10115 Berlin, Germany.

⁴Humboldt Universität zu Berlin, Unter den Linden 6, 10099 Berlin, Germany.

*Corresponding author: agustinortiz13@hotmail.com. Telephone: +54-387-4255441.

Submitted to Gondwana Research.

Abstract

To better comprehend the crustal evolution of the Lower Paleozoic Orogen at the Southwestern Gondwana margin, we present new combined U–Pb and Hf isotope analyses on zircon by LA-MC-ICP-MS from monzogranite, granodiorite and diorite facies of the Diablillos Intrusive Complex, Eastern Magmatic Belt, Southern Puna. We display $^{206}\text{Pb}/^{238}\text{U}$ concordant weighted average ages of 517 ± 3 Ma and 515 ± 6 Ma for the monzogranite and diorite facies of the complex respectively, and a concordant age of 521 ± 4 Ma for the granodiorite facies. These ages permit to constrain the magmatic activity climax in the Diablillos Complex around ~ 515 - 520 Ma. Major and trace element data, initial $^{87}\text{Sr}/^{86}\text{Sr}$ values varying from 0.70446 to 0.71278, positive and negative Nd(t) values between +2.5 and -4, as well as Hf(t) for zircon data between +3 and -3 indicate that the analyzed samples represent contaminated magmas. The Hf(t) and the Nd(t) values for this complex specify that the rocks from the Diablillos Intrusive Complex are derived from an interaction of a dominant Mesoproterozoic crustal source and juvenile mantle-derived magmas, with a T_{DM} model age range of ~ 1.2 - 1.5 Ga, that were reworked during lower Paleozoic times. The combined data obtained in this contribution allow us to suggest that the Eastern Magmatic Belt in the Puna represents a long-lived magmatic event. Supporting the model for the evolution of the Central Andean basement involving the formation of a mobile belt, whereby the Pampean and Famatinian cycles do not represent distinct events but comprise a single, non-differentiable event from Neoproterozoic to Lower Paleozoic times.

Key words: Western Gondwana; Puna Argentina; Lower Paleozoic Arc; Zircon U-Pb geochronology; Hf isotopes.

1. Introduction

The evolution of the Gondwana supercontinent has been the focus of numerous investigations during the past years (e.g., **Pimentel et al., 2000; Rapela et al., 2007; Piper, 2007; Ramos, 2008; Cordani et al., 2009; Rapela et al., 2015**). The main models to explain the formation of this supercontinent are, the assembly of two blocks: a western block comprising Africa and South America, and an eastern block with India, East Antarctica, Madagascar, Australia, and Sri Lanka (**Squire et al., 2006; Yoshida and Upreti, 2006; Yoshida, 2007**). It has also been suggested that there existed a long-lived supercontinent from Paleoproterozoic until Mesoproterozoic times (**Piper, 2000; Piper, 2007**). There seems to be general consensus that Western Gondwana represents the amalgamation of descendants of the first supercontinent – Rodinia, which existed from Neoproterozoic to Cambrian times (e.g., **Pimentel and Fuck, 1992; Pimentel et al., 2000; Alkmim et al., 2001; Escayola et al., 2007; Rapela et al., 2007; Fuck et al., 2007; Ramos, 2008; Cordani et al., 2009**).

The evolution of the Eastern Cordillera and Puna in the Central Andes, NW Argentina (**Fig. 1**), which is part of the Southwestern Gondwana margin, has been widely debated. Different authors (e. g., **Ramos et al., 1986; Ramos, 1988; Loewy et al., 2004; Rapela et al., 2007; Ramos, 2008; Cordani et al., 2009; Collo et al., 2009; Drobe et al., 2009; Hauser et al., 2011; among others**) have traditionally recognized two orogenic events: the *Pampean* (Upper Precambrian–Lower Cambrian) and *Famatinian* (Upper Cambrian–Lower Silurian) stages involving subduction processes with formation of magmatic arcs, followed by successive collision of peri-Gondwana or exotic terranes. Due to the lack of evidence and indicators for these collision processes, such as sutures zones, presence of ophiolites related to oceanic crust, or high P/low T metamorphism indicative of subduction-accretion regimes, others (e.g., **Becchio et al., 1999; Bock et al., 2000; Lucassen et al., 2000; Buttner et al., 2005; Zimmermann et al., 2014; Rapela et al., 2015**) proposed an alternative model, suggesting a geodynamic evolution dominated by intracrustal recycling with minor contributions from juvenile materials. In this regard, **Lucassen et al. (2000)** proposed for the Central Andes basement an evolution in a long-

lived mobile belt, where the Pampean and Famatinian cycles are not distinct events but rather represent a single, non-differentiable event between 600 and 400 Ma. The mobile belt peaked in a low-P/high-T metamorphism at approximately 525-500 Ma. This was then followed by a long-lasting high-thermal gradient regime in the mid-crust until Silurian times (**Lucassen et al., 2000**).

The Puna geological province is a high-plateau region (4000 meter above sea level) that comprises the Salta and Jujuy, and part of the Catamarca, provinces (**Fig. 1**). The magmatic record in this region has been associated with the Famatinian orogeny, initiated in the Lower Tremadoc and reaching its peak in the Arenig (**Rapela et al., 1992; Coira et al., 1999**). It involves two N-S trending magmatic belts of ~200 km extension; they define an Eastern Eruptive Belt (**Méndez et al., 1973**) represented by calc-alkaline and peraluminous granitoids, metadacites and metarhyolites, and a Western Eruptive Belt (**Palma et al., 1986**) characterized by metaluminous I-type granitoids (**Fig. 1**). Taking into account that the so-called eruptive belts also involve plutonic rocks, we, here, prefer to use the term Magmatic Belts, in order to include volcanic, subvolcanic and plutonic rocks.

In the Eastern Magmatic Belt, **Becchio et al. (2011)** defined the Diablillos Intrusive Complex (CID by its Spanish name *Complejo Intrusivo Diablillos*; **Fig. 2**). This complex is mainly composed of granitoids, diorites, and basic dykes. Recently, **Suzano et al. (2015)** presented an extensive work on the petrography and magmatic differentiation of this Complex. They proposed that the main process related to the origin and evolution of this Complex was magma mixing between granites and diorites.

In the past years, the advances of zircon isotope geochemistry have provided a formidable means to date magmatic and metamorphic events by U-Pb geochronology (e.g., **Hoskin and Schaltegger, 2003**), and to employ zircon successfully for the tracing of petrogenetic processes in metamorphic and magmatic rocks (**Hawkesworth and Kemp, 2006; Castañeiras et al., 2011**). Some recent compositional investigations of zircon have not been directly related to geochronology, but instead based on the ability of zircon to record petrogenetic processes in igneous systems through analysis of Hf isotopes (e.g., **Zeh et al. 2007; Dong et al. 2013; Li et al. 2014**; and references therein). This isotope system provides a useful tool to discriminate the origin of rocks in general, and potentially to

Geocronologia e isotopia do magmatismo paleozoico na zona de Diablillos, borda oriental da Puna austral (NW da Argentina): Evolução crustal do orôgeno paleozoico inferior na margem ocidental de Gondwana

reveal the source and nature of protoliths (e.g., **Claiborne et al., 2010; Guo et al., 2007; Liu et al., 2009; Nardi et al., 2012**) - thus giving us important parameters for modelling the crustal evolution of rocks (e.g., **Hawkesworth and Kemp, 2006**).

The general lack of isotopic data (there is only one datum for the CID, a U-Pb weighted average age of 501 Ma with a 1σ error of ± 17 Ma, **Suáñez et al., 2015**) makes it imperative to determine the emplacement age of this complex. Moreover, the scarce amount of geological and geochemical data available for this sector of the Southern Puna make the CID an essential place to study and provide new evidence for the development of the Eastern Magmatic Belt at the SW Gondwana margin.

We have obtained three new zircon U-Pb ages by Laser Ablation Inductively Coupled Plasma Mass Spectrometry (LA-ICP-MS) for the main facies of the Diablillos Intrusive Complex, namely: diorite, granodiorite, and monzogranite. Additionally, we present the first Lu-Hf isotope data for this complex and in the Southern Puna, as well as new geochemical and Sr-Nd isotope data for the igneous rocks of the CID. The aim is to contribute to the understanding of sources, magmatic processes and emplacement of magmas during Cambrian-Ordovician times in this sector of the Puna and thus, contribute to better comprehend the crustal evolution of the Lower Paleozoic Orogen at the Southwestern Gondwana Margin.

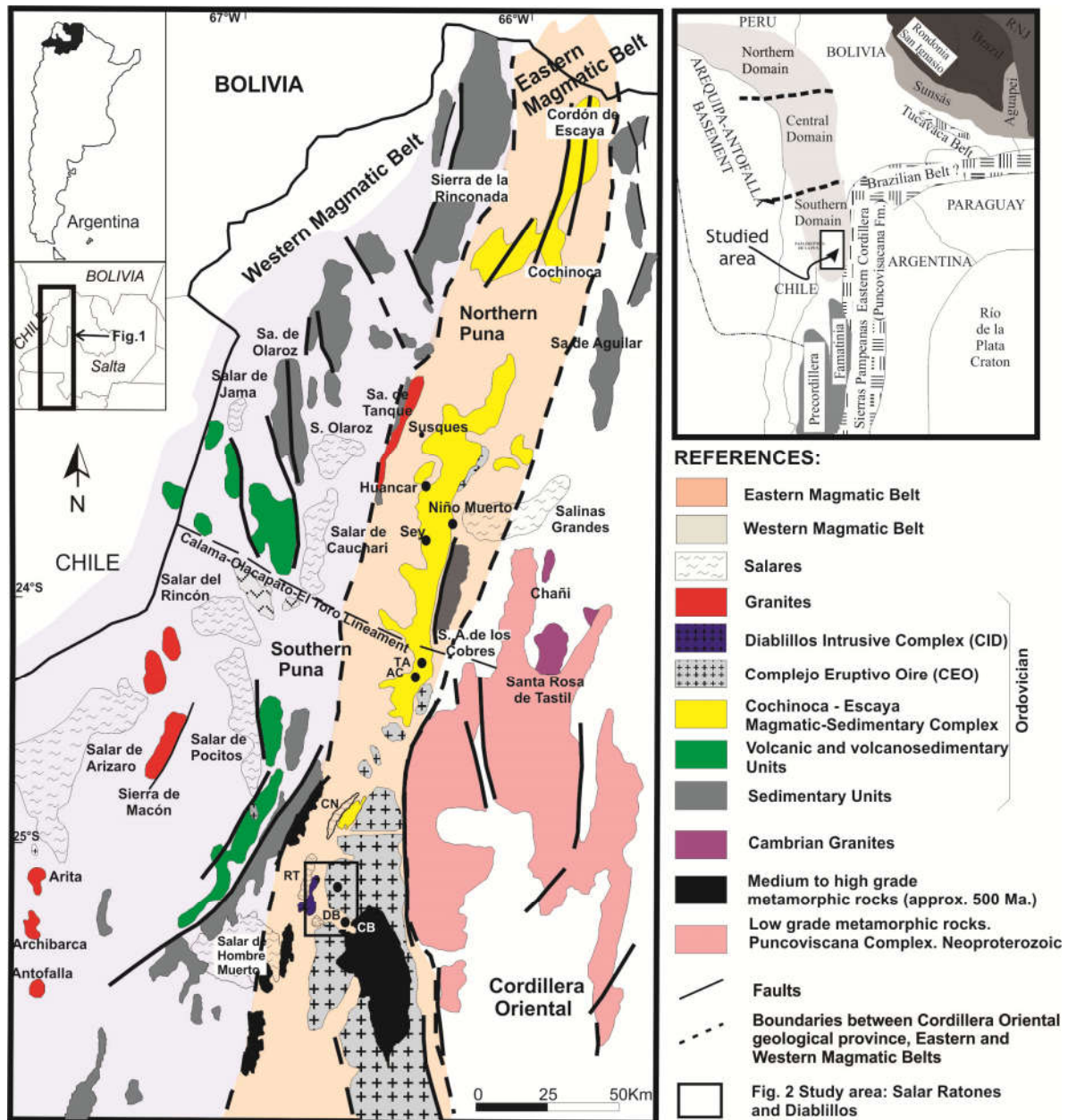


Fig. 1: Regional map, showing the main geological units in the geological provinces of NW Argentina. CN: Salar Centenario. DB: Salar Diablillos. RT: Salar Ratones. CB: Cerro Blanco. TA: Tajamar. AC: Acazoque. Inset shows a geotectonic sketch map of the South American basement. Modified after Viramonte et al. (2007) and Hauser et al. (2011).

REFERENCES:

- Eastern Magmatic Belt
- Western Magmatic Belt
- Salares
- Granites
- Diablillos Intrusive Complex (CID)
- Complejo Eruptivo Oire (CEO)
- Cochinoca - Escaya Magmatic-Sedimentary Complex
- Volcanic and volcanosedimentary Units
- Sedimentary Units
- Cambrian Granites
- Medium to high grade metamorphic rocks (approx. 500 Ma.)
- Low grade metamorphic rocks. Puncoviscana Complex. Neoproterozoic
- Faults
- Boundaries between Cordillera Oriental geological province, Eastern and Western Magmatic Belts
- Fig. 2 Study area: Salar Ratones and Diablillos

Ordovician

2. Geological setting

The origin of the Eastern and Western Magmatic Belts was variably interpreted due to collision of allochthonous, parauthochthonous, or autochthonous terranes with the southwestern margin of Gondwana (e.g., Coira et al., 1982; Ramos, 1986; Conti et al., 1996). Other authors (e.g., Dalziel and Forsythe, 1985; Ramos 1988; Rapela et al., 1992) interpreted these magmatic belts as two magmatic arcs related to subduction processes. In contrast, for Aceñolaza and Toselli (1981) the Eastern Magmatic Belt originated from an extensional ensialic regime, developed between the Arequipa Craton to the west and the Brasiliano Craton to the east. Coira et al. (1999) proposed a model whereby the magmatism of the Western Magmatic Belt (Upper Cambrian-Lower Arenig) occurred progressively in an active to waning arc setting. In the Eastern Belt, an oblique convergence regime occurred at that time, generating important strike faults, resulting to the north in partial melting of the crust, and in a subduction zone to the south.

The Southern Puna basement in the surroundings of the Centenario, Ratones and Diablillos salars is represented by medium to high grade Neoproterozoic metamorphic rocks of the Pachamama Formation (Hongn and Seggiaro, 2001). They comprise mica schist and gneisses (ortho and paragneisses) intercalated with calksilicates and amphibolites (Fig. 1). These salars are surrounded by low- to medium- grade Neoproterozoic-Cambrian basement (Fig. 1) consisting of slates, phyllites, metaquartzites, and sillimanite schists that constitute the Rio Blanco Metamorphic Complex (Hongn and Seggiaro, 2001). Becchio et al. (1999) and Lucassen and Becchio (2003), indicated a metamorphic peak of high T and low to- medium P at approx. 510 Ma (Sm-Nd isochron of plagioclase, clinopyroxene, garnet data, and U-Pb in titanites from calksilicate layers). In addition, these rocks are intruded by Ordovician granitoids of the Oire Eruptive Complex (CEO; Hongn and Seggiaro, 2001) from the Eastern Magmatic Belt. The granitoids of the CEO comprise fine- to coarse- grained, equigranular or porphyritic granites and granodiorites that occur over a ~100 km long N-S trending belt to the east of the Centenario, Ratones and Diablillos salars (Fig. 1). Further to the east, these granitoids gradually change to orthogneiss with different degrees of mylonitization. The CEO is interpreted as a syn-kinematic to post-

kinematic magmatic episode associated with the Guandacol and Ocloyic deformation phases that took place in the early and late Ordovician, respectively (**Mon and Hongn, 1996; Hongn and Seggiaro, 2001**).

The Ordovician basement rocks are represented by low-grade marine metasediments with intercalated volcanic rocks of the Falda Ciénaga Formation (Llanvirn-Llandeilian, **Aceñolaza et al., 1976**) outcropping at the western edge of the Centenario salar (Filo Copalayo, **Fig. 1**) and at Filo de Oire Grande. In tectonic contact, on the Filo Copalayo (**Mon and Hongn, 1996**), medium- to high- grade metamorphic units of mica schist and granitic-granodioritic-tonalitic orthogneiss crop out (**Fig. 1**). They have an apparent crystallization age of 467 ± 10 Ma (U-Pb age on zircon, **Domínguez et al., 2006**). At the eastern edge of the Centenario salar, a volcano-sedimentary unit (Cochinoca- Escaya Magmatic-Sedimentary Complex, **Coira et al., 2004**) is formed by slates, metapsammites, and low- to medium- grade mica schist (**Fig. 1**). This sequence is intercalated with the products of bimodal magmatism: metarhyolite, metadacite, and metabasalt (**Fig. 1**). These facies, in turn, are intruded by syenogranites and leucogranites of the CEO, whereby hornfels and mottled schist were generated. **Viramonte et al. (2007)** constrained U-Pb crystallization ages for metarhyolites between 485 and 472 Ma and concluded that the plutonic units of the CEO were emplaced between 475 and 462 Ma.

2.1. Local Geology and Petrography

The Diablillos Intrusive Complex (CID) was emplaced in the Inca Viejo Range of the Southeastern Magmatic Belt. The Inca Viejo Range, located to the west of the Filo de Oire Grande, is a mountain that separates the Ratones and Centenario salars to the northwest from the Diablillos salar to the southeast (**Fig. 2, 3a**).

Based on geographic location and macroscopic characteristics of the rocks (e.g., occurrences of blue quartz, **Seifert et al., 2011**), **Becchio et al. (2011)** associated the granitic facies of the CID with the granitoids of the Oire Eruptive Complex (CEO) (Filo de Oire Grande, **Fig. 2**).

Geocronologia e isotopia do magmatismo paleozoico na zona de Diablillos, borda oriental da Puna austral (NW da Argentina): Evolução crustal do orôgeno paleozoico inferior na margem ocidental de Gondwana

Recently, **Suáñez et al. (2015)** identified the main lithologies of this Complex, namely monzogranite, granodiorite and tonalite, diorites, and a facies of basic dykes (**Fig. 2**).

On the eastern side of the Inca Viejo range, the facies of the CID intrude low-grade metamorphic rocks of the Rio Blanco Metamorphic Complex (**Hongn and Seggiaro, 2001**). On the western side, the monzogranite facies intrudes moderate grade metamorphic rocks, such as mica schists, and para- as well as ortho-gneisses (**Fig. 2**) that are included with the Pachamama Formation (**Hongn and Seggiaro, 2001**). In addition, subvolcanic bodies of the Ratones Andesites and Inca Viejo Formation of Miocene age (**González, 1984**) crop out to the north and south of the range. They are associated with hydrothermal alteration and mineral concentrations of economic interest. Lastly, the basement rocks and the Neogene subvolcanic intrusives are covered by Quaternary volcanics of the Incahuasi Formation (**Aceñolaza et al., 1976**), and by alluvial/fluvial materials including the occurrences of salars that are of particular economic interest for lithium and borate brines.

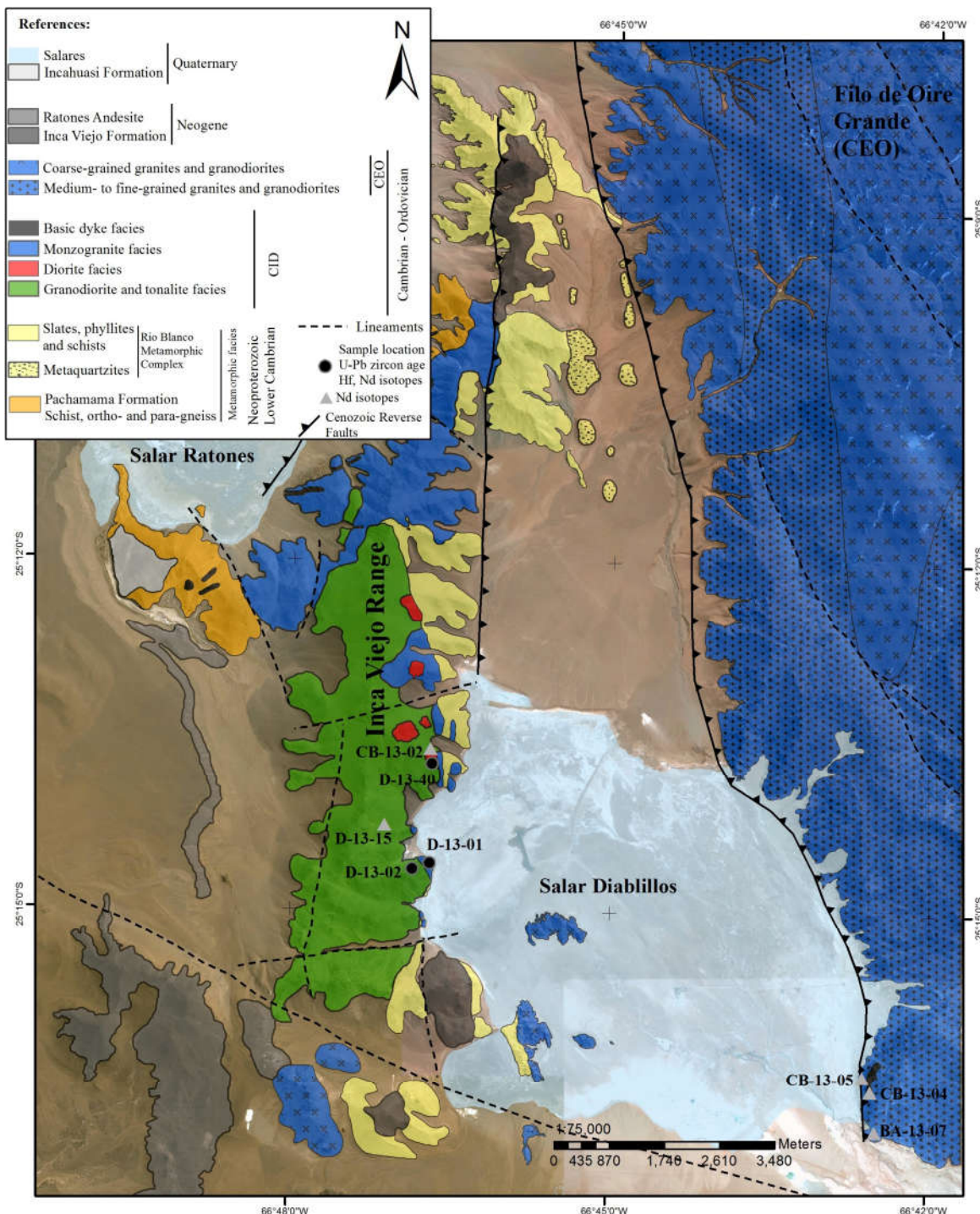


Fig. 2: Detailed geological map showing the main units in the Diablillos Intrusive Complex. Modified after Nieves (2014). The positions of the sampling sites for this study are also shown.

Geocronologia e isotopia do magmatismo paleozoico na zona de Diablillos, borda oriental da Puna austral (NW da Argentina): Evolução crustal do orôgeno paleozoico inferior na margem ocidental de Gondwana

Suzaño et al. (2015) recognized the following facies in the Diablillos Intrusive Complex:

Monzogranite facies: This unit crops out on the northern and eastern sides of the range and intrudes phyllites, slates, and mottled slates of the Rio Blanco Metamorphic Complex to the east (**Fig. 3e**), as well as mica schist, para- and ortho-gneiss of the Pachamama Formation to the west. In the central part of the range, this facies occurs in transitional contact with granodiorite and tonalite (**Fig. 2**).

The distribution of the monzogranite unit has an irregular shape. The rock is medium- to coarse-grained, with a porphyritic texture. It varies from a light to dark grey color, according to biotite content in the matrix. Occasionally, a slight magmatic foliation is observed by the preferred orientation of Mafic Magmatic Enclaves (MME) and syn-magmatic pegmatite dykes. On the northern side of the range, this facies has scarce MME. On the eastern side of the Inca Viejo Range, this facies forms lobate and elongate (less than 700 m long) bodies and includes abundant enclaves of various compositions, such as MME, granodiorite, tonalite, and diorite in the form of dismembered bodies of irregular shape (**Fig. 2**). The dismembered diorite bodies (up to 5 m long), granodiorite, and tonalite enclaves, and the MME have a heterogeneous distribution and are of irregular shape and varied size. The enclaves have rounded and elliptical shapes, with varying sizes up to 1.5 m. The contacts with the monzogranite are sharp (for mafic dismembered bodies and MME) (**Fig. 3b, c**), and variably sharp, transitional, or lobate (for granodiorite and tonalite enclaves) (**Fig. 3b, d**).

The porphyritic monzogranites have euhedral to subhedral K-feldspar (1 to 3 cm large) and plagioclase (1 to 1.5 cm) phenocrysts embedded in a coarse-grained matrix composed by K-feldspar, plagioclase, blue quartz, and abundant biotite.

Some subhedral (even subrounded) phenocrysts seemingly migrated mechanically from the monzogranite to the granodiorite enclaves (**Fig. 3d**). In areas where the monzogranites are intruded by the mafic dismembered bodies, subrounded K-feldspar phenocrysts, plagioclase and quartz are incorporated into the mafic bodies, showing typical

magma mixing-mingling textures, such as mantled plagioclase and ocelli quartz (**Hibbard, 1991**).

The modal composition shown in **Fig. 4** classifies sample D-13-01 as a monzogranite with ~55 vol.% K-feldspar, ~24 vol.% plagioclase, and ~21 vol.% quartz. In thin section (**Fig. 5a**), this facies has a holocrystalline, porphyritic texture of medium to coarse grain size. It is formed mainly by K-feldspar and plagioclase phenocrysts, with K-feldspar, quartz, plagioclase and abundant biotite in the matrix. Accessory minerals are muscovite, apatite, titanite, zircon, and undifferentiated opaque minerals.

The 0.5 to 1 cm phenocrysts are microperthite, and are subhedral with irregular rims and inclusions of euhedral plagioclase, quartz, biotite and muscovite; some K-feldspar is slightly altered to sericite and other phyllosilicate. The plagioclase phenocrysts (1-4 mm) are oligoclase to andesine (by the Michael-Levy method) and are overgrown by K-feldspar; other phenocrysts are zoned. Some quartz has undulous extinction and forms triple points in the matrix, owing to the occasionally observed ductile foliation. Biotite crystals are subhedral, frequently forming assemblages with zircon and titanite. Muscovite is subhedral and occurs as fine-grained aggregates (**Fig. 5a**).

Geocronologia e isotopia do magmatismo paleozoico na zona de Diablillos, borda oriental da Puna austral (NW da Argentina): Evolução crustal do orôgeno paleozoico inferior na margem ocidental de Gondwana

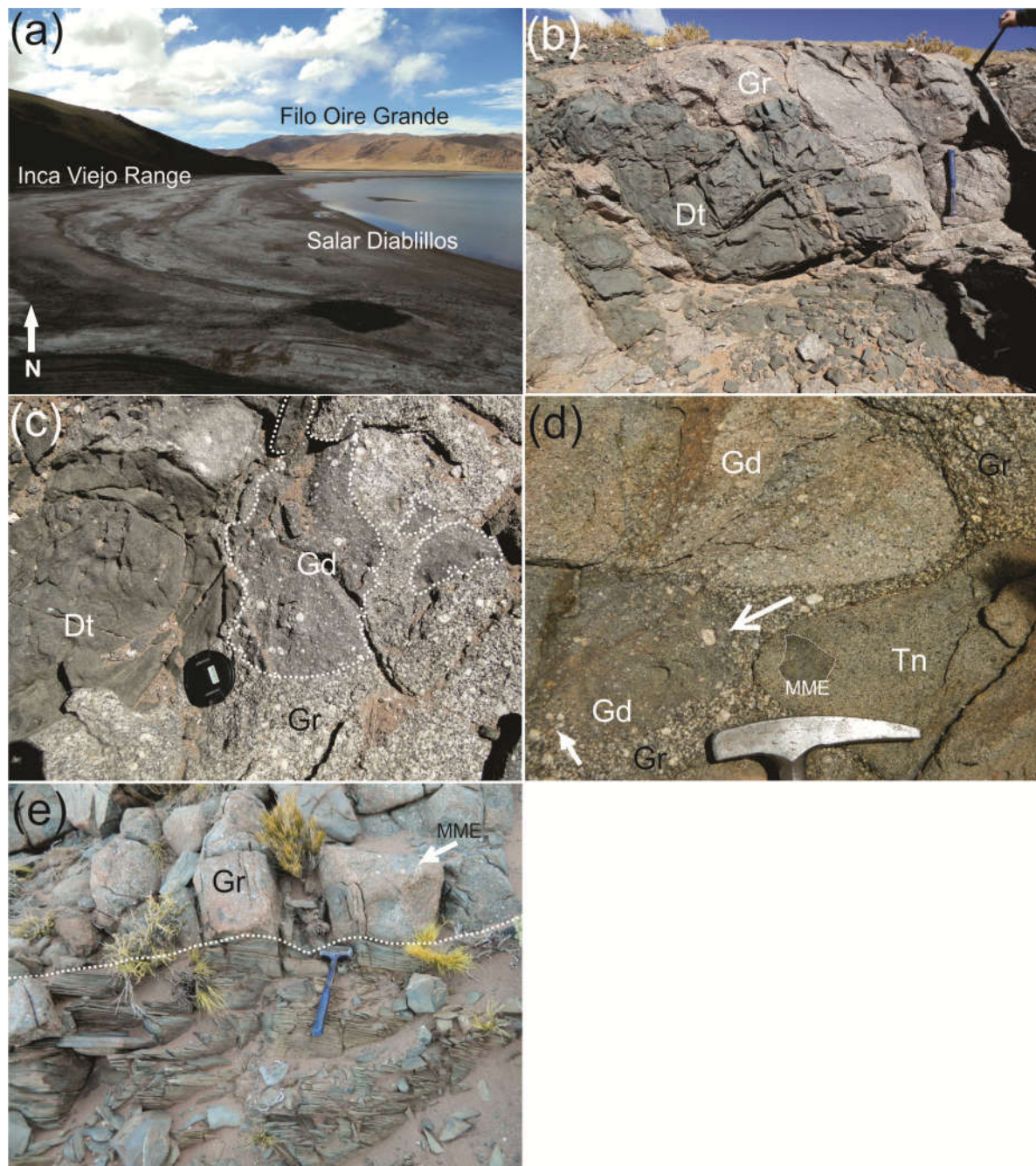


Fig. 3: (a) Panoramic view of the Diablillos salar and the Inca Viejo Range. (b) Contact relationship between a porphyritic monzogranite and parts of a mafic dismembered body. Hammer is 40 cm long. (c) Contact relationships between a porphyritic monzogranite, a granodiorite enclave, and a mafic dismembered body. White dotted lines delimit granodiorite enclave with K-feldspar phenocrysts. Black cover lens is 4 cm in diameter. (d) Field image showing the transitional contact between the monzogranite and the granodiorite

facies, and a contact with a tonalite enclave. Black arrows show K-feldspar phenocrysts that migrated from the monzogranite to the granodiorite. Note the MME included into the tonalite enclave. (e) Intrusive contact, delimited with a white dotted line, between the monzogranite and slates from the Rio Blanco Metamorphic Complex. Hammer is 40 cm long. Dt: Diorite. Gr: Monzogranite. Gd: Granodiorite. Tn: Tonalite.

Granodiorite facies: This unit, together with the tonalite facies, is the most widespread unit in the Inca Viejo Range, occurring over an area ~7 km long and 2 km wide. The granodiorite facies has dark to light grey color, crops out on the mid-eastern side of the range, has a transitional contact with the monzogranite facies to the east, and is intercalated with the tonalite facies to the west. On the northeastern side of the range, the granodiorite facies intrudes pyllites, slates and mottled slates of the Rio Blanco Metamorphic Complex.

The granodiorite facies is porphyritic. It is characterized by blue quartz and subhedral (subrounded) K-feldspar and plagioclase phenocrysts (up to 2 cm in size) (**Fig. 3c, d**). They are immersed in a medium- to fine-grained matrix composed of the same minerals plus biotite. Abundant concentrations of MME (similar to those in the monzogranite) of 7 to 50 cm size, with sharp to transitional contacts were observed in some parts of the granodiorite (**Fig. 3c**). Also, tonalite enclaves and minor meta-wacke xenoliths (probably from the Rio Blanco Metamorphic Complex) were identified occasionally.

The modal composition shown in **Fig. 4** classifies sample D-13-02 as a granodiorite with ~40 vol.% plagioclase, ~35 vol.% K-feldspar, and ~25 vol.% quartz. At the microscopic scale, the granodiorite facies (**Fig. 5b**) has a holocrystalline porphyritic texture with plagioclase, microcline and quartz as phenocrysts. The matrix is formed by medium- to fine-grained quartz, plagioclase, K-feldspar, abundant biotite, and muscovite. Accessory minerals are zircon, titanite, apatite, and opaques.

Phenocrysts of K-feldspar (microcline, 0.5-1 cm) are surrounded by and have in their cores and along their rims inclusions of euhedral plagioclase, quartz and biotite. Some K-feldspar and plagioclase are altered to sericite in their cores (**Fig. 5b**). In some cases, these K-feldspar phenocrysts have a plagioclase rim defining a rapakivi texture, typically formed in a magma mixing environment (**Hibbard, 1991**). The plagioclase phenocrysts (0.2-1 cm) are subhedral. Less frequently, zoned plagioclase phenocrysts are mantled with biotite and overgrown by plagioclase. The quartz phenocrysts (4 cm) are subrounded and

Geocronologia e isotopia do magmatismo paleozoico na zona de Diablillos, borda oriental da Puna austral (NW da Argentina): Evolução crustal do orôgeno paleozoico inferior na margem ocidental de Gondwana

some are closely aggregated with matrix. Biotite is abundant; ilmenite crystals may be partially replaced by titanite along the rims.

Tonalite facies: This facies was mapped together with the Granodiorite facies due to their close relationship (**Suzaño et al., 2015**). The tonalite facies crops out on the top of the Inca Viejo Range. It forms a ~50-70 m wide continuous body, in gradational contact with the granodiorite facies to the east. It has a dark grey color and varies from equigranular and fine-grained to slightly porphyritic, with quartz (2 cm) and plagioclase (2-2.5 cm) phenocrysts. The matrix is composed of plagioclase, quartz, and abundant biotite. This facies also has MME (less than 2 m wide) with sharp contacts (**Fig. 3d**), small granodiorite enclaves (5-7 cm), and some cross-cutting, small (<30 cm) pegmatite dykes.

The modal composition shown in **Fig. 4** classifies sample D-13-15 as a tonalite with ~48 vol.% plagioclase, ~24 vol.% K-feldspar, and ~28 vol.% quartz. In thin section, the tonalite facies (**Fig. 5c**) is porphyritic to equigranular, with some small (3 mm) plagioclase phenocrysts. The matrix has medium- to fine grain size and is composed of plagioclase, poikilitic quartz, and abundant biotite; accessory minerals are zircon, apatite, and opaques.

Some plagioclase phenocrysts have a biotite rim and may carry biotite inclusions (**Fig. 5c**); some plagioclase phenocrysts are slightly altered to sericite. Biotite, in some instances, forms crystal aggregates with opaque minerals and has euhedral epidote inclusions. The poikilitic quartz has inclusions of plagioclase, biotite (**Fig. 5c**), acicular apatite, fine grained epidote, and amphibole.

Diorite facies represents the least widespread unit in the complex; it is distributed as dismembered bodies and as MME in the monzogranite, granodiorite and tonalite facies. On the eastern side of the range, it crops out as globular bodies up to 200 m wide and 400 m long (**Fig. 2**). At the southern edge of the range diorite occurs as dismembered bodies and MME.

This facies has a dark green color, with a fine-grained, equigranular to porphyritic texture. It has mantled plagioclase phenocrysts up to 1 cm in size, and blue ocelli pheno-xenocrysts of quartz immersed in an aphanitic, dark green matrix. The contacts with the

monzogranite facies are sharp, but with the granodiorite and tonalite facies they are transitional and lobate. There are places where the diorites have monzogranite enclaves with sharp contacts and irregular or tabular shapes (up to 1 m size) (**Fig. 3b, c**).

The modal composition for sample D-13-40 is ~96.5 vol.% plagioclase, ~1.4 vol.% K-feldspar, and ~2.1 vol.% Quartz, which allows to classify (**Fig. 4**). The very fine grained matrix is composed of plagioclase, amphibole, quartz, biotite, apatite, epidote and opaque minerals (**Fig. 5d**). Several disequilibrium features are observed in the plagioclase, such as individual crystals with poikilitic texture, zoned crystals with polysynthetic twinning, and porphyritic agglomerates with quartz exsolution (**Fig. 5d**). Some plagioclase phenocrysts have hornblende rims, and some of these rims are altered to biotite. The quartz phenocrysts are rare, anhedral, and surrounded; others have reaction rims displaying hornblende and biotite along grain margins.

Basic dyke facies: On the northwestern side of the Inca Viejo Range, thick (40 m) basic dykes crop out. These concordant dykes intrude the monzogranite facies of the CID and the medium grade metamorphic rocks along a NE-SW strike. In addition, this facies intrudes the granitic facies of the CEO in the southern Filo de Oire Grande, east of the range (**Fig. 2**). The dykes have fine-grained, equigranular to porphyritic textures with plagioclase phenocrysts in a fine-grained, dark green matrix.

The monzogranites and the mafic bodies are intruded by syn-magmatic concordant and discordant tabular pegmatite dykes (<2m wide), that are composed of K-feldspar, quartz, muscovite, tourmaline and epidote. Both dyke types –diorite and pegmatite varieties- represent later stages of the magmatic event of the CID (**Suzaño et al., 2015**).

Geocronologia e isotopia do magmatismo paleozoico na zona de Diablillos, borda oriental da Puna austral (NW da Argentina): Evolução crustal do orôgeno paleozoico inferior na margem ocidental de Gondwana

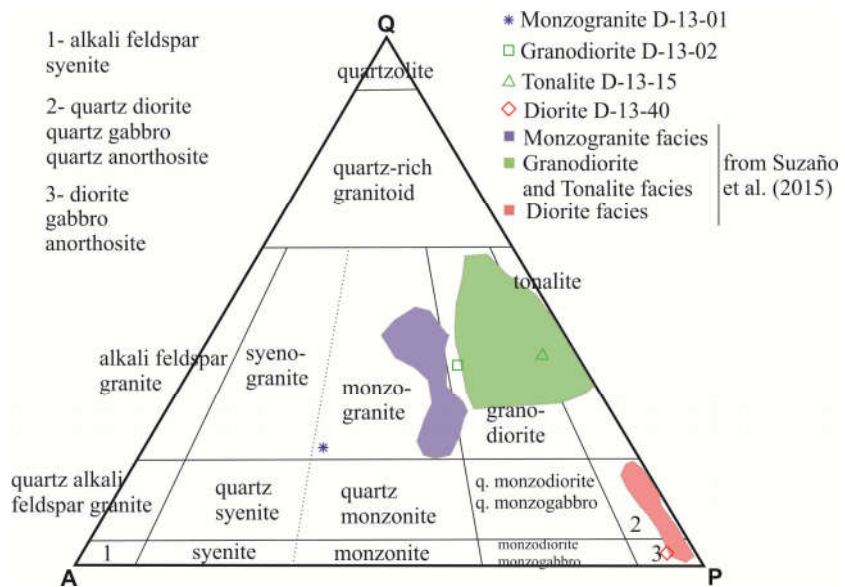


Fig. 4: Q-A-P diagram showing the modal classification of the analyzed samples from the CID, in comparison with the samples from **Suzaño et al. (2015)**. The modal classification was made by counting approximately 800 points in a thin section, for the four analyzed samples.

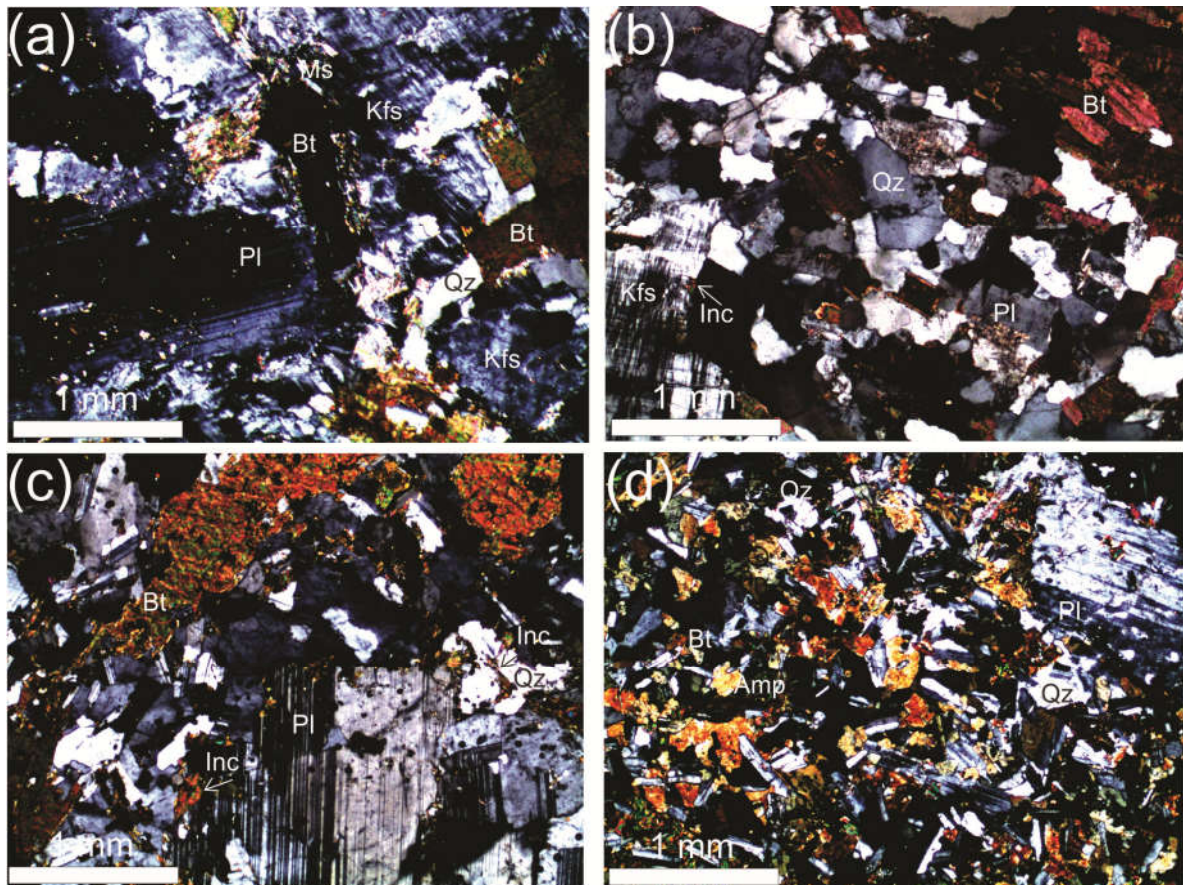


Fig. 5: Microphotographs of the facies of the Diablillos Intrusive Complex. **(a)** Monzogranite facies (sample D-13-01) with holocrystalline porphyritic texture. It is composed mainly of K-feldspar (Kfs) and plagioclase (Pl) phenocrysts, and the matrix is composed of Kfs, quartz (Qz), and Pl. **(b)** Granodiorite facies (sample D-13-02). Holocrystalline porphyritic texture with Pl, Kfs and Qz phenocrysts. The matrix is formed by fine- to medium-grained Qz, Pl, Kfs. Biotite (Bt) is abundant. The microcline phenocrysts have Bt inclusions (Inc) along the rims. **(c)** Tonalite facies (sample D-13-15) showing porphyritic to equigranular textures. Some Pl phenocrysts have a rim of Bt as well as Bt inclusions (Inc). Poikilitic Qz with inclusions of Bt (Inc) is shown. **(d)** Porphyritic diorite with Pl phenocrysts (sample D-13-40). The fine-grained matrix is formed by Pl, amphibole (Amp), Bt and Qz. All images taken in cross-polarized light. Mineral abbreviations after **Whitney and Evans (2010)**. Kfs: K-feldspar. Pl: Plagioclase. Qz: Quartz. Bt: Biotite. Ms: Muscovite. Amp: Amphibole.

3. Analytical Procedures

3.1. Geochemical analyses

Sample preparation for major and trace element analyses was performed at the Geochemistry Laboratory of Geonorte Institute, Salta National University, Argentina. This consisted of washing of the field samples, cutting off weathered and veined portions, crushing, quartering, sieving, and grinding the samples with a Herzog mill with oscillatory rings of tungsten carbide. Major elements, Ni and Sc (ppm) were analyzed by ICP-OES and trace element analyses were carried out by ICP-MS at the ACME Laboratories in Canada (**Table 1**). For information about standards, limits of detection, etc., refer to <http://acmelab.com/services/>.

3.2. U-Pb and Lu-Hf isotope analytical procedures

After crushing, grinding and panning of approximately 5 kg of each of the selected samples zircon concentrates were extracted with a Frantz isodynamic separator at the Geochemistry Laboratory in the Geonorte Institute, Salta National University, Argentina. Final purification was achieved by hand-picking using a binocular microscope at the Geochronology Laboratory of the University of Brasilia, Brazil. Zircon was hand-picked with an acupuncture needle and mounted on a glass wafer covered with a double sided sticky tape in order to secure the grains. Then a 9 mm plastic ring was placed around the zircon grains and filled with epoxy+hardener. After a day, once the resin was dry, the mounts were removed from the tape. Finally, mounts were polished to expose zircon surfaces. In order to target zircon grains, cathodoluminescence (CL) images were obtained with a JEOL Quantas 450 Scanning Electron Microscope at the same facility. The grains were polished and cleaned with 3% nitric acid.

U-Pb and Lu-Hf analyses were performed on zircon grains from three selected samples, using a Thermo-Fisher Neptune MC-ICP-MS coupled with a Nd:YAG UP213 New Wave laser ablation system, in the Laboratory of Geochronology at the University of Brasilia. For

the U-Pb analyses (**Table 2**) the diameter of the laser spot beam was 30 μm . A frequency of 7 Hz was used, at 80% energy and 40 counts per second. GJ-1 zircons were used as standards to normalize isotopic fractionation during isotope analyses. To monitor precision and accuracy over the course of this study the TEMORA reference zircon was measured as an unknown. Common lead ^{204}Pb was monitored using the ^{202}Hg and ($^{204}\text{Hg}+^{204}\text{Pb}$) masses. In all analyzed zircon grains the common Pb correction, commonly calculated following **Stacey and Kramers (1975)**, was not necessary due to the very low signal of mass ^{204}Pb (< 30 cps) and high $^{206}\text{Pb}/^{204}\text{Pb}$. Reported errors are propagated by quadratic addition $[(2SD^2 + 2SE^2)^{1/2}]$ of external reproducibility and within-run precision. The external reproducibility is represented by the standard deviation (SD) obtained from repeated analyses ($n = 20$, ~1.1 % for $^{207}\text{Pb}/^{206}\text{Pb}$ and up to ~2 % for $^{206}\text{Pb}/^{238}\text{U}$) of the standard zircon GJ-1, performed during the analytical session, and the within-run precision is the standard error (SE) calculated for each analysis. During the analytical sessions the zircon standard TEMORA was also analyzed as an unknown in order to monitor accuracy and precision during the analyses. Concordia diagrams (2σ error ellipses), Concordia ages and upper intercept ages were calculated using the Isoplot/Ex software (**Ludwig, 2003**). The U-Pb analyses on zircon grains were carried out using the standard-sample bracketing method (**Albarède et al., 2004**) using the GJ-1 standard zircon in order to quantify the amount of ICP-MS fractionation. Two to four unknowns were analyzed between GJ-1 analyses and $^{206}\text{Pb}/^{207}\text{Pb}$ and $^{206}\text{Pb}/^{238}\text{U}$ ratios were time corrected. On smaller zircon grains single spot laser induced fractionation of the $^{206}\text{Pb}/^{238}\text{U}$ ratio was corrected using the linear regression method (**Košler et al., 2002**). The raw data were processed off-line and reduced using an Excel worksheet (**Buhn et al., 2009**). A full description of the methods and procedures is given by **Buhn et al. (2009)**.

Lu-Hf isotopes (**Table 3**) were analyzed on selected zircon grains previously analyzed for U-Pb isotopes. When possible, the two spot analyses were as close as possible in order to analyze portions of the zircon grain with the same U and Pb isotopic characteristics. Lu-Hf isotopic data were collected during 40-50 seconds of ablation time and with a 40 μm diameter spot size at 85% energy. The signals of the interference-free isotopes ^{171}Yb , ^{173}Yb and ^{175}Lu were monitored during analysis in order to correct for isobaric interferences of ^{176}Yb and ^{176}Lu on the ^{176}Hf signal. The ^{176}Yb and ^{176}Lu

Geocronologia e isotopia do magmatismo paleozoico na zona de Diablillos, borda oriental da Puna austral (NW da Argentina): Evolução crustal do orôgeno paleozoico inferior na margem ocidental de Gondwana

contribution was calculated using the isotopic abundances of Lu and Hf proposed by **Chu et al. (2002)**. The contemporaneous measurements of ^{171}Yb and ^{173}Yb provide a method to correct for mass-bias of Yb using a $^{173}\text{Yb}/^{171}\text{Yb}$ normalization factor of 1.132685 (**Chu et al., 2002**). Hf isotope ratios were normalized to the $^{179}\text{Hf}/^{177}\text{Hf}$ value of 0.7325 (**Patchett, 1983**). A detailed description of the procedures and methods is given by **Matteini et al. (2010)**.

The $\varepsilon_{\text{Hf}}(t)$ values were calculated using the decay constant $\lambda=1.865*10^{-11}$ proposed by **Scherer et al. (2006)**, and the $^{176}\text{Lu}/^{177}\text{Hf}$ and $^{176}\text{Hf}/^{177}\text{Hf}$ CHUR values of 0.0332 and 0.282772 proposed by **Blichert-Toft and Albarède (1997)**. A two-stage T_{DM} age was calculated from the initial Hf isotopic composition of the zircon, using an average crustal Lu/Hf ratio (**Gerdes and Zeh, 2009; Nebel et al., 2007**). The initial Hf composition of zircon represents the $^{176}\text{Hf}/^{177}\text{Hf}$ value calculated at the time of zircon crystallization, namely the U-Pb age, possibly concordant, previously obtained on the same crystal. The two-stage depleted mantle Hf model ages ($T_{\text{DM}} \text{ Hf}$) were calculated using $^{176}\text{Lu}/^{177}\text{Hf}=0.0384$ and $^{176}\text{Hf}/^{177}\text{Hf}=0.28325$ for the depleted mantle (**Chauvel and Blichert-Toft, 2001**) and $^{176}\text{Lu}/^{177}\text{Hf}$ value of 0.0113 for the average crust (**Taylor and McLennan, 1985; Wedepohl, 1995**). Before Hf isotope measurements on zircon, replicate analyses of 200 ppb Hf JMC 475 standard solution doped with Yb (Yb/Hf=0.02) were carried out ($^{176}\text{Hf}/^{177}\text{Hf}=0.282162\pm13$ 2s, n=4). During the analytical session replicate analyses of GJ-1 standard zircon were done obtaining a $^{176}\text{Hf}/^{177}\text{Hf}$ ratio of 0.282006 ± 16 2 σ (n =25), in agreement with the reference value for GJ standard zircon obtained by **Morel et al. (2008)**. The ε_{Hf} values for each single grain were recalculated to the U-Pb age previously obtained on the same zircon grain. For slightly discordant analyses, the $^{206}\text{Pb}/^{238}\text{U}$ and $^{207}\text{Pb}/^{206}\text{Pb}$ ages were used for younger (<1 Ga) and older (>1 Ga) grains, respectively.

3.3. Microprobe analysis

Microprobe analysis (**Table 4**) was performed on zircon grains previously analyzed by the U-Pb laser ablation method using a JEOL JXA-8230 Superprobe at the University of Brasilia, Brazil. Concentrations for HfO₂, SiO₂, ZrO₂, Y₂O₃, UO₂ and ThO₂ were determined. The conditions for analysis included 20kV energy, and 10nÅ of current for Si, Zr and Hf, and 100nÅ for U, Th and Y. Counting times on peaks were, 10 s for Si and Zr, and 60 s for the other elements. Counting times on background were 5 s for Si and Zr, and 30 s for the other elements.

3.4. Sr-Nd isotope analytical procedures

Bulk rock Sm-Nd isotopic analysis of eight selected samples (**Table 5**) was carried out at the Geochronology Laboratory of the University of Brasília, Brazil. Sample dissolution was done in Teflon Savillex beakers or in Parr-type Teflon bombs. Sm and Nd extraction from whole-rock powders followed the technique of **Gioia and Pimentel (2000)**, in which the separation of the REE as a group using cation-exchange columns precedes reversed-phase chromatography for the separation of Sm and Nd using columns loaded with HDEHP (di-2-ethylhexyl phosphoric acid) supported on Teflon powder. We also used the RE-Spec and Ln-Spec resins for REE and Sm–Nd separation. A mixed ¹⁴⁹Sm–¹⁵⁰Nd spike was used. Sr, Sm and Nd samples were loaded onto Re filaments of a double filament assembly. Sm and Nd isotopic analyses were carried out using a Finnigan Triton mass spectrometer. Uncertainties on ⁸⁷Sr/⁸⁶Sr ratios are considered to be better than 0.01% (2σ) and uncertainties on ¹⁴⁷Sm/¹⁴⁴Nd e ¹⁴³Nd/¹⁴⁴Nd ratios are considered to be better than ± 0.05% (1σ) and ± 0.003% (1σ), respectively, based on repeated analyses of the international rock standards BCR-1 and BHVO-1. The ¹⁴³Nd/¹⁴⁴Nd ratios were normalized to a ¹⁴⁶Nd/¹⁴⁴Nd ratio of 0.7219. The Nd procedure blanks were smaller than 100 pg.

4. Results

4.1. Geochemistry

4.1.1. Major, trace and rare earth elements

Major and trace - including rare earth - element whole rock compositions of samples from the different facies of the Diablillos Intrusive Complex are shown in **Table 1**. Samples of the Oire Eruptive Complex from the Filo de Oire Grande (**Fig. 2**) were also analyzed in order to compare the characteristics between the CID and CEO described by **Becchio et al. (2011)**.

In the TAS diagram for granitoids (**Middlemost, 1994**) (**Fig. 6a**), the Monzogranite facies is represented by samples D-13-01 (CID) and CB-13-05 (CEO); the former plots into the quartz monzonite field. However, we continue to refer to this sample as monzogranite, based on its modal composition and field evidence. We assume that the low silica content shown by this sample is due to the mixed nature of samples from the CID.

The Granodiorite and Tonalite facies are represented by samples D-13-02 (granodiorite, CID) and D-13-15 (tonalite, CID) that plot into the granodiorite and tonalite fields, respectively; BA-13-07 (granodiorite, CEO) plots into the granodiorite field as well. Finally, the Diorite facies is represented by samples D-13-40 (CID), CB-13-02 (CID) and CB-13-04 (CEO), all plotting into the quartz diorite field.

In the A/CNK vs A/NK plot (**Shand, 1943**) (**Fig. 6b**) the diorites fall into the metaluminous field representing I-type rocks; in contrast, the tonalites, granodiorites and monzogranites lie in the peraluminous field representing S-type granitoids. There is one sample (D-13-15, tonalite) that falls into the metaluminous field, near the boundary to the peraluminous field. In the AFM diagram (**Irvine and Baragar, 1971**) (**Fig. 6c**), the intermediate rocks of the CID and CEO show a calk-alkaline trend, whereas the mafic rocks show a slight tendency towards a more primitive origin, with tholeiitic characteristics (sample CB-13-04, dioritic basic dyke). **Figure 6d** shows the geotectonic Rb vs Y+Nb diagram (**Pearce et al., 1984**), where the CID and CEO rocks plot into the Volcanic Arc Granite field (VAG), even though the intermediate and felsic rocks display a minor tendency towards the Within Plate Granite field (WPG).

The Harker diagrams (**Harker, 1909**) illustrate two contrasting groups (**Fig. 7**): on the one hand, the basic plutonic rocks and on the other, the intermediate plutonic rocks. Al_2O_3 contents of all samples do not vary significantly (~14 to 16 wt.%). The SiO_2 content in the diorite facies varies from ~50 to 54 wt.%; the granodiorite and tonalite facies show SiO_2 values of ~60-65 wt.%; and the monzogranite facies has ~61 to 69 wt.%. The mafic rocks have values of FeOt (~8-10 wt.%), MgO (~4-8 wt.%), CaO (~7-11 wt.%), Na_2O (~2-3 wt.%) and K_2O (~0.5-2.5 wt.%); the felsic rocks have contents of FeOt (~4-8 wt.%), MgO (~2-4 wt.%), CaO (~1.5-4 wt.%), Na_2O (~2.5-3.5 wt.%) and K_2O (~2-5 wt.%). The two main groups have regular variation trends. MgO , FeOt , TiO_2 and CaO are negatively correlated with increasing SiO_2 , whereas Na_2O and K_2O show positive correlations (**Fig. 7**).

Trace element versus silica variation diagrams (**Fig. 8**) show decreasing Sr with increasing SiO_2 , suggesting plagioclase fractionation. Rb and Ba display positive correlation trends with increasing silica. In the same way, the Zr content in the felsic rocks shows the same pattern with increasing SiO_2 due to zircon saturation. Sample CB-13-04 (Diorite basic dyke) has 94 ppm Ni and is the most primitive rock of the basic group (in the AFM diagram, **Fig. 6c**, with slight tholeiitic character).

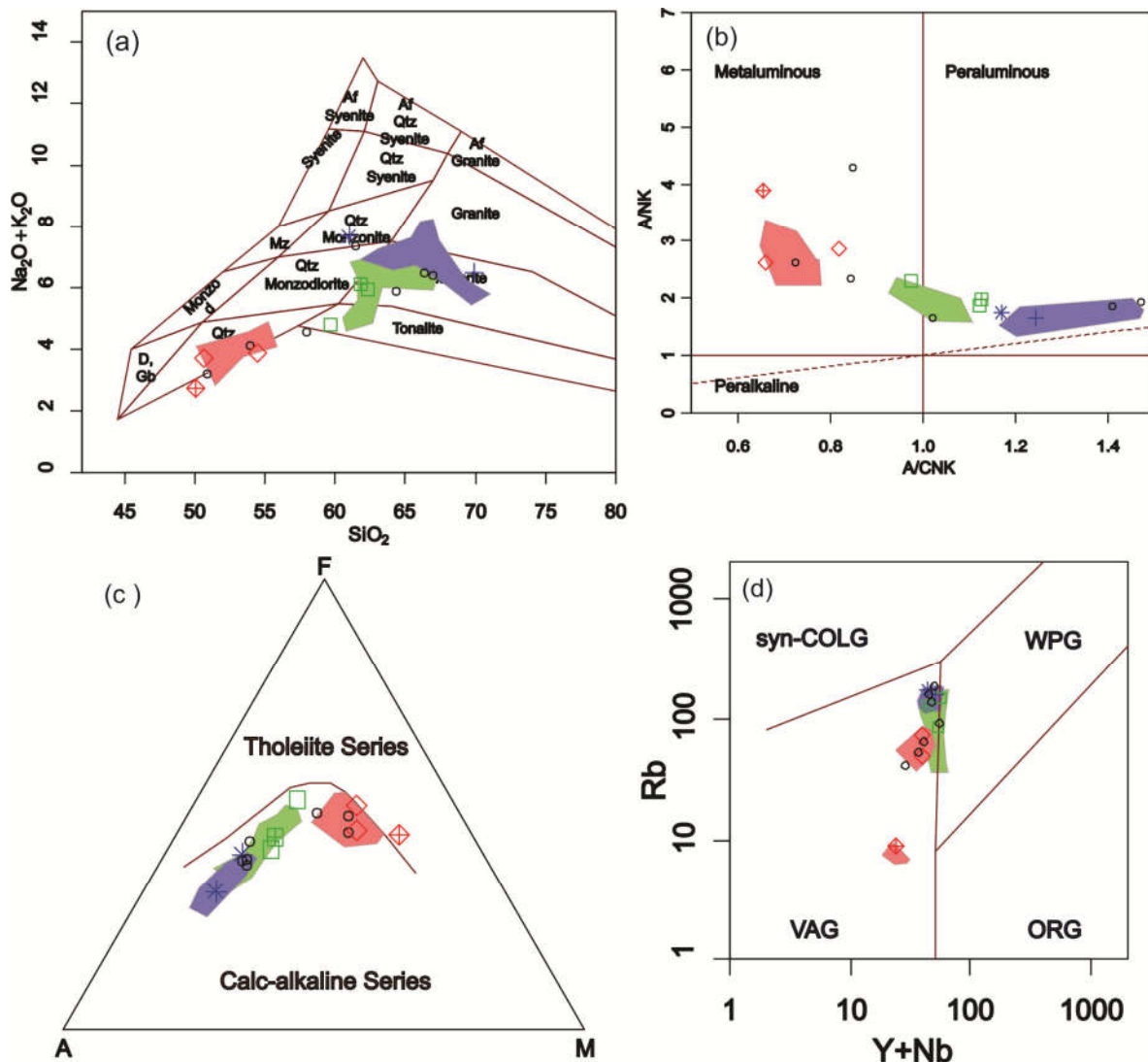
In the trace elements spider diagram (**Fig. 9a**) normalized to chondrite values (**Thompson, 1982**), the intermediate rocks show enrichment in the Large-Ion Lithophile Elements (LILE) (i.e., Ce , Rb , Th and K), compared to the basic rocks. Besides, the felsic group shows a slight depletion in High Field Strength Elements (HFSE) (i.e., Nb , P , Zr and Ti), showing crustal characteristics. Also, this group shows negative anomalies for Sr and Ba , suggesting plagioclase fractional crystallization during melting and magma evolution (**Dong et al., 2013**). In **Fig. 9a** the basic rocks show a minor depletion of LILE and strong depletion of HFSE compared to the intermediate rocks, with the exception of sample CB-13-04 (CEO, diorite basic dyke) that has a stronger depletion of the LILE and HFSE.

The chondrite-normalized REE patterns (**Fig. 9b**) for the intermediate rocks show enrichment of the LREE ($\text{LaN/YbN}=3.91 - 11.84$) and a negative slope for the HREE, compared to the basic rocks including those of **Zimmermann et al. (2014)** from the Western Magmatic Belt, with $\text{LaN/YbN}=1.62-3.67$ have a crustal signatures. In addition, the intermediate rocks display a discernible negative Eu anomaly ($\text{Eu/Eu}^*= 0.50-0.70$),

Geocronologia e isotopia do magmatismo paleozoico na zona de Diablillos, borda oriental da Puna austral (NW da Argentina): Evolução crustal do orôgeno paleozoico inferior na margem ocidental de Gondwana

indicative of plagioclase fractionation. The mafic rocks show a slight depletion of the HREE compared to the felsic rocks, and with the exception of sample CB-13-04 (CEO, diorite basic dyke), with even stronger depletion of the REE (**Fig. 9b**).

In the upper crust-normalized trace element spider diagram (**Boynton, 1984**), the mafic rocks display slightly negative patterns of the LILE (i.e., Ce, Rb, Th and K) and a slight depletion of the HFSE (i.e., Nb, Zr and Ti), compared to the patterns for the intermediate rocks, with the exception of sample CB-13-04 (CEO, diorite basic dyke), even stronger depleted compared to the felsic rocks (**Fig. 9c**).

**References:**

- ◆ Diorite (CID) ◆ Diorite (CEO) * Monzogranite (CID)
- Diorite from Suzaño et al. (2015) + Monzogranite (CEO)
- Granodiorite-tonalite (CID) ■ Monzogranite from Suzaño et al. (2015)
- Granodiorite-tonalite (CEO) ○ CID Enclaves from Suzaño et al. (2015)
- Granodiorite-tonalite from Suzaño et al. (2015)

Fig. 6: (a) Granitoid TAS diagram (Middlemost, 1994) for the various facies of the CID. Rocks are classified as granites, granodiorites, tonalities, and quartz diorites. (b) In the A/CNK vs A/NK plot (Shand, 1943) diorites fall into the metaluminous field, whereas the tonalites, granodiorites and monzogranites fall into the peraluminous field. (c) In the AFM diagram (Irvine and Baragar 1971), the CID rocks show a calk-alkaline trend. The diorites show a slight tendency towards tholeiitic characteristics. (d) Geotectonic Rb vs Y+Nb

Geocronologia e isotopia do magmatismo paleozoico na zona de Diablillos, borda oriental da Puna austral (NW da Argentina): Evolução crustal do orôgeno paleozoico inferior na margem ocidental de Gondwana

diagram (Pearce et al., 1984). The CID and CEO rocks plot in the VAG field, with a minor tendency towards the WPG field.

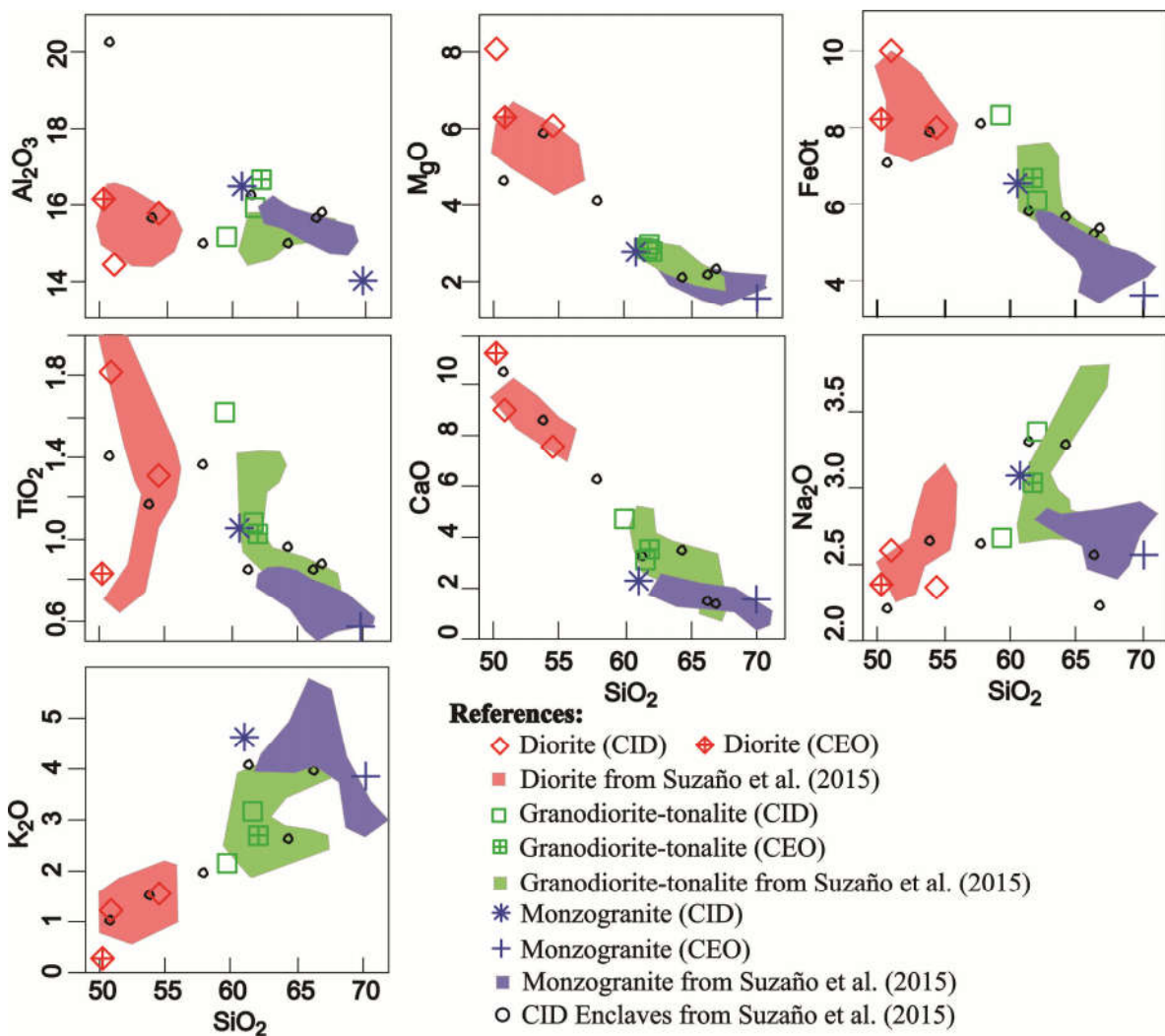


Fig. 7: Harker diagrams for the basic plutonic rocks and, the intermediate plutonic rocks. With increasing values of SiO_2 , a negative correlation trend is evidenced, for MgO , FeOt , TiO_2 and CaO , whereas the Na_2O and K_2O values show a positive correlation trend with increasing SiO_2 . Data in wt.%.

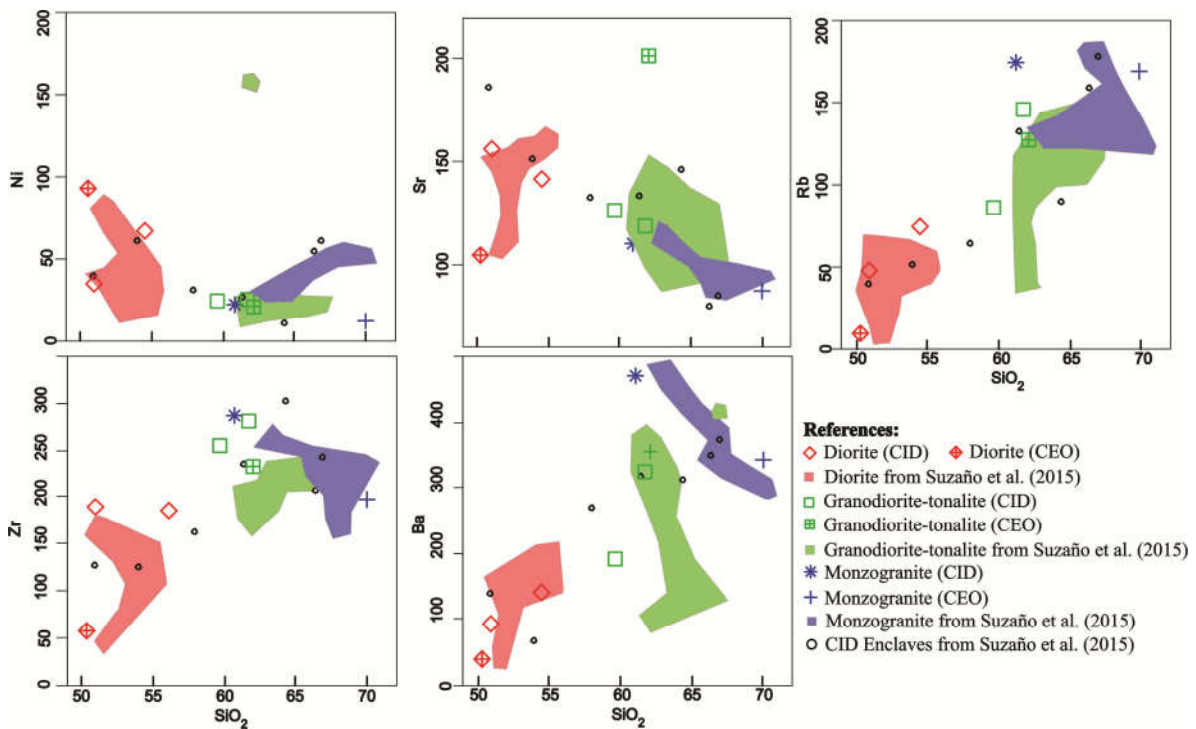


Fig. 8: Harker-style trace element variation diagrams, showing decreasing Sr with increasing SiO_2 . Rb and Ba show positive correlation trends with increasing SiO_2 . The intermediate rocks show increasing values of Zr with increasing SiO_2 . Trace element data in ppm, SiO_2 contents in wt.%.

Geocronologia e isotopía do magmatismo paleozoico na zona de Diablillos, borda oriental da Puna austral (NW da Argentina): Evolução crustal do orôgeno paleozoico inferior na margem ocidental de Gondwana

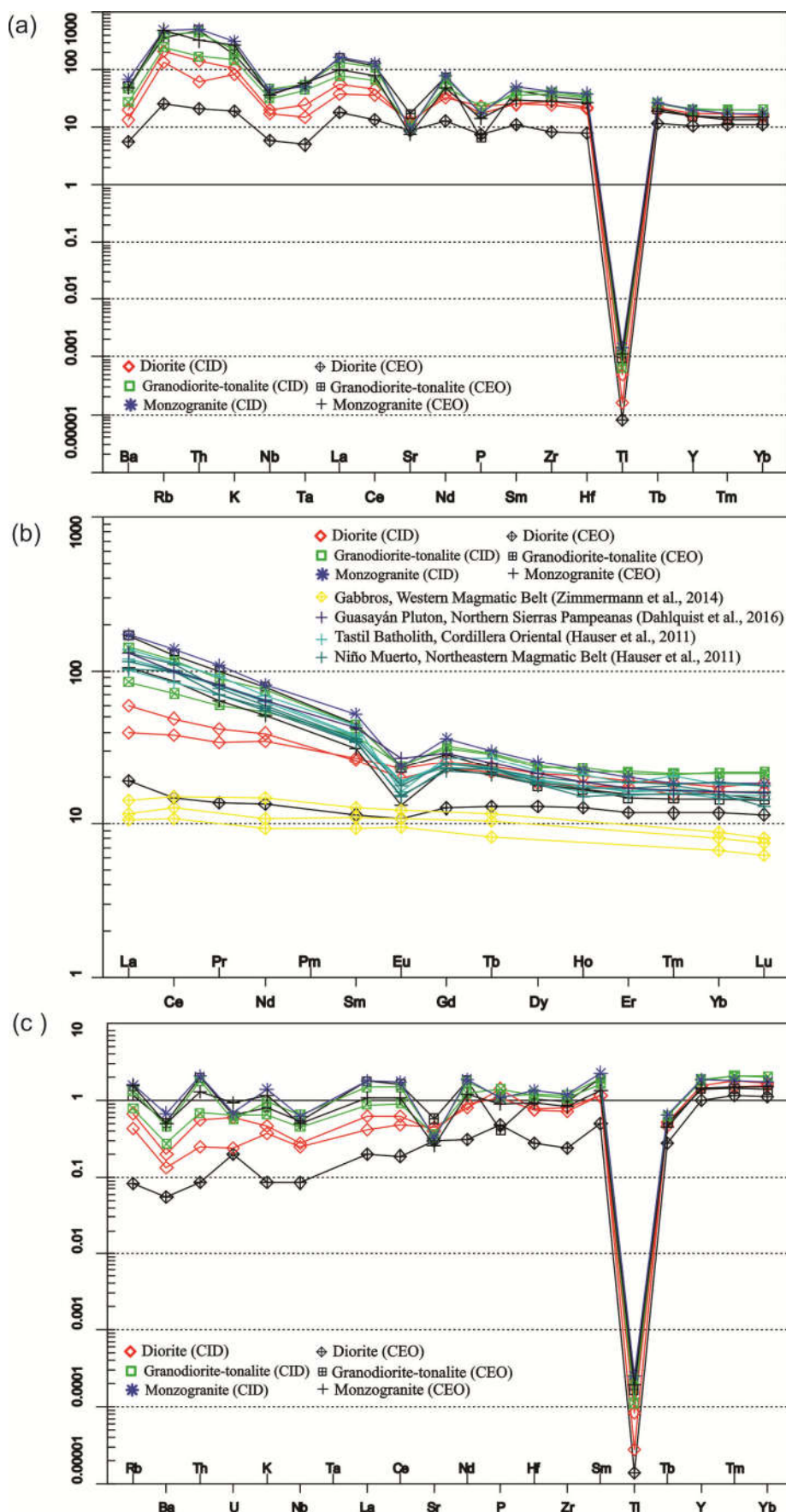


Fig. 9: (a) Chondrite-normalized trace element spider diagram (Thompson, 1982). Intermediate-felsic rocks show enrichment in the LILE compared to the basic rocks. Also, note in the more evolved group depletion in the HFSE. The basic rocks show a slight depletion in the LILE and illustrate a stronger depletion in the HFSE than the intermediate rocks. (b) REE abundances normalized to chondrite (Boynton, 1984). The intermediate rocks show enrichment of the LREE and a decreasing HREE pattern, compared to the basic rocks. Note the similarities between the CID and CEO rocks with those from the Ojo de Colorados Complex, Western Magmatic Belt (Zimmermann et al., 2014), Guasayán Pluton, Northern Sierras Pampeanas (Dahlquist et al., 2016), a Metadacite from Niño Muerto, Northeastern Magmatic Belt (Hauser et al., 2011) and the Tastil batholith, Cordillera Oriental (Hauser et al., 2011). (c) Upper crust-normalized trace element abundances (normalization after Taylor and McLennan, 1985). The mafic rocks display slightly negative patterns of the LILE and illustrate a stronger depletion in the HFSE than observed for the intermediate rocks.

4.2. Zircon U-Pb geochronology

Due to its refractory nature and low elemental diffusivity (e.g., Cherniak et al., 1997a; Cherniak et al., 1997b; Cherniak and Watson, 2003), and resulting ability to retain its compositional zoning through time and under varying conditions, zircon is invaluable for investigating the evolution of long-lived and complex silicic magmatic systems (Clairborne et al., 2010).

Three samples representing the main units of the Diablillos Intrusive Complex, namely monzogranite, granodiorite and diorite, were selected to try to determine the emplacement age of this magmatic complex.

Sample D-13-01, Monzogranite facies:

Sixty hand-picked zircon crystals were analyzed from this sample, but only fifty four were used due to their relatively better concordance fit ($100 \pm 2\%$) (Table 2). These grains have varied sizes from 150 to 300 μm and are colorless to pinkish brown. Cathodoluminescence (CL) images show that the grains have variable shapes (Fig. 10b), from elongate euhedral and subhedral, to bipyramidal to subrounded. Some grains display internal magmatic zonation, whereas others have inherited zircon cores (Fig. 10b).

Zircon grains from this sample have varied concentrations of U and Th, with Th/U ratios ranging from 0.14 to 2.0 (Table 4), which denotes a magmatic origin (Hoskin and Schaltegger, 2003).

In **Fig. 10a** the zircon data display a continuous and good concordant age distribution in the Concordia diagram (from ~490 Ma to 540 Ma), resulting in a weighted average $^{206}\text{Pb}/^{238}\text{U}$ age of 517 ± 3 Ma (inset **Fig. 10a**), which is here interpreted as the emplacement age of this facies (see Discussion below).

In addition, the Probability Density Plot (PDP, **Fig. 11a**) resolves various zircon populations with similar elongate euhedral and subhedral bipyramidal crystal shapes. The PDP displays a small, four grain population of ~490 Ma age; a major population (27 grains) of ~515-520 Ma age, a significant (13 grains) population of ~530-540 Ma age, and another (3 grains) of ~600-630 Ma age. In addition, there is a group of three zircon core analyses representing a ~1000-1100 Ma population.

Sample D-13-40, Diorite facies:

Forty seven hand-picked zircon crystals were analyzed from this sample, but only thirty data were used because of their superior concordance fit ($100 \pm 2\%$) (**Table 2**). These grains are of varied sizes from 100 to 200 μm , and are colorless to pinkish brown. In CL, the grains show different shapes (**Fig. 10d**), from elongate euhedral and subhedral bipyramidal to subrounded. Some grains have internal zonation or irregularly shaped dark cores, whereas others have inherited cores. Some grains display irregular shapes with irregularly segmented zonation (**Fig. 10d**).

Zircon grains from this sample have different concentrations of U and Th, with Th/U ratios ranging from 0.52 to 2.1 (**Table 4**), consistent with a magmatic origin as well (**Hoskin and Schaltegger, 2003**).

The analyses of the Diorite facies exhibit a continuous and concordant age distribution in the Concordia diagram from ~490 Ma to 540 Ma (**Fig. 10c**). This results in a $^{206}\text{Pb}/^{238}\text{U}$ weighted average age of 515 ± 6 Ma (inset **Fig. 10c**), which is interpreted as the emplacement age of this facies.

In the PDP (**Fig. 11b**) several zircon populations with varied ages and similar habit characteristics (elongate euhedral and subhedral bipyramidal to subrounded) are distinguished. First, a five grain population of ~490 Ma occurs; second, a large population of ~515-520 Ma ages (15 grains); a significant population of ~530-540 Ma ages (7 grains); one grain of ~630 Ma, and one at ~1100 Ma.

Sample D-13-02, Granodiorite facies:

Thirty hand-picked zircon grains were analyzed from this sample, but only fifteen data were used because of their better concordance fit ($100 \pm 5\%$) (**Table 2**). Zircon grains from this sample have varied sizes from 150 to 250 μm , and are colorless to pinkish brown. Also, CL images reveal grains with different morphologies but that are similar the geometries in the other facies (**Fig. 10f**): elongate euhedral and subhedral bipyramidal to subrounded. Some grains have internal zonation or irregularly shaped dark cores, others display irregular shapes with obliquely cut zonation (**Fig. 10f**).

Zircon grains from this sample have variable concentrations of U and Th, with Th/U ratios ranging from 0.14 to 1.2 (**Table 4**) typical for a magmatic origin (**Hoskin and Schaltegger, 2003**).

Zircon U-Pb data correspond to a $^{206}\text{Pb}/^{238}\text{U}$ Concordia age of 521 ± 4 Ma (**Fig. 10e**), assumed to be the emplacement age of this facies. As shown for the other samples, the PDP characterizes several zircon populations with similar mineral characteristics (elongate euhedral and subhedral bipiramidals). **Fig. 11c** displays two data of ~ 490 Ma age; a significant population of ~ 515 - 520 Ma ages (5 grain), a grain of ~ 540 Ma age, an older population of ~ 600 Ma (5 grain), and a single older zircon grain of ~ 1300 Ma age.

Geocronologia e isotopía do magmatismo paleozoico na zona de Diablillos, borda oriental da Puna austral (NW da Argentina): Evolução crustal do orôgeno paleozoico inferior na margem ocidental de Gondwana

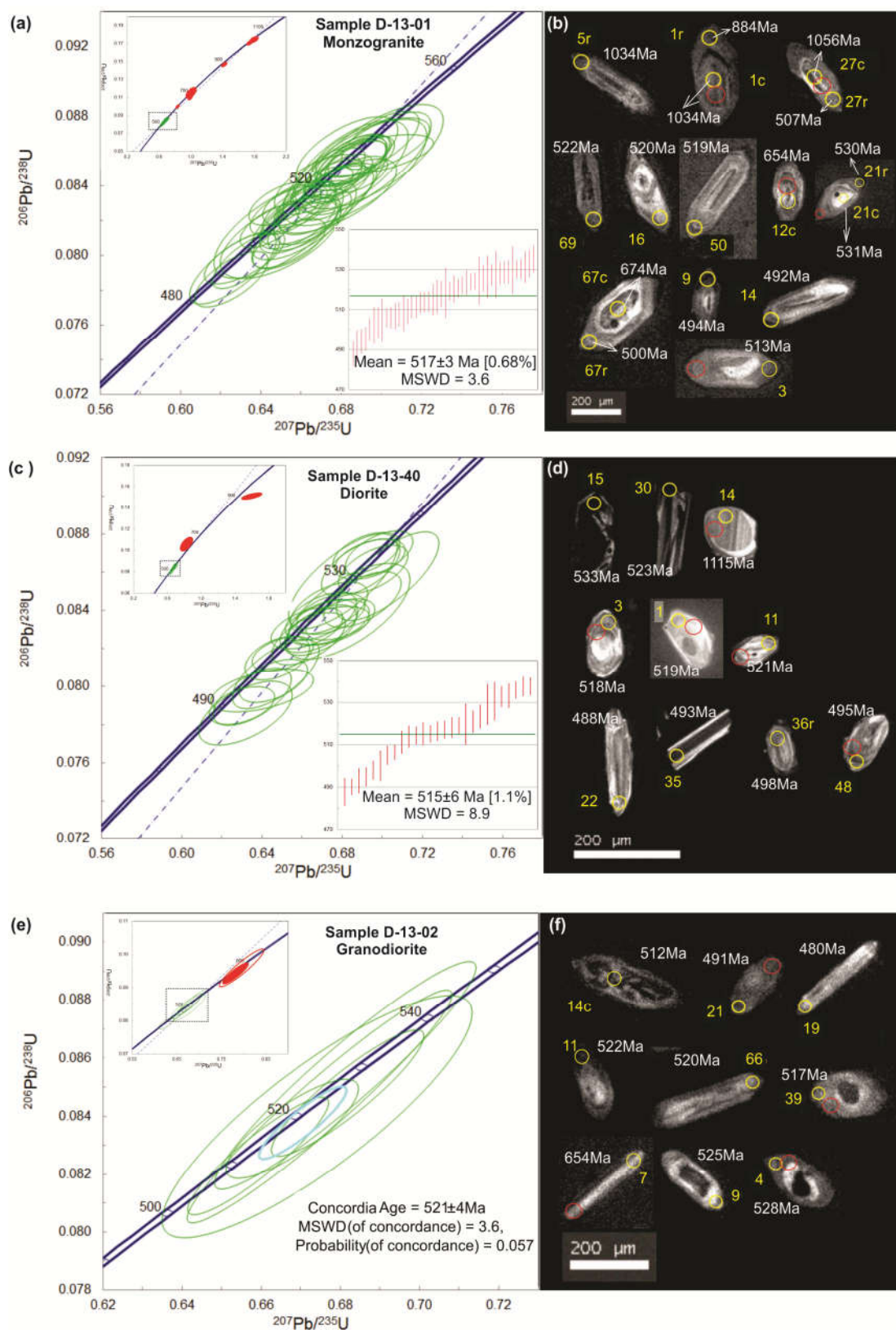


Fig. 10: (a) U-Pb isotope data. (a) Concordia diagram (Wetherill, 1956) displaying the scatter of concordant U-Pb ages for zircon from monzogranite sample D-13-01. Errors are shown as ellipses at the 1σ level. Upper left inset shows the Concordia diagram for U-Pb ratios of all zircon grains analyzed. Lower right inset shows the weighted average age diagram (data in Ma) for the monzogranite facies. (b) CL images of representative zircon crystals from the monzogranite sample. Age results are shown for the spots analyzed. (c) Concordia diagram displaying the scatter of concordant U-Pb ages for zircon from diorite sample D-13-40. Errors are shown as ellipses at the 1σ level. Upper left inset shows the Concordia diagram for U-Pb ratios of all zircon grains analyzed. Lower right inset shows the weighted average age diagram (data in Ma) for the diorite facies. (d) CL images of representative zircon crystals from the diorite sample. (e) Concordia diagram displaying the concordant U-Pb ages for zircon from granodiorite sample D-13-02. Errors are shown as ellipses at the 2σ level. Upper left inset shows the Concordia diagram for U-Pb ratios of all zircon analyses. (f) CL images of representative zircon crystals from the granodiorite sample. Note: In (b), (d), and (f), yellow circles mark the spots of U-Pb analyses. r: rim; c: core. Red circles mark the locations of Hf analyses.

Geocronologia e isotopía do magmatismo paleozoico na zona de Diablillos, borda oriental da Puna austral (NW da Argentina): Evolução crustal do orôgeno paleozoico inferior na margem ocidental de Gondwana

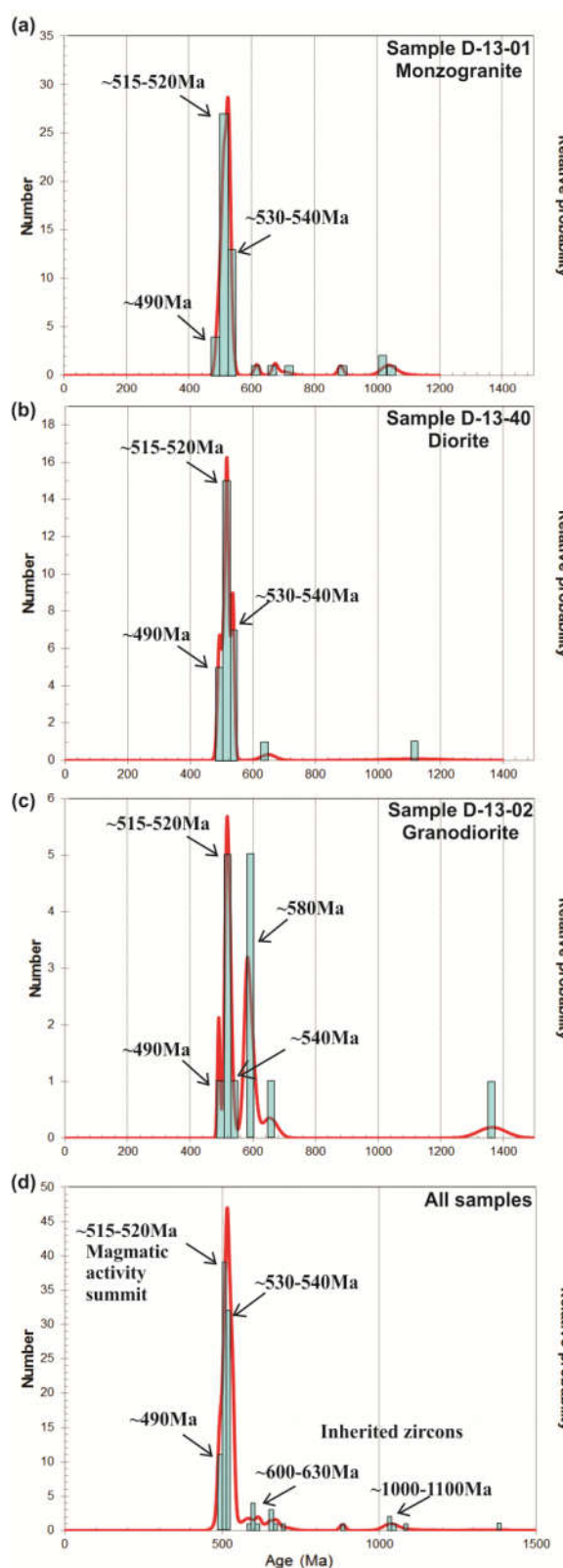


Fig. 11: Probability Density Plots. Ages for the various peak populations are given in black letters. **(a)** Monzogranite facies, **(b)** Diorite facies, and **(c)** Granodiorite facies, and **(d)** the combined data set from all three samples from the Diablillos Intrusive Complex. For explanation see text.

4.3. Lu-Hf isotope data for zircon

Hf isotopes are a useful tool for discriminating the origin of granitoids through revealing the source and nature of the protolith rocks (e.g., **Claiborne et al., 2010; Guo et al., 2007; Liu et al., 2009; Nardi et al., 2012**). This can provide important parameters for the modelling of crustal evolution (e.g., **Hawkesworth and Kemp, 2006**).

Lu-Hf analyses (**Table 3**) were performed on zircon grains previously analyzed by the U-Pb method.

Sample D-13-01, Monzogranite facies:

Eight zircon crystals with varied U-Pb ages were analyzed in this sample, showing $^{176}\text{Lu}/^{177}\text{Hf}$ and $^{176}\text{Hf}/^{177}\text{Hf}$ ratios between 0.001257 - 0.003581 and 0.282285 - 0.282465 respectively (**Table 3**).

Zircon grains with ages between ~515 to 530 Ma show Hf(t) around zero, ranging from -2.61 to +0.41 (**Fig. 12**), with Hf T_{DM} model ages between 1.5 and 1.3 Ga. Three Neoproterozoic zircon crystals with ages between 616 and 703 Mashow positive to negative Hf(t) between +1.19 (age=616 Ma) and -1.88 (age=703 Ma) with Hf T_{DM} model ages between 1.39 and 1.60 Ga. Two zircon cores with Mesoproterozoic ages (1034 and 1056 Ma) gave positive Hf(t) values of 7.02 and 5.9 (**Fig. 12a**), with Hf T_{DM} model ages between 1.3 and 1.5 Ga.

Sample D-13-40, Diorite facies:

Eight zircon crystals with varied U-Pb ages were analyzed in this sample, yielding $^{176}\text{Lu}/^{177}\text{Hf}$ ratios between 0.001075 - 0.005571 and $^{176}\text{Hf}/^{177}\text{Hf}$ ratios between 0.282192 - 0.282706 (**Table 3**).

Zircon grains with ages between ~518 and 536 Ma show Hf(t) values from -9.51 to +9.07 (**Fig. 12**), with Hf T_{DM} model ages between 1.87 and 0.85 Ga. A younger zircon (Z48, of 495 Ma) yielded a positive Hf(t) of +2.08 and Hf T_{DM} model age of 1.21 Ga, and a zircon crystal with a Mesoproterozoic age (1115 Ma) a positive Hf(t) of +3.98 and Hf T_{DM} model age of 1.6 Ga.

Geocronologia e isotopía do magmatismo paleozoico na zona de Diablillos, borda oriental da Puna austral (NW da Argentina): Evolução crustal do orôgeno paleozoico inferior na margem ocidental de Gondwana

Sample D-13-02, Granodiorite facies:

Eight zircon crystals with different U-Pb ages were analyzed in this sample, disregarding one analysis (Grain N° Z8c) due to an anomalous Hf(t). Otherwise, this sample yielded $^{176}\text{Lu}/^{177}\text{Hf}$ ratios of 0.000979 - 0.004253 and $^{176}\text{Hf}/^{177}\text{Hf}$ ratios of 0.282341 - 0.282536.

Zircon grains from this sample with ages between ~485 to 540 Ma show Hf(t) values from +2.1 and -2.2 (**Fig. 12**), with Hf T_{DM} model ages between 1.2 and 1.6 Ga. Also, this sample presents a negative peak Hf(t) of -3.80 (Age=538 Ma), and a positive peak Hf(t) of +4.20 (Age=654 Ma) (**Fig. 12**), and Hf T_{DM} model ages of 1.6 Ga and 1.2 Ga, respectively.

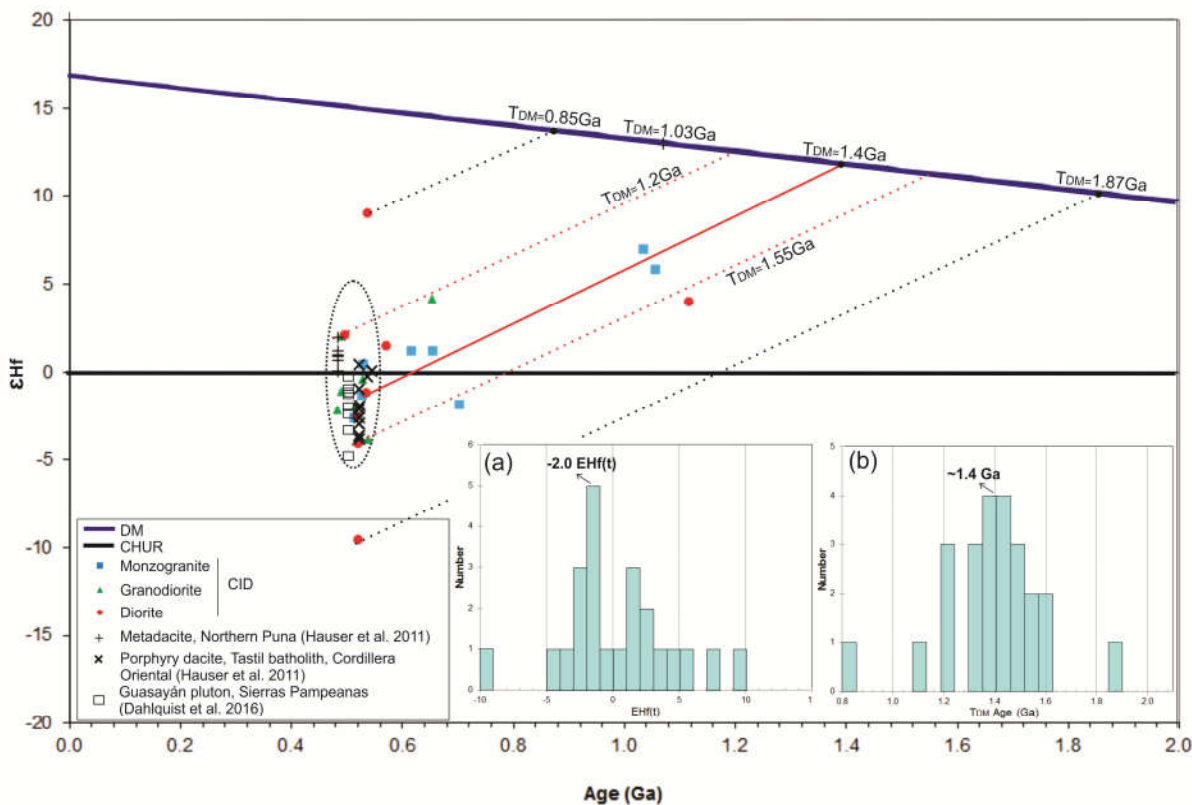


Fig. 12: Plot of $\epsilon\text{Hf}_{(t)}$ vs. U-Pb ages for zircon from the CID facies. Black dotted ellipse shows that most of the analyzed samples with ages between ~490-540 Ma are plotting near the CHUR line. The majority of the T_{DM} ages are constrained between the red dotted lines, denoting T_{DM} ages from 1.2 to 1.55 Ga. The red solid line indicates the most frequent T_{DM} observed is 1.4 Ga. For comparison, the Ordovician

metadacite $\epsilon\text{Hf(t)}$ data from the Northern Eastern Magmatic Belt, the Cambrian Tastil batolith $\epsilon\text{Hf(t)}$ data from the Cordillera Oriental (**Hauser et al., 2011**), and the data by **Dahlquist et al. (2016)** for the Cambrian Guasayán Pluton in the Sierras Pampeanas are also shown. Inset (a) Hf(t) histogram: The Hf(t) values for the selected samples range from +2.0 to -2.0, whereby the latter value is observed more frequently. Inset (b) shows a T_{DM} age histogram for the analyzed samples. The most frequent T_{DM} age for the ~490-540 Ma zircon U/Pb ages is ~1.4 Ga.

4.4. Sr-Nd isotope data

Whole-rock Sr and Nd isotope analyses (**Table 4**) were performed on eight monzogranite, granodiorite, tonalite, and diorite samples from the CID and CEO complexes (**Fig. 13**). The Sr and Nd isotopic ratios were recalculated to 518 Ma, the proposed age of emplacement.

The two monzogranites (D-13-01, CID; CB-13-05, CEO) have $^{147}\text{Sm}/^{144}\text{Nd}$ ratios of 0.12 – 0.13 and $^{143}\text{Nd}/^{144}\text{Nd}$ ratios of 0.511745 and 0.511833, respectively. The $\epsilon\text{Nd}_{(t)}$ values are -4.3 (CB-13-05) and -2.6 (D-13-01), with T_{DM} model ages of 1.6 and 1.3 Ga, respectively (**Fig. 13a**). The $^{87}\text{Sr}/^{86}\text{Sr}$ values are 0.71065 and 0.71278 (**Fig. 13b**).

The two granodiorites (D-13-02, CID; BA-13-07, CEO) and one tonalite (D-13-15, CID) sample yielded $^{147}\text{Sm}/^{144}\text{Nd}$ ratios between 0.11 and 0.15 and $^{143}\text{Nd}/^{144}\text{Nd}$ ratios of 0.511722 to 0.511860 (**Table 4**). The $\epsilon\text{Nd}_{(t)}$ values range from -4.8 (BA-13-07), over -3.4 (D-13-02), to -2.1 (D-13-15), with T_{DM} model ages of 1.38 Ga, 1.4 Ga and 1.55 Ga, respectively (**Fig. 13a**). These samples gave $^{87}\text{Sr}/^{86}\text{Sr}$ values of 0.71112 – 0.71526 (**Table 4**) (**Fig. 13b**).

The three diorites (D-13-40 and CB-13-02, CID; CB-13-04 basic dyke, CEO) yielded $^{147}\text{Sm}/^{144}\text{Nd}$ ratios between 0.15 and 0.18 and $^{143}\text{Nd}/^{144}\text{Nd}$ ratios between 0.511942 and 0.512088 (**Table 4**). These samples have $\text{Nd}_{(t)}$ values of +2.3 (CB-13-04), +1.8 (CB-13-02), and -0.5 (D-13-40), with T_{DM} model ages of 1.5 Ga, 1.3, and 1.4 Ga, respectively (**Fig. 13a**). The $^{87}\text{Sr}/^{86}\text{Sr}$ values range from 0.70446 to 0.70569 (**Table 4**) (**Fig. 13b**).

Geocronologia e isotopía do magmatismo paleozoico na zona de Diablillos, borda oriental da Puna austral (NW da Argentina): Evolução crustal do orôgeno paleozoico inferior na margem ocidental de Gondwana

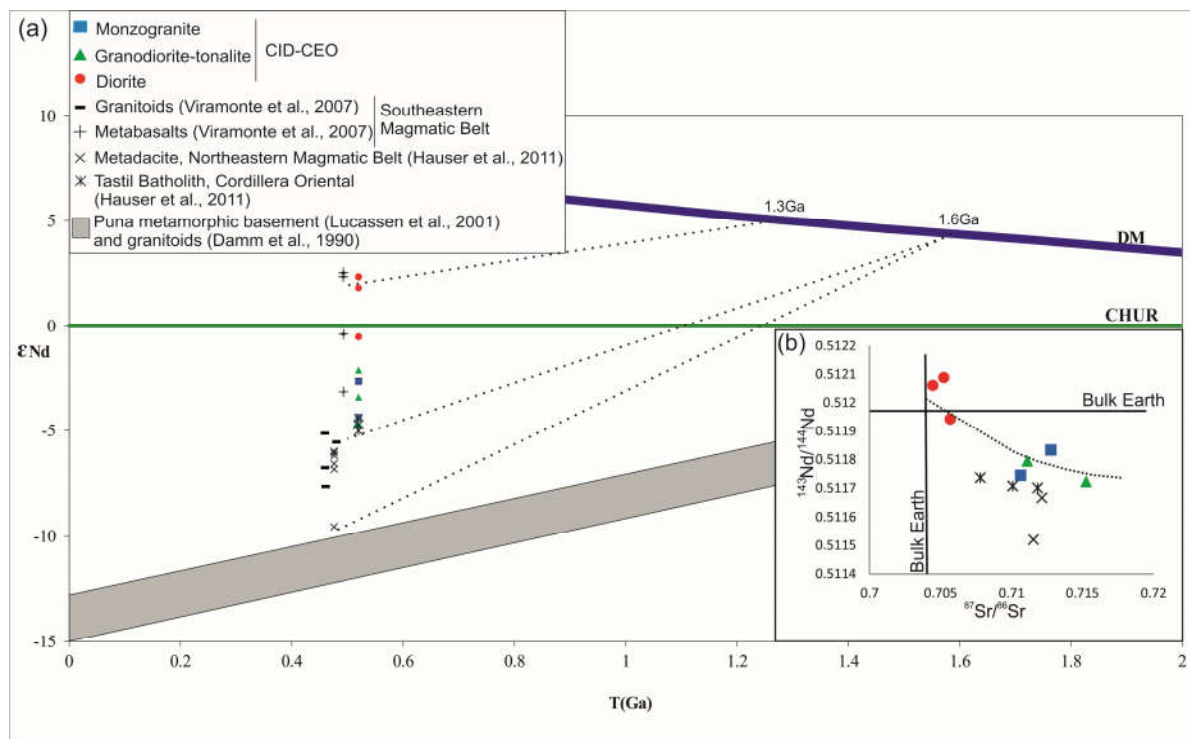


Fig. 13: (a) Nd isotope evolution diagram for the CID and CEO rocks. T_{DM} ages vary from ~1.3 to ~1.6 Ga (black dotted lines); the most frequent T_{DM} age is ~1.4 Ga. Note that the samples show similar $\text{Nd}(t)$ values and T_{DM} ages to the results from **Viramonte et al. (2007)** for the Centenario salar area, Southeastern Magmatic Belt, Puna, and to the data by **Hauser et al. (2011)** for the Northeastern Magmatic Belt, Puna and the Tastil batholith, Cordillera Oriental. (b) Nd isotopic ratios plotted versus Sr isotopic ratios for the CID and CEO rocks. There is a negative correlation trend from the basic rocks towards the felsic rocks (black dotted line). Felsic facies display similar Nd and Sr ratios to the rocks from the Cordillera Oriental and Eastern Magmatic Belt, Northern Puna (**Hauser et al., 2011**).

5. Discussion

5.1. Emplacement age of the Diablillos Intrusive Complex

A weighted average $^{206}\text{Pb}/^{238}\text{U}$ age of 517 ± 3 Ma (**Fig. 10a**) was obtained from zircon grains of the monzogranite facies (Sample D-13-01), an age of 515 ± 6 Ma (**Fig. 10c**) for the diorite facies (Sample D-13-40), and a concordant U-Pb age of 521 ± 4 Ma for the granodiorite facies (Sample D-13-02) (**Fig. 10e**). As the ages for all three samples overlap with each other within error, it is reasonable to take these results as the best current estimate of the emplacement age of this complex.

The age variations in the Concordia diagrams for the three samples (**Fig. 10a, b**) could reflect analytical scatter (**Castiñeiras et al., 2010**); but the age range is similar in the three analyzed samples regardless of during which analytical session data were acquired. No evidence for Pb loss was observed either.

Furthermore, a combination of Pb loss and inheritance of older Pb could provide a possible explanation for the age scatter (**Castiñeiras et al., 2010**). Excluding the oldest grains with comparatively higher Th/U ratios, the remaining slight variation in the Th/U ratios of the samples suggests that the inherited component involved in the analyzed zircon crystals is insignificant.

Another possibility for the observed age variation is a true difference in age, for example when a sequence of different geological processes, such as metamorphism or magmatism, occurred over a limited time span (**Castiñeiras et al., 2010**). **Hoskin and Schaltegger (2003)** concluded that zircon crystals of Th/U ratios ≥ 0.5 have a magmatic origin, whereas zircon crystals with a metamorphic origin should have Th/U ratios < 0.07 . Hence, the slight variation observed in the zircon fractionation indices in the monzogranite and granodiorite samples, namely Th/U = 0.14 to 2 (**Table 4**), suggests that zircon crystals from the CID could have developed during a combination of an igneous and a metamorphic event. Such an event combination could be correlated with the low-P/high-T metamorphic event at approximately 525-500 Ma described by **Becchio et al. (1999)** and **Lucassen et al. (2000)** for the Puna basement.

On the other hand, a long-lived magma chamber that could have given rise to the CID could also explain the age variation for these three facies, resulting in a continuous age distribution in the Concordia diagram (for instance, data obtained in samples D-13-01 and D-13-40, ranging between ~ 540 Ma - 490 Ma; **Fig. 11 a, b**). This variation would be explained by the recrystallization of older cores - not entirely crystallized, at

lower levels of the magma chamber - during the intrusion of new pulses of hot magma; or possibly the age range could result from minor mixing of new zircon crystals from newly intruded magma with older zircon cores (**Dong et al., 2013; Folkes et al., 2011; Castiñeiras et al., 2010**). Furthermore, the observed internal zonation, irregular dark cores or irregular shapes with irregular dissolution zonation displayed by some zircon grains (**Fig. 10b, d, f**), may support such mixing ideas. Such zonations may indicate periods of zircon undersaturation followed by zircon-saturation in a melt (e.g., **Vavra 1994; de la Rosa et al., 2002; Zeck and Williams, 2002**). In addition, **Hoskin and Schaltegger (2003)** concluded that such crystals preserved compositional information for the melt prior to, and after, dissolution. Consequently, they recorded a change in composition related to an event such as magma-mixing.

The meaning of this age variation could be further investigated with a more precise geochronological and isotopic study, such as SIMS whereby a smaller laser beam spot could possibly allow more accurate determination of ages, especially for zircon crystals with internal zonation. In addition, *in situ* REE analysis of zircon could provide detailed evidence for such mixing process in zircon crystals with internal zonation.

One way of comparing the individual age distributions of the three analyzed samples is **Fig. 11** with the Probability Density Plots that specify different zircon age populations. Thereby, in **Fig. 11d** the combined data base for the three facies types is considered.

Clearly, the zircon population at ~490 Ma (**Fig. 11d**) is present in the data for all three samples but the meaning of this age is unclear as the number of data for this combined population is limited (10 zircon grains). A possible interpretation could be that this age group may indicate the last magmatic activity in the complex.

The largest population at ~515-520 Ma (39 zircon minerals) (**Fig. 11d**) could represent the peak of magmatic activity related to the CID, whereas the population at ~530-540 Ma (32 zircon grains) (**Fig. 11d**) may represent zircon antecrysts (incorporated from previous crystallization events in the magmatic system, **Schmitt, 2011**). This would mean that they represent early magmatic activity in the CID.

Finally, the oldest zircon populations at ~580-600-630 and 1000-1300 Ma (**Fig. 11d**) signify inherited xenocrysts from the source rock. These data are mostly from the cores of analyzed zircon grains. These data illustrate the presence of Neo-

Mesoproterozoic sources in the region, i.e., the metasedimentary Puncoviscana Formation (Turner, 1960; Escayola et al., 2011), which has also detritic Mesoproterozoic zircon crystals.

As a result, after analyzing the age populations in the rock facies of the CID, we interpret that this Intrusive Complex was emplaced between 540-490 Ma, possibly over a ca. 50 Ma magmatic event. This emplacement would have been coeval with the low-P/high-T metamorphism event at 500-525 Ma described by **Becchio et al. (1999)** and **Lucassen et al. (2000)** in the Puna basement rocks evidenced in this case by the medium- to high-grade metamorphic rocks of the Pachamama Formation.

5.2. Magma sources for the Diablillos Intrusive Complex

5.2.1. Geochemistry and Sr-Nd isotopes

Based on field observation, petrography, and geochemistry - including Sr-Nd isotope analysis, two groups of rocks can be differentiated in the CID and CEO: the intermediate group (monzogranite, granodiorite and tonalite rocks) with silica contents between 69.99 and 59.65 wt.% and the basic group (diorites) with silica contents between 54.50 and 50.27 wt.%.

The Monzogranite and Granodiorite-Tonalite facies is enriched in LILE (i.e., Ce, Rb, Th and K), has negative anomalies of Ba, Sr, Eu compared to the Diorite facies (**Fig. 9a**), and is enriched in the LREE compared to the basic rocks (**Fig. 9b**). In the A/CNK vs. A/NK plot diagram (**Shand, 1943**) the tonalites, granodiorites and monzogranites plot in the peraluminous field (**Fig. 6b**). The geotectonic Rb vs Y+Nb diagram (**Pearce et al., 1984**) shows the felsic rocks of the CID and CEO plotting in the Volcanic Arcs Granite field. These samples show slightly negative $\epsilon_{\text{Nd}}(t)$ values, between -4.8 (Granodiorite from CEO, BA-13-07) and -2.11 (tonalite from CID, D-13-15) and initial $^{87}\text{Sr}/^{86}\text{Sr}$ values between 0.71526 (granodiorite from CEO, BA-13-07) and 0.71064 (monzogranite from CEO, CB-13-05) (**Fig. 13b**). They display T_{DM} model ages between 1.56 and 1.32 Ga (**Fig. 13a**), suggesting that a Mesoproterozoic crust was involved in the generation of these rocks. All these data together indicate that these lithologies represent S-type granitoids derived from a crustal source (**Shaw et al., 1986**).

The Diorite facies plots in the metaluminous field (**Fig. 6b**) of the A/CNK vs. A/NK diagram (**Shand, 1943**), representing I-type rocks; in the AFM diagram (**Irvine and Baragar, 1971**) (**Fig. 6c**) it shows a calc-alkaline trend, with a slight tendency

Geocronologia e isotopía do magmatismo paleozoico na zona de Diablillos, borda oriental da Puna austral (NW da Argentina): Evolução crustal do orôgeno paleozoico inferior na margem ocidental de Gondwana

towards a more primitive origin, with tholeiitic characteristics. Besides, an enrichment in incompatible elements (i.e., Ce, Rb, Th and K) (**Fig. 9a**) and a slight depletion of the HREE (**Fig. 9b**), compared to the intermediate rocks, agrees with a crust-contaminated mafic magma source origin for the basic rocks (**Kleine et al., 2004**).

Contamination of mafic magma with crust is also evident in the Sr-Nd data where the diorites show low initial $^{87}\text{Sr}/^{86}\text{Sr}$ values of 0.70446 (diorite from CID, CB-13-02) to 0.70523 (diorite from CEO, CB-13-04) (**Fig. 13b**). They also show positive to slightly negative Nd(t) values between +2.34 (diorite from CEO, CB-13-04) and -0.51 (diorite from CID, D-13-04) and Mesoproterozoic T_{DM} model ages (**Fig. 13a**). In addition, the Diorite facies is characterized in the upper crust-normalized spider diagram for trace elements (**Fig. 9c**) with slightly negative patterns compared to those of the intermediate rocks, suggesting that the Diorite facies derived from a contaminated mafic magma. With the exception of sample CB-13-04 (CEO, diorite basic dyke), with a more primitive origin as this dyke facies was recognized by **Suzaño et al. (2015)** as being related to a later stage of the evolution of the CID. Similarly these basic dykes have the same REE pattern with the gabbros from the Ojo de Colorados Complex in Western Magmatic Belt, Puna, described by **Zimmermann et al. (2014)**, which suggests the involvement of analogous mantle-derived sources.

Likewise, the negative correlation trend towards the felsic rocks (**Fig. 13b**), evidenced by the moderate to high $^{87}\text{Sr}/^{86}\text{Sr}$ and low $^{143}\text{Nd}/^{144}\text{Nd}$ ratios of the intermediate rocks, and the moderate to low $^{87}\text{Sr}/^{86}\text{Sr}$ and low $^{143}\text{Nd}/^{144}\text{Nd}$ ratios of the basic rocks from the CID, supports the magma source origin – i.e., contamination of primary magma with crustal material and suggests a magma-mixing origin of the CID. These conclusions are in agreement with field relationships and petrographic findings (**Fig. 3 and 5**), such as subrounded phenocrysts that migrated mechanically from the monzogranites to the granodiorite enclaves, subrounded K-feldspar phenocrysts, mantled and zoned plagioclase, *inter alia*.

5.2.2. Crustal evolution evidences from Hf isotopes

Zircon with a Hf isotopic composition similar to depleted mantle could not be identified; closest to this comes a zircon grain from the diorite sample with an $\text{Hf}(536)$ value of +9.07, with a T_{DM} age of 0.85 Ga (**Fig. 12**). The two Mesoproterozoic zircon cores of the monzogranite sample have juvenile magma component signatures, with

Hf(t) values of +7.02 and +5.86 and T_{DM} ages of 1.3 and 1.4 Ga, respectively (**Fig. 12**). A zircon from the granodiorite gave a Hf(654) value of +4.20 and T_{DM} age of 1.2 Ga. On the other hand, zircon minerals indicating magmas with an extensive reworked crustal source are exemplified in the diorite sample with Hf(519) of -9.51, with a T_{DM} age of 1.87 Ga, and Hf(521) of -4.09, with a T_{DM} age of 1.57 Ga, and in the granodiorite sample with a grain characterized by Hf(538) of -3.80, giving a T_{DM} age of 1.5 Ga (**Fig. 12**).

The presence of slightly positive and negative Hf(t) values between +3 and -3 (**Fig. 12**) for the three analyzed samples emplaced between ca. 490-540 Ma (**Fig. 11d**) indicates that the rocks from the Diablillos Intrusive Complex derived from an interaction of a dominant Mesoproterozoic crustal source (most frequent T_{DM} age at ~1.4 Ga) and juvenile mantle-derived magma, that were reworked during lower Paleozoic times. In addition, the Sm-Nd whole rock isotope data (**Fig. 13a**) agree with this idea, whereby similar Nd(t) (+2.5 to -4) and Nd T_{DM} model ages between 1.3 to 1.6 Ga, with a most frequently observed T_{DM} age of ~1.4 Ga, were obtained.

The zircon grain from the diorite with an Hf(536) positive value of 9.07 indicates that new juvenile magma was formed at T_{DM} of 0.85 Ga (**Fig. 12**). In the Northeastern Magmatic Belt Puna, **Hauser et al. (2011)** analyzed a Mesoproterozoic zircon grain in a metadacite, with an Hf(1070) of +13.0 value and a T_{DM} of 1.03 Ga (**Fig. 12**). Consequently, a magmatic event took place in the magmatic arc at the SW Gondwana margin between ca. 0.85 and 1.03 Ga (around the Meso/Neoproterozoic boundary). This lends further support to the models of depleted mantle evolution by **Condie et al. (2005)** and **Andersen et al. (2007)**, whereby only little evidence for juvenile magmatic rocks had been actually recognized worldwide for the ca. 1-1.20 Ga period.

The samples from the CID present similar Hf(t) and T_{DM} ages to those previously obtained for ca. 480 Ma subvolcanic rocks from the Northeastern Magmatic Belt Puna (**Hauser et al., 2011**) (**Fig. 12**). Additionally, in the Centenario salar and nearby areas (**Fig. 1**) of the Southern Puna, **Viramonte et al. (2007)** obtained whole rock Nd(t) data ranging from +2.5 to -7 and Nd (T_{DM}) ages between 1.5 to 1.7 Ga for granitoids (460-475 Ma) and metavolcanics (485 Ma) (**Fig. 13a**), similar to the Nd(t) (+2.5 to -4) and model Nd (T_{DM}) ages of this study (1.3 to 1.6 Ga) (**Fig. 13a**). Similar to

Geocronologia e isotopia do magmatismo paleozoico na zona de Diablillos, borda oriental da Puna austral (NW da Argentina): Evolução crustal do orôgeno paleozoico inferior na margem ocidental de Gondwana

the CID facies, the samples of **Viramonte et al. (2007)** have low $^{143}\text{Nd}/^{144}\text{Nd}$ isotope ratios, indicative of recycling of older crustal material without development of great volumes of new crust (**Damm et al., 1990; Becchio et al., 1999; Lucassen et al., 2000**). These similarities between the CID facies and the Centenario salar igneous rocks support the interaction of a dominant Mesoproterozoic crustal protolith and juvenile mantle-derived magmas for the evolution of the CID and magmatic complexes in the Centenario salar area in the Southeastern Magmatic Belt.

Similarly, the apparent magma source similarities shown for the Southern and Northern Puna (**Fig. 12**) indicate that the evolution of the Eastern Magmatic Belt at the SW Gondwana margin was analogous in both sectors, as already discussed by **Viramonte et al. (2007)**.

The whole rock Nd(t) (**Fig. 13a**) and zircon Hf(t) values (**Fig. 12**) presented in this study and by **Hauser et al. (2011)** and **Dahlquist et al. (2016)**, show that the interaction of a Mesoproterozoic crustal source of ~1.4 Ga and juvenile mantle-derived magmas, that were reworked during lower Paleozoic times in the Eastern Magmatic Belt, extended not only to the Cordillera Oriental geological province, east of the magmatic belt, but also to the Northern Sierras Pampeanas geological province (**Fig. 14**) south of the Eastern Magmatic Belt. Thus, this Mesoproterozoic event represents a regional episode that could be correlated with the Grenvillian/Sunsas Orogenic Belt (**Condie et al., 2005**).

5.3. Eastern Magmatic Belt, Lower Paleozoic Arc, SW Gondwana margin: A long-lived magmatic event?

The magmatic history of a continental arc can be characterized as a “punctuated equilibrium”, whereby long periods – between 30 and 50 Ma; **Ducea et al. (2015)** - of low-level activity (so-called “Lulls”) are interrupted periodically by short bursts – 5–20 Ma (**Ducea et al., 2015**) - of high-volume magmatism (so-called “Flare-ups”) (**De Silva et al., 2015**). On average, a magmatic arc enters a flare-up mode every 30–70 Ma (**De Celles et al., 2009**). One of the processes proposed to trigger this enhanced magmatic episode is repeated magmatic underplating: the intrusion of new melts generated in the mantle below and stalled in the lower crust by basalts from above the subduction zone (**Ducea et al., 2015**). The tempos of continental arc magmatism, thus, reflect

modulation of the mantle-power input as it is progressively filtered through the continental crust (**De Silva et al., 2015**).

Gehrels et al. (2009) determined that the Coast Mountain batholith at the north-western coast of North America was active nearly continuously from ca. 170 Ma to ca. 50 Ma, but that there were dramatic variations in magmatic flux during this time.

As stated in the previous section, the magma source similarities of both the Northern and Southern Magmatic Belt of the Puna, and the zircon U-Pb age ranges presented in this contribution (CID: 540-490 Ma), and in other recent studies such as that of the granitoids and metavolcanics of 485 to 460 Ma age in the Southeastern Magmatic Belt of the Puna (**Viramonte et al., 2007**). Furthermore, the ca. 480 Ma (metavolcanics, **Hauser et al., 2011**), and 469 to 445 Ma granitoids (**Bahlburg et al., 2014**) in the Northeastern Magmatic Belt of the Puna, allow us to suggest that, the magmatism in the Eastern Magmatic Belt in the Puna region represent a long-lived magmatic event. It started at ca. 540 Ma (Diablillos Intrusive Complex) and lasted till 460 Ma in the Southern Puna (Salar Centenario and nearby areas), with proven younger activity in the Northern Puna, until ca. 440 Ma (**Fig. 14, inset a**).

The mentioned episodes of low and high level magmatic activity, underline the long-lived magmatic event in the Eastern Magmatic Belt, where the early stages of ~540-530 Ma magmatism in the CID and the peak magmatic activity (~520-515 Ma) in the CID would represent a lull episode, whereas the most voluminous magmatic activity registered in the Eastern Magmatic Belt between 485-470 Ma (**Viramonte et al., 2007; Hauser et al., 2011; Bahlburg et al., 2014**) would represent a Flare-up episode (**Fig. 14, inset a**).

Zimmermann et al. (2014) presented for the Western Magmatic Belt, Southern Puna, U-Pb zircon ages for gabbroic bodies of 543 Ma (Complejo Ojo de Colorados), highlighting the early stages of the magmatic event that took place in the Southern Puna at ~540 Ma. In addition, **Dahlquist et al. (2016)** defined a ~533 Ma U-Pb age for the Guasayán Pluton in the Northern Sierras Pampeanas (near the boundary of the Puna and Cordillera Oriental, **Fig. 14, inset b**). **Aparicio González et al. (2011)** presented a ~533 Ma U-Pb age for granitic dykes in the Sierra de Mojotoro, Cordillera Oriental (**Fig. 14, inset b**), and there is the ~530 to ~515 Ma U-Pb age range by **Hauser et al. (2011)** for the Tastil batholith, Cordillera Oriental (**Fig. 14, inset b**). Furthermore, these granitoids present similar REE patterns to those of the in the Eastern Magmatic Belt (Puna), as illustrated in Fig. 9c.

Geocronologia e isotopía do magmatismo paleozoico na zona de Diablillos, borda oriental da Puna austral (NW da Argentina): Evolução crustal do orôgeno paleozoico inferior na margem ocidental de Gondwana

This evidence for a number of contiguous regions suggests that the likely long-lived magmatic event in the Eastern Magmatic Belt of the Puna, proposed in this contribution, was a regional event. It could be related to the model of **Lucassen et al. (2000)**, who proposed for the Central Andean basement an evolution in a mobile belt, where the Pampean and Famatinian cycles are not distinct events but belong to a single, non-differentiable event from ~600 to 400 Ma.

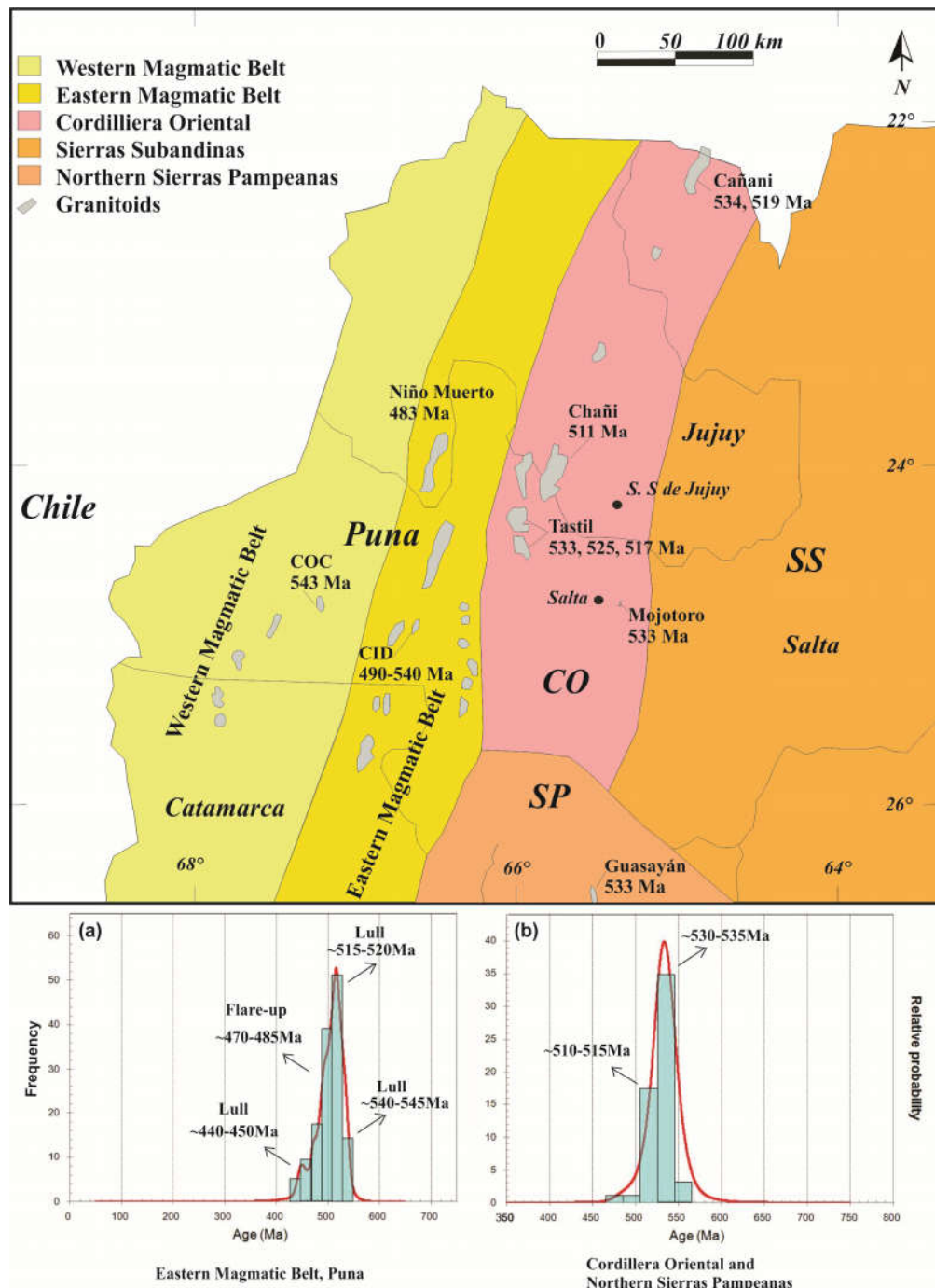


Fig. 14: Schematic map showing the main geological provinces, and sampling positions and related ages of some Lower Paleozoic granitoids in NW Argentina: the Complejo Ojo de Colorados (**Zimmermann et al., 2014**) in the Western Magmatic Belt (Puna); the Tastil batholith (**Hauser et al., 2011**), the granitic dykes in Mojotoro (**Aparicio González et al., 2011**), and the Nevado de Chañi and Cañañi granitoids (**Zapettini et al., 2008; Escayola et al., 2011**, respectively) in the Cordillera Oriental. Also shown is the Guasayán pluton in the Northern Sierras Pampeanas (**Dahlquist et al., 2016**). Inset (a) shows the Probability Density Plot illustrating zircon U-Pb ages for the Eastern Magmatic Belt (Puna), from the CID, and the North and Southeastern Magmatic Belt; data from **Viramonte et al. (2007); Hauser et al. (2011)**, and **Bahlburg et al. (2014)**. Inset (b) shows the Probability Density Plot for zircon U-Pb ages for the Cordillera Oriental and Northern Sierras Pampeanas from **Hauser et al. (2011)**, **Aparicio González et al. (2011)**, and **Dahlquist et al. (2016)**. CID: Diablillos Intrusive Complex. COC: Complejo Ojo de Colorados. CO: Cordillera Oriental. SP: Sierras Pampeanas. SS: Sierras Subandinas. Modified from **Aparicio González et al. (2011)**.

6. Conclusions

The findings reported here provide a contribution to the understanding of the magmatic activity in the Diablillos Intrusive Complex of the Eastern Magmatic Belt in the Southern Puna. The U-Pb data on zircon indicate that the emplacement of the complex took place between ~540 Ma and 490 Ma (possibly representing a ca. 50 Ma magmatic event). The main magmatic activity related to this complex was at ~515-520 Ma.

The combined major and trace, including rare earth element, data, and whole rock $^{87}\text{Sr}/^{86}\text{Sr}$ and Nd(t), as well as Hf(t) on zircon results indicate that all analyzed samples represent contaminated magmas.

The Hf(t) values of +3 and -3 and the Nd(t) values of +2.5 and -4 indicates that the facies from the Diablillos Intrusive Complex derived from an interaction of a dominant Mesoproterozoic crustal source and juvenile mantle-derived magmas - with a T_{DM} model age range of ~1.2 - 1.5 Ga - that were reworked during lower Paleozoic times.

These data, along with the whole rock Nd(t) and zircon Hf(t) values, of this study and from other authors demonstrate that the interaction of a crustal source of ~1.4 Ga and juvenile mantle-derived magmas in the Eastern Magmatic Belt is related to a similar evolution in the Cordillera Oriental and Northern Sierras Pampeanas geological provinces, emphasizing that the reworking process during lower Paleozoic times was a regional episode.

The magma source similarities and the zircon U-Pb age range presented in this contribution and in different studies of both the Northern and Southern Puna allows to propose that the Eastern Magmatic Belt in the Puna region was possibly created in a long-lived magmatic event, initiated at ca. 540 Ma with the intrusion of the Diablillos Intrusive Complex, and lasting to 460 Ma in the Southeastern Magmatic Belt of the Puna, with even younger activity in the Northern Magmatic Belt of the Puna, until ca. 440 Ma.

Further detailed study, involving additional geochronology not only on the plutonic rocks but also on the basement rocks from the study area and environs may

provide a test for the existence of such a long-lived magmatic event in the Eastern Magmatic Belt of the Puna.

7. Acknowledgements

Financial support from the CNPq program and from CONICET is acknowledged. We thank Alejandro Nieva (GEONORTE-Universidad Nacional de Salta) for help with sample preparation for chemical analysis. And we would like to thank Luciana Pereira and Bárbara Lima (Laboratório de geocronologia - Universidade de Brasília) for technical assistance with the CL imaging and isotope analyses. And we acknowledge the Rodinia Lithium-Silver Standard Company of Salta for field assistance and hospitality.

Geocronologia e isotopía do magmatismo paleozoico na zona de Diablillos, borda oriental da Puna austral (NW da Argentina): Evolução crustal do orôgeno paleozoico inferior na margem ocidental de Gondwana

CAPITULO IV

4. CONCLUSÕES

Os dados reportados neste estudo tiveram como resultado uma contribuição no entendimento da atividade magmática no Complexo Intrusivo Diablillos, Faixa Magmática Leste, Puna Sul. Os dados de U-Pb em zircão indicaram que o emprazamento do complexo teve lugar entre ~540 Ma e poderia haver durado até 490 Ma (evento magmático de ca. 50 Ma); com a maior atividade magmática do complexo aos ~515-520 Ma.

Os dados combinados de análises geoquímicas de elementos majoritários, traços e terras raras, valores de $^{87}\text{Sr}/^{86}\text{Sr}$ e Nd(t) em rocha total e Hf(t) em zircão, indicaram que as amostras analisadas representam magmas contaminados.

Os valores de Hf(t) de +3 até -3, e valores de Nd(t) +2.5 até -4, indicam que as facies do Complexo Intrusivo Diablillos derivaram de uma interação entre uma fonte crustal Mesoproterozoica e magmas juvenis -com uma idade modelo T_{DM} entre ~1.2 - 1.5 Ga- que foi retrabalhada durante o Paleozoico Inferior.

Além disso, os valores em rocha total de Nd(t) e aqueles de Hf(t) em zircão apresentados nesta contribuição e os dados apresentados por outros autores, demonstraram que a interação entre uma fonte crustal Mesoproterozoica e magmas juvenis de ~1.4 Ga na Faixa Magmática Leste, foi estendida nas províncias geológicas Cordilheira Oriental e Norte das Serras Pampeanas, com uma evolução similar, enfatizando que o evento de retrabalhamento durante tempos do Paleozoico Inferior foi regional.

As semelhanças entre as fontes magmáticas e o intervalo de idades U-Pb apresentadas neste estudo e em diferentes estudos na Puna Norte e Sul, sugerem que a Faixa Magmática Oriental na região Puna foi um evento magmático de longa duração, iniciando aos ca. 540 Ma com a intrusão do Complexo Intrusivo Diablillos até 460 Ma na Puna Sul, com idades mais jovens na Puna Norte até ca. 440 Ma.

Geocronología e isotopía do magmatismo paleozoico na zona de Diablillos, borda oriental da Puna austral (NW da Argentina): Evolución crustal do orógeno paleozoico inferior na margem occidental de Gondwana

5. REFERENCIAS BIBLIOGRÁFICAS

- Aceñolaza, F., Toselli, A., González, O. 1976. Geología de la región comprendida entre el Salar de Hombre Muerto y Antofagasta de la Sierra, Provincia de Catamarca. Revista de la Asociación Geológica Argentina 31, 127- 136.
- Aceñolaza, E.G. and Toselli, A.J. 1981. Geología del Noroeste Argentino. Universidad Nacional de Tucumán. Facultad de Ciencias Naturales. Publicación Especial 1287, 212 p. San Miguel de Tucumán.
- Albarède, F., Telouk, S., Blichert-Toft, J., Boyet, M., Agranier, A., Nelson, B., 2004. Precise and accurate isotopic measurements using multiple-collector ICPMS. *Geochimica and Cosmochimica Acta* 68 (12), 2725–2744.
- Alkmim, F.F., Marshak, S., Fonseca, M.A. 2001. Assembling West Gondwana in the Neoproterozoic: clues from the São Francisco craton region, Brazil. *Geology* 29, 319–322.
- Andersen, T., Griffin, W.L., Sylvester, A.G. 2007. Sveconorwegian crustal underplating in southwestern Fennoscandia: LAM-ICPMS U-Pb and Lu-Hf isotope evidence from granites and gneisses in Telemark, southern Norway. *Lithos* 93 (3), 273-287, doi:10.1016/j.lithos.2006.03.068.
- Aparicio González, P. A., Pimentel, M. M., Hauser, N. 2011. Datacion U-PB por LA-ICP-MS de diques graníticos del Ciclo Pampeano, Sierra de Mojotoro, Cordillera Oriental. Revista de la Asociación Geológica Argentina 68 (1), 33-38.
- Bahlburg, H., Berndt J., Gerdes, A. 2014. The ages of the Faja Eruptiva de la Puna Oriental Northwestern Argentina. Resumen. Simposio Tectónica Preandina. 19º Congreso Geológico Argentino, S21-4. Córdoba.
- Becchio, R., Lucassen, F., Kasemann, S., Franz, G., Viramonte, J.G. 1999. Geoquímica y sistemática isotópica de rocas metamórficas del Paleozoico Inferior. Noroeste de Argentina y Norte de Chile (21 - 27 S). *Acta Geológica Hispanica* 34, 273–299.
- Becchio, R., Suzaño N., Arnosio M., Nieves, A., Lopez Solano F. 2011. La mezcla de magma como proceso de diferenciación cortical durante la evolución del

- Orógeno famatiniano. Salar de Diablillos. Noroeste argentino. Actas del XVIII Congreso Geológico Argentino. Neuquén. 142-143.
- Belousova, E.A., Griffin, W.L., O'Reilly, S.Y. 2006. Zircon crystal morphology, trace element signatures and Hf isotope composition as a tool for petrogenetic modelling: examples from eastern Australian granitoids. *J. Petrol.* 47, 329–353.
- Blichert-Toft, J. and Albarède, F. 1997. The Lu–Hf isotope geochemistry of chondrites and the evolution of the mantle–crust system. *Earth and Planetary Science Letters* 148, 43–258.
- Bock, B., Bahlburg, H., Worner, G., Zimmermann, U. 2000. Tracing crustal evolution in the Southern Central Andes from late Precambrian to Permian with geochemical and Nd and Pb isotope data. *Journal of Geology* 108, 515–535.
- Boynton, W. V. 1984. Cosmochemistry of the rare earth elements: meteorite studies. In *Rare earth element geochemistry*. Vol. 2.
- Bühn, B., Pimentel, M. M., Matteini, M., Dantas, E. L. 2009. High spatial resolution analysis of Pb and U isotopes for geochronology by laser ablation multi-collector inductively coupled plasma mass spectrometry (LA-MC-ICP-MS). *Anais da Academia Brasileira de Ciências* (2009) 81(1), 99-114.
- Büttner, S.H., Glodny, J., Luccasen, F., Wemmer, K., Erdmann, S., Handler, R., Franz, G. 2005. Ordovician metamorphism and plutonism in the Sierra de Quilmes metamorphic complex: implications for the tectonic setting of the northern Sierras Pampeanas (NW Argentina). *Lithos* 83, 143–181.
- Castiñeiras, P., Díaz García, F., Gómez Barreiro, J. 2010. REE-assisted U-Pb zircon age (SHRIMP) of an anatetic granodiorite: constraints on the evolution of the A Silva granodiorite, Iberian allochthonous complexes. *Lithos* 116, 153–166.
- Castiñeiras, P., Navidad, M., Casas, J. M., Liesa, M., Carrera, J. 2011. Petrogenesis of Ordovician Magmatism in the Pyrenees (Albera and Canigó Massifs) Determined on the Basis of Zircon Minor and Trace Element Composition. *The Journal of Geology* 119, 521–534.

Geocronologia e isotopía do magmatismo paleozoico na zona de Diablillos, borda oriental da Puna austral (NW da Argentina): Evolução crustal do orôgeno paleozoico inferior na margem ocidental de Gondwana

- Chauvel, C. and Blichert-Toft, J.E. 2001. A hafnium isotope and trace element perspective on melting of the depleted mantle. *Earth and Planetary Science Letters* 190, 137– 151.
- Cherniak, D. J., Hanchar, J. M., Watson, E. B. 1997a. Rare-earth diffusion in zircon. *Chemistry Geology* 134, 289-301.
- Cherniak, D. J., Hanchar, J. M., Watson, EB. 1997b. Diffusion of tetravalent cations in zircon. *Contributions Mineral Petrology* 127, 383-390
- Cherniak, D. J. and Watson, E. B. 2003. Diffusion in zircon. In: Hanchar, J. M, Hoskin, P. W. O. (eds) *Zircon, Reviews in Mineralogy and Geochemistry* 53, 113–144. Mineralogical Society of America, Washington
- Christensen, N.I., Mooney, W.D.J. 1995. Seismic velocity structure and composition of the continental crust: a global view. *Journal of Geophysical Research* 100 (B6), 9761–9788.
- Chu, N.C., Taylor, R.N., Chavagnac, V., Nesbitt, R.W., Boella, R.M., Milton, J.A., German, C. R., Bayon, G., Burton, K. 2002. Hf isotope ratio analysis using multi-collector inductively coupled plasma mass spectrometry: an evaluation of isobaric interference corrections. *Journal of Analytical Atomic Spectrometry* 17, 1567– 1574.
- Claiborne, L.L., Miller, C.F., Wooden, J.L. 2010. Trace element composition of igneous zircon: a thermal and compositional record of the accumulation and evolution of a large silicic batholith, Spirit Mountain, Nevada. *Contrib. Mineral. Petrol.* 160, 511–531.
- Coira, B., Davidson, J., Mpodozis, C., Ramos, V. 1982. Tectonic and magmatic evolution of the Andes of northern Argentina and Chile. *Earth-Science Reviews* 18, 303–332.
- Coira, B., Perez, B., Flores, P., Kay, S., Woll, B., Hanning, M. 1999. Magmatic sources and tectonic setting of Gondwana margin Ordovician magmas, northern Puna of Argentina and Chile. In: Ramos, V.A. and Keppie, J.D. (Eds.), Laurentia-

- Gondwana Connections before Pangea: Boulder. Colorado. Geological Society of America. Special paper 336.
- Coira, B., Caffe, P., Ramirez, A., Chayle, W., Diaz, A., Rosas, S., Perez, A., Perez, B., Orosco, O., Martínez, M. 2004. Hoja Geológica Mina Pirquitas 2366-I/2166-III, (1:250.000). SEGEMAR- IGRM, Boletín 269, 1-123.
- Coira, B. 2008. Volcanismo del Paleozoico inferior de la Puna jujeña. Relatorio del XVII Congreso Geológico Argentino, capítulo 2, 140-154.
- Collo, G., Astini, R., Cawood, P.A., Buchan, C., Pimentel, M. 2009. U– Pb detrital zircon ages and Sm– Nd isotopic features in low-grade metasedimentary rocks of the Famatinia belt: implications for the late Neoproterozoic– Early Palaeozoic evolution of the proto-margin of Gondwana. Journal of the Geological Society of London 166, 303– 319.
- Condie, K.C., Beyer, E., Belousova, E., Griffin, W.L., O'Reilly, S.Y. 2005. U– Pb isotopic ages and Hf isotopic composition of single zircons: the search for juvenile Precambrian continental crust. Precambrian Research 139, 42– 100.
- Conti, C.M., Rapallini, A., Coira, B., Koukharsky, M., 1996. Paleomagnetic evidence of an early Paleozoic rotated terrane in northwest Argentina: a clue for Gondwana-Laurentia interaction? Geology 24, 953–956.
- Cordani, U.G., Teixeira, W., D'Agrella-Filho, M.S., Trindade , R.I. 2009. The position of the Amazonian Craton in supercontinents. Gondwana Research 15, 396– 407.
- Dahlquist, J. A., Verdecchia, S. O., Baldo, E. G., Basei, M. A., Alasino, P. H., Urán, G. A., Zandomeni, P. S. 2016. Early Cambrian U-Pb zircon age and Hf-isotope data from the Guasayán pluton, Sierras Pampeanas, Argentina: implications for the northwestern boundary of the Pampean arc. Andean geology, 43(1), 137-150.
- Dalziel, I.W.D. and Forsythe, R.D. 1985. Andean evolution and the terrane concept. In Howell, D. G. (Ed), Tectonostratigraphic terrains of the Circum-Pacific region: Circum- Pacific-Council for energy and Mineral Resources. Earth Science Series 1, 565–581.
- Damm, K.W., Pichowiak, S., Harmon, R.S., Todt, W., Kelley, S., Omarini, R., Niemeyer, H. 1990. Pre-Mesozoic evolution of the central Andes; The basement

Geocronologia e isotopía do magmatismo paleozoico na zona de Diablillos, borda oriental da Puna austral (NW da Argentina): Evolução crustal do orôgeno paleozoico inferior na margem ocidental de Gondwana

- revisted. In: Kay, S.M. and Rapela, C.W. (Eds.), Plutonism from Antarctica to Alaska: Boulder, Colorado, Geological Society of America. Special paper 241.
- De Celles, P.G., Ducea, M.N., Kapp, P., Zandt, G. 2009. Cyclicity in Cordilleran orogenic systems. *Nature Geoscience* 2, 251-257.
- De la Rosa, J. D., Jenner, G. A., Castro, A. 2002. A study of inherited zircons in granitoid rocks from the South Portuguese and Ossa-Morena Zones, Iberian Massif: support for the exotic origin of the South Portuguese Zone. *Tectonophysics* 352, 245-256.
- De Silva, S.L., Riggs, N.R., Barth, A.P. 2015. Quickening the pulse: fractal tempos in continental arc magmatism. *Elements* 11, 113-118.
- Dominguez, R., Becchio, R., Martino, R., Viramonte, J., Pimentel, M. 2006. El basamento ígneo metamórfico del borde occidental del salar Centenario. Petrografía y estructura. Avances en microtectónica y geología estructural. Revista de la Asociación Geológica Argentina, Serie D. I, 161 -168.
- Dong, M., Dong, G., Mo X., Santosh, M., Zhu, D., Yu, J., Nie, F., Hu, Z. 2013. Geochemistry, zircon U-Pb geochronology and Hf isotopes of granites in the Baoshan Block, Western Yunnan: Implications for Early Paleozoic evolution along the Gondwana margin. *Lithos* 179, 36–47.
- Drobe, M., de Luchi, N.L., Steenken, A., Frei, R., Naumann, R., Siegesmund, S., Wemmer, K. 2009. Provenance of the late Proterozoic to early cambrian metaclastic sediments of the Sierra de San Luis (Eastern Sierras Pampeanas) and Cordillera Oriental, Argentina. *Journal of South American Earth Sciences* 28, 239– 262.
- Ducea, M.N., Paterson, S.R., DeCelles, P.G. 2015. High-volume magmatic events in subduction systems. *Elements* 11, 99-104.
- Escayola, M.P., Pimentel, M.M., Amstrong, R. 2007. Neoproterozoic backarc basin: sensitive high-resolution ion microprobe U– Pb and Sm– Nd isotopic evidence from the Eastern Pampean Ranges, Argentina. *Geology* 35, 495– 498.

- Escayola, M. P., van Staal, C. R., Davis, W. J. 2011. The age and tectonic setting of the Puncoviscana Formation in northwestern Argentina: An accretionary complex related to Early Cambrian closure of the Puncoviscana Ocean and accretion of the Arequipa-Antofalla block. *Journal of South American Earth Sciences* 32(4), 438-459.
- Folkes, C. B., de Silva, S. L., Schmitt, A. K., Cas, R. A. F. 2011. A reconnaissance of U-Pb zircon ages in the Cerro Galán system, NWArgentina: Prolonged magma residence, crystal recycling, and crustal assimilation. *Journal of Volcanology and Geothermal Research* 206, 136–147.
- Fuck, R.A., Brito Neves, B.B., Schobbenhaus, C. 2007. Rodinia descendants in South America. *Precambrian Research* 160, 108– 126.
- Gerdes, A. and Zeh, A. 2009. Zircon formation versus zircon alteration — new insights from combined U– Pb and Lu– Hf in-situ LA– ICP-MS analyses, and consequences for the interpretation of Archean zircon from the Central Zone of the Limpopo Belt. *Chemical Geology* 261, 230– 243.
- Gehrels, G., Rusmore, M., Woodsworth, G., Crawford, M., Andronicos, C., Hollister, L., Girardi, J. 2009. U-Th-Pb geochronology of the Coast Mountains batholith in north-coastal British Columbia: Constraints on age and tectonic evolution. *Geological Society of America Bulletin* 121(9-10), 1341-1361.
- Gioia, S.M.C. and Pimentel, M. 2000. The Sm– Nd isotopic method in the Geochronology Laboratory of University of Brasilia. *Annals of the Brazilian Academy of Sciences* 2, 219– 245.
- González, O.E. 1984. Las ignimbritas «Ojo de Ratones» y sus relaciones regionales. Provincia de Salta. 9º Congreso Geológico Argentino, Actas 1, 206– 220, Buenos Aires.
- Guo, F., Fen, W. M., Li, C. W., Gao, X. F. 2007. U–Pb ages, Hf isotope and trace element compositions of captured zircons of the Paleocene adakites in the Yanji area, NE China: implications for magmatic evolution of intermediate-felsic magmas. *Acta Petrol. Sin.* 23, 413–422 (in Chinese with English abstract).
- Harker, A., 1909. *The Natural History of Igneous Rocks*. Methuen, London.

Geocronologia e isotopía do magmatismo paleozoico na zona de Diablillos, borda oriental da Puna austral (NW da Argentina): Evolução crustal do orôgeno paleozoico inferior na margem ocidental de Gondwana

- Hauser, N., Matteini, M., Omarini, R., Pimentel, M. M. 2011. Combined U–Pb and Lu–Hf isotope data on turbidites of the Paleozoic basement of NW Argentina and petrology of associated igneous rocks: Implications for the tectonic evolution of western Gondwana between 560 and 460 Ma. *Gondwana Research* 19, 100-127. doi:10.1016/j.gr.2010.04.002.
- Hawkesworth, C. J. and Kemp, A. I. S. 2006. Using hafnium and oxygen isotopes in zircons to unravel the record of crustal evolution. *Chemical Geology* 226, 144-162.
- Hibbard, M. J., 1991. Textural anatomy of twelve magma-mixed granitoid systems: Enclaves and granite petrology, Elsevier, Amsterdam, 431-444.
- Hong, F. D., and Seggiano, R. E. 2001. Hoja Geológica 2566-III., escala 1:250.000: Cachi. Provincias de Salta y Catamarca, Programa Nacional de Cartas Geológicas de la República Argentina, Servicio Geológico Minero Argentino, Boletín Nro. 548, 88pp.
- Hoskin, P. W. O. and Schaltegger, U. 2003. The composition of zircon and igneous and metamorphic petrogenesis. *Reviews in Mineralogy and Geochemistry* 53, 27–55.
- Irvine, T. and Baragar, W. 1971. A guide to the chemical classification of the common volcanic rocks. *Canadian journal of earth sciences* 8(5), 523-548.
- Kleine, T., Mezger, K., Zimmermann, U., Münker, C., Bahlburg, H. 2004. Crustal Evolution along the Early Ordovician Proto-Andean Margin of Gondwana: Trace Element and Isotope Evidence from the Complejo Igneo Pocitos (Northwest Argentina). *The Journal of geology* 112(5), 503-520.
- Košler, J., Fonneland, H., Sylves ter, P., Tubrett, M., Pedersen, R.B. 2002. U– Pb dating of detrital zircons for sediment provenance studies, a comparison of laser ablation ICP-MS and SIMS techniques. *Chemical Geology* 182, 605– 618.
- Li, H., Watanabe, K., Yonezu, K. 2014. Zircon morphology, geochronology and trace element geochemistry of the granites from the Huangshaping polymetallic deposit, South China: Implications for the magmatic evolution and mineralization processes. *Ore Geology Reviews* 60, 14–35.

- Liu, R., Zhou, H. W., Zhang, L., Zhong, Z. Q., Zeng, W. 2009. Paleoproterozoic reworking of ancient crust in the Cathaysia Block, South China: evidence from zircon trace elements, U–Pb and Lu–Hf isotopes. *Chin. Sci. Bull.* 54, 1543–1554.
- Loewy, S. L., Connelly, J. N., Dalziel, I. W. D. 2004. An orphaned basement block: the Arequipa-Antofalla Basement of the Central Andean margin of South America. *GSA Bulletin* 116 (1/2), 171–187.
- Lucassen, F., Becchio, R., Wilke, H., Franz, G., Thirwall, M., Viramonte, J.G., Wemmer, K. 2000. Proterozoic-Paleozoic development of the basement of the central andes (18–26°) a mobile belt of the South America craton. *Journal of South America Earth Science* 13, 697–715.
- Lucassen, F., Becchio, R., Harmon, R., Kasemann, S., Franz, G., Trumbull, R., Wilke, H.G., Romer, R.L., Dulski, P. 2001. Composition and density model of the continental crust in an active continental margin — the Central Andes between 18° and 27°S. *Tectonophysics* 341, 195–223.
- Lucassen, F. and Becchio, R. 2003. Timing of highgrade metamorphism: Early Palaeozoic U-Pb formation ages of titanite indicate long-standing high-T conditions at the western margin of Gondwana (Argentina, 26-29°S): *Journal of Metamorphic Geology* 21, 649-662.
- Ludwig, K. R., 2003. User's Manual for Isoplot 3.0: a geochronological Toolkit for Microsoft Excel. Berkeley Geochronology Center, Special, publication, no.4 1–71.
- Matteini, M., Dantas, E. L., Pimentel, M. M., Bühn, B. 2010. Combined U-Pb and Lu-Hf isotope analyses by laser ablation MC-ICP-MS: methodology and applications. *Anais da Academia Brasileira de Ciências* 82(2), 479-491.
- Méndez, V., Navarini, A., Plaza, D., Viera, O. 1973. Faja Eruptiva de la Puna Oriental: Actas 5to Congreso Geológico Argentino. 4, 89–100, Córdoba.
- Middlemost, E. A. 1994. Naming materials in the magma/igneous rock system. *Earth-Science Reviews* 37(3), 215-224.

Geocronologia e isotopía do magmatismo paleozoico na zona de Diablillos, borda oriental da Puna austral (NW da Argentina): Evolução crustal do orôgeno paleozoico inferior na margem ocidental de Gondwana

- Mon, R. and Hongn, F. D. 1996. Estructura del basamento proterozoico y paleozoico inferior del norte argentino. *Revista de la Asociación Geológica Argentina* 51(1), 3-14.
- Morel, M.L.A., Nebel, O., Nebel-Jacobsen, Y.L., Miller, J.S., Vroon, P.Z. 2008. Hafnium isotope characterization of the GJ-1 zircon reference material by solution and laser ablation MC-ICPMS. *Chemical Geology* 255, 231 –235.
- Nardi, L. V. S., Formoso, M. L. L., Jarvis, K., Oliveira, L., Bastos Neto, A. C., Fontana, E. 2012. REE, Y, Nb, U, and Th contents and tetrad effect in zircon from a magmatic–hydrothermal F-rich system of Sn-rare metal-cryolite mineralized granites from the Pitinga Mine, Amazonia, Brazil. *J. S. Am. Earth Sci.* 33, 34–42.
- Nebel, O., Nebel-Jacobsen, Y., Mezger, K., Berndt, J. 2007. Initial Hf isotope compositions in magmatic zircon from early Proterozoic rocks from the Gawler Craton, Australia: a test for zircon model ages. *Chemical Geology* 241, 23–37.
- Nieves, A. I. 2014. Aspectos petrológicos de procesos de mezcla de magmas en el basamento Ígneo Metamórfico del NOA. Contrafuertes del salar de Diablillos. Universidad Nacional de Salta. Tesis Profesional. Inédito. 100 pág.
- Palma, M. A., Parica, P. D., Ramos, V. A. 1986. El granito Archibarca: su edad y significado tectónico, Provincia de Catamarca. *Revista de la Asociación Geológica Argentina* 41, 414–419.
- Patchett, P.J. 1983. Importance of the Lu–Hf isotopic system in studies of planetary chronology and chemical evolution. *Geochimica and Cosmochimica Acta* 47, 81.
- Pearce, J. A., Harris, N. B., Tindle, A. G. 1984. Trace element discrimination diagrams for the tectonic interpretation of granitic rocks. *Journal of Petrology* 25(4), 956–983.
- Pimentel, M.M., Fuck, R.A. 1992. Neoproterozoic crustal accretion in central Brazil. *Geology* 20, 375–379.

- Pimentel, M.M., Fuck, R.A., Jost, H., Ferreiro Filho, C.F., Aráujo, S.M. 2000. The basement of the Brasília Fold Belt and the Goiás Magmatic Arc. In: Cordani, U.G., Milani, E.J., Thomaz Filho, A., Campos, D.A. (Eds.), Tectonic Evolution of South America. Rio de Janeiro. 31st International Geological Congress, Rio de Janeiro, Brazil, pp. 195–229.
- Piper, J.D.A. 2000. The Neoproterozoic supercontinent: Rodinia or Paleopangea? *Earth and Planetary Science Letters* 59, 61–89.
- Piper, J.D.A. 2007. The Neoproterozoic supercontinent Palaeopangea. *Gondwana Research* 12, 202–227.
- Ramos, V. A., Jordan, T. E., Allmendinger, R. W., Mpodozis, C., Kay, S. M., Cortés, J. M., Palma, M. A. 1986. Palaeozoic terranes of the central Argentine - Chilean Andes. *Tectonics* 5, 855–880.
- Ramos, V. 1988. Late Proterozoic-Early Paleozoic of South America, a collisional history. *Episodes* 11 (3), 168–175.
- Ramos, V.A. 2008. The Basement of the central Andes: the Arequipa and related Terranes. *Annual Review in Earth Planetary Sciences* 36, 289–324.
- Rapela, C. W., Coira, B., Toselli, A. J., Saavedra, J. 1992. El magmatismo del Paleozoico inferior en Sudoeste de Gondwana. In: Gutiérrez Marco, J. G., Saavedra, J., Rábano, I. (Eds.), *Paleozoico Inferior de Ibero-América, Tomo I*, Universidad de Extremadura, España, pp. 22-67.
- Rapela, C.W., Pankhurst, R.J., Casquet, C., Fanning, C.M., Baldo, E.G., González Casado, J.M., Galindo, C., Dahlquist, J. 2007. The Rio de la Plata craton and the assembly of SW Gondwana. *Earth Science Reviews* 83, 49–82.
- Rapela, C. W., Verdecchia, S. O., Casquet, C., Pankhurst, R. J., Baldo, E. G., Galindo, C., Fanning, C. M. 2015. Identifying Laurentian and SW Gondwana sources in the Neoproterozoic to Early Paleozoic metasedimentary rocks of the Sierras Pampeanas: Paleogeographic and tectonic implications. *Gondwana Research* 32, 193-212.

Geocronologia e isotopía do magmatismo paleozoico na zona de Diablillos, borda oriental da Puna austral (NW da Argentina): Evolução crustal do orôgeno paleozoico inferior na margem ocidental de Gondwana

- Seifert, W., Rhede, D., Thomas, R., Förster, H. J., Lucassen, F., Dulski, P., Wirth, R., 2011. Distinctive properties of rock-forming blue quartz: inferences from a multi-analytical study of submicron mineral inclusions: *Mineralogical Magazine* 75(4), 2519–2534.
- Shaw, D. M., Cramer, J. J., Higgins, M. D., Truscott, M. G. 1986. Composition of the Canadian Precambrian shield and the continental crust of the earth. In: Dawson, J.B., Hall, J., Wedepohl, K.H. (Eds.), *The Nature of the Lower Continental Crust*. Blackwell Scientific Publication, Oxford, 394 pp.
- Scherer, E., Münker, C., Mezger, K. 2006. Calibration of the lutetium–hafnium clock. *Science* 293, 683–687.
- Schmitt, A., 2011. Uranium series accessory crystal dating of magmatic processes. *Annual Review of Earth and Planetary Sciences* 39, 321–349.
- Shand, S. J. 1943. Eruptive rocks: Their genesis, composition, and classification, with a chapter on meteorites. J. Wiley & sons, Incorporated.
- Squire, R.J., Campbell, I.H., Allen, C.M., Wilson, C.J.L. 2006. Did the Transgondwanan supermountain trigger the explosive radiation of animals on Earth? *Earth and Planetary Science Letters* 250, 116–133.
- Stacey, J.S. and Kramers, J.D. 1975. Approximation of terrestrial lead isotope evolution by a two-stage model. *Earth Planetary Science Letters* 26, 207–221.
- Streckeisen, A., 1976. To each plutonic rock its proper name. *Earth-science reviews* 12(1), 1–33.
- Suzaño, N., Becchio, R., Nieves, A., Sola, A., Ortiz, A. 2015. Mezcla de magmas en el arco magmático Famatiniano del noroeste de Argentina: ejemplo en el Complejo Intrusivo Diablillos. Puna Austral. *Revista Mexicana de Ciencias Geológicas* 32, (3), 433–454.
- Taylor, S.R. and McLennan, S.M. 1985. *The Continental Crust: its Composition and Evolution*. Blackwell, Oxford. 312 pp.

- Thompson, R. N. 1982. Magmatism of the British Tertiary volcanic province. *Scottish Journal of Geology* 18(1), 49-107.
- Turner, J.C.M., 1960. Estratigrafía de la Sierra de Santa Victoria y adyacencias, Boletín de la Academia Nacional de Ciencias Córdoba 41,163-196.
- Vavra, G. 1994. Systematics of internal zircon morphology in major Variscan granitoid types. *Contributions Mineral Petrology* 117, 331-334.
- Viramonte, J. M., Becchio, R. A., Viramonte, J. G., Pimentel, M. M., Martino, R. D. 2007. Ordovician igneous and metamorphic units in southeastern Puna: New U–Pb and Sm–Nd data and implications for the evolution of northwestern Argentina. *Journal of South American Earth Sciences* 24, 167–183.
- Wedepohl, K.H. 1995. The compositions of the continental crust. *Geochimica et Cosmochimica Acta* 59, 1217–1232.
- Wetherill, G. W. 1956. An interpretation of the Rhodesia and Witwatersrand age patterns. *Geochimica et Cosmochimica Acta* 9(5), 290-292.
- Whitney, D. L. and Evans, B.W. 2010. Abbreviations for names of rock-forming minerals. *American mineralogist* 95(1), 185.
- Yoshida, M. and Upreti, B.N. 2006. Neoproterozoic India within East Gondwana: constraints from recent geochronologic data from Himalaya. *Gondwana Research* 10, 349– 356.
- Yoshida, M. 2007. Geochronologic data evaluation: implications for the Proterozoic tectonics of East Gondwana. *Gondwana Research* 12, 228– 241.
- Zappettini, E., Coira, B., Santos, J. O. 2008. Edad U/Pb de la Formación Chañi: granito del arco magmático tilcárico. In B. Coira, & E. O. Zappettini (Eds.), XVII Congreso Geológico Argentino, Actas (pp. 248-249).
- Zeck, H. P. and Williams, I. S. 2002. Inherited and magmatic zircon from Neogene Hoyazo cordierite dacite, SE Spain—anatetic source rock provenance and magmatic evolution. *J. Petrol* 43, 1089-1104.

Geocronologia e isotopía do magmatismo paleozoico na zona de Diablillos, borda oriental da Puna austral (NW da Argentina): Evolução crustal do orôgeno paleozoico inferior na margem ocidental de Gondwana

Zeh, A., Gerdes, A., Klemd, R., Barton Jackson, M., J. R. 2007. Archaean to Proterozoic Crustal Evolution in the Central Zone of the Limpopo Belt (South Africa-Botswana): Constraints from Combined U-Pb and Lu-Hf Isotope Analyses of Zircon. *Journal of Petrology* 48 (8), 1605-1639. doi:10.1093/petrology/egm032.

Zimmermann, U., Bahlburg, H., Mezger, K., Berndt, J., Kay, S. M. 2014. Origin and age of ultramafic rocks and gabbros in the southern Puna of Argentina: an alleged Ordovician suture revisited. *International Journal of Earth Sciences* 103(4), 1023-1036.

6. AGRADECIMENTOS

Em primer lugar, eu quero agradecer a minha orientadora, Dra. Natalia Hauser por sua paciência e valiosa orientação; por os momentos compartilhados, no campo, jantares e discussões entre uns gostosos “mates”, sem dúvida ela me ajudara a me converter em um melhor profissional e uma melhor pessoa. Muchisimas gracias por todo Naty.

Ao tribunal, Dr. Valmir Souza da Silva, Dr. Miguel Basei, por enriquecer com suas boas correções e sugestões o manuscrito.

A Dra. Poliana Dutra Maia por sua ajuda e correções com o português do texto.

A meus professores, Massimo Matteini, Maria Emilia Schutesky Della Giustina, Nilson F. Botelho, Reinhardt Fuck e Márcio M. Pimentel; em suas disciplinas, eles me ensinaram olhar além e abrir mais minha mente.

Ao Dr. Raúl Becchio, por estabelecer o vínculo com a UnB e minha orientadora, e por as ideias e sugestões fornecidas para elaboração do artigo científico.

A meus amigos e colegas Geólogo Alexis Nieves, Dr. Nestor Suárez e Dr. Alfonso Sola, por sua ajuda nos trabalhos de campo.

Ao pessoal do Laboratório de Geoquímica da Universidad Nacional de Salta e o Laboratório de Geocronologia da UnB, Alejandro Nieva, Luciana Pereira e Bárbara Lima, pela preparação das amostras, pela obtenção das imagens no MEV e por me ensinar a trabalhar com o NEPTUNE.

A minha família, por me apoiar sempre, em cada novo projeto que decido iniciar na minha vida, sempre me motivando para mais.

Por ultimo, mas não menos importante, a meu amorzinho –Eli- por estar ao meu lado sempre, além da distancia, me dando apoio incondicional em tudo momento. Muchísimas gracias por aguantarme mi amorcito.

Geocronologia e isotopía do magmatismo paleozoico na zona de Diablillos, borda oriental da Puna austral (NW da Argentina): Evolução crustal do orôgeno paleozoico inferior na margem ocidental de Gondwana

7. ANEXO

Table 1. Whole rock geochemical analyses for major and trace, including rare earth element data for the CID and CEO, Eastern Magmatic Belt, Southern Puna. Major element data in wt.%, trace element data in ppm.

Sample	D-13-01 (CID)	CB-13-05 (CEO)	D-13-02 (CID)	BA-13-07 (CEO)	D-13-15 (CID)	CB-13-04 (CEO)	D-13-40 (CID)	CB-13-02 (CID)
Petrology/ Element	Monzogranite	Monzogranite	Granodiorite	Granodiorite	Tonalite	Diorite basic dyke	Diorite	Diorite
SiO ₂	60.93	69.99	61.69	62.05	59.65	50.27	54.50	50.93
TiO ₂	1.06	0.55	1.08	1.03	1.69	0.83	1.31	1.82
Al ₂ O ₃	16.53	13.95	15.93	16.69	15.01	16.13	15.80	14.54
Fe ₂ O ₃	7.26	4.00	7.39	6.74	9.12	9.10	8.87	11.13
MgO	2.73	1.60	2.98	2.74	3.26	8.08	6.09	6.31
MnO	0.10	0.07	0.12	0.08	0.14	0.15	0.14	0.17
CaO	2.36	1.56	3.16	3.50	4.84	11.26	7.56	9.05
Na ₂ O	3.07	2.56	3.04	3.37	2.65	2.36	2.35	2.59
K ₂ O	4.60	3.84	3.15	2.68	2.15	0.28	1.54	1.21
P ₂ O ₅	0.18	0.15	0.19	0.07	0.24	0.08	0.18	0.24
LOI	0.9	1.5	1.0	0.8	1.0	1.1	1.4	1.7
Sum	99.73	99.78	99.74	99.74	99.76	99.76	99.75	99.74
Cr	100	100	100	100	100	600	300	300
V	125.0	67.0	143.0	144.0	235.0	245.0	205.0	303.0
Co	61.5	67.9	58.0	41.0	52.6	63.3	56.1	53.0
Ni	23.0	<20.0	25.0	21.0	26.0	94.0	67.0	35.0
Ga	23.1	16.2	20.2	20.6	19.8	13.8	16.7	17.7
Rb	173.8	168.5	145.7	126.8	86.1	9.0	74.5	47.7
Sr	110.9	89.5	116.3	201.5	126.1	104.4	141.1	155.6
Y	40.9	31.8	39.5	31.0	41.5	21.7	31.8	34.1
Zr	286.7	197.1	281.3	231.9	254.3	57.4	170.3	190.4
Nb	15.4	12.4	16.3	13.4	11.2	2.1	7.0	6.1
Cs	6.7	13.3	5.5	10.2	5.7	1.1	6.3	4.4
Ba	474.0	342.0	324.0	355.0	190.0	39.0	140.0	92.0
Hf	7.8	5.4	7.0	6.0	6.6	1.6	4.3	4.4
Ta	1.0	1.2	1.1	1.1	0.9	0.1	0.5	0.3
Th	21.7	13.5	18.6	20.7	7.2	0.9	5.9	2.6
U	1.7	2.3	1.4	1.6	1.6	0.5	1.5	0.6
Be	3.0	2.0	2.0	<1.0	2.0	<1.0	<1.0	3.0
As	6.7	4.2	7.8	8.0	6.9	2.4	19.5	26.5
Au	<0.5	1.2	0.9	1.3	<0.5	0.9	0.9	0.8
Bi	0.2	1.0	<0.1	0.1	<0.1	<0.1	0.1	<0.1
Cu	14.6	3.0	31.1	16.4	37.2	95.2	83.6	73.5

Pb	3.8	1.2	3.1	3.3	2.2	0.8	3.0	1.3
Sb	<0.1	<0.1	<0.1	<0.1	<0.1	<0.1	<0.1	0.1
Sc	18	10	22	15	28	37	30	42
Sn	4.0	4.0	3.0.	3.0	3.0	<1.0	2.0	2.0
Ti	0.9	0.7	0.8	0.6	0.4	<0.1	0.3	0.1
Zn	107.0	62.0	104.0	98.0	74.0	6.0	43.0	21.0
La	53.1	32.7	44.2	52.9	26.2	5.9	18.5	12.3
Ce	111.6	68.9	94.4	102.6	57.8	12.0	39.6	30.9
Pr	13.2	7.8	10.8	12.1	7.3	1.7	5.08	4.2
Nd	48.8	30.7	44.9	47.1	32.4	8.1	23.6	21.1
Sm	10.3	6.1	8.6	8.8	7.3	2.2	5.1	5.2
Eu	1.7	0.9	1.8	1.7	1.8	0.8	1.5	1.7
Gd	9.4	5.9	8.4	7.5	8.1	3.3	6.0	6.7
Tb	1.4	0.9	1.4	1.1	1.4	0.6	1.0	1.1
Dy	8.2	5.8	7.8	5.7	7.6	4.2	5.9	6.8
Ho	1.6	1.2	1.6	1.2	1.7	0.9	1.3	1.5
Er	4.2	3.3	4.6	3.1	4.5	2.5	3.6	4.0
Tm	0.6	0.5	0.7	0.5	0.7	0.4	0.5	0.6
Yb	3.8	3.2	4.4	3.0	4.5	2.5	3.4	3.6
Lu	0.6	0.5	0.7	0.5	0.7	0.4	0.5	0.6
LaN/YbN	9.4	6.8	6.7	11.9	3.9	1.6	3.7	2.3
Eu/Eu*	0.5	0.5	0.6	0.7	0.7	0.9	0.8	0.9

Geocronologia e isotopia do magmatismo paleozoico na zona de Diablillos, borda oriental da Puna austral (NW da Argentina): Evolução crustal do orôgeno paleozoico inferior na margem ocidental de Gondwana

Table 2. Results of in situ U-Pb isotope analysis of zircon from rocks of the Diablillos Intrusive Complex, Eastern Magmatic Belt, Southern Puna. R: rim analysis. C: core analysis.

Monzogranite D-13-01		Isotopic Ratios						Apparent Ages							
Grain N°		$^{207}\text{Pb}/^{206}\text{Pb}$	1σ(%)	$^{207}\text{Pb}/^{235}\text{U}$	1σ(%)	$^{206}\text{Pb}/^{238}\text{U}$	1σ(%)	$^{207}\text{Pb}/^{206}\text{Pb}$	1σ(Ma)	$^{207}\text{Pb}/^{235}\text{U}$	1σ(Ma)	$^{206}\text{Pb}/^{238}\text{U}$	1σ(Ma)	Rho	Conc(%)
Z5C		0.058	1.4	0.625	1.9	0.079	1.3	517.5	30.6	493.2	7.5	488.0	6.3	0.68	98.9
Z14		0.057	1.5	0.626	2.3	0.079	1.7	502.6	32.9	493.6	8.9	491.7	8.1	0.75	99.6
Z9		0.058	1.2	0.633	1.8	0.08	1.3	514.3	25.6	497.8	6.9	494.2	6.2	0.74	99.3
Z17		0.057	1.7	0.632	2.1	0.08	1.3	505.7	36.9	497.3	8.2	495.4	6.0	0.69	99.6
Z67R		0.059	1.4	0.654	1.8	0.081	1.2	559.7	30.7	511.0	7.4	500.1	5.7	0.63	97.9
Z36		0.058	2.4	0.65	3.0	0.081	1.9	536	51.9	508.3	12	502.2	9.2	0.62	98.8
Z66		0.059	1.5	0.658	2.2	0.081	1.6	556.2	33.7	513.3	9.0	503.7	7.9	0.72	98.1
Z60C		0.058	2.4	0.649	3.3	0.081	2.2	520.8	52.2	507.8	13.0	504.9	11.0	0.68	99.4
Z19		0.057	1.1	0.644	1.5	0.082	1.0	500.2	24.8	505.0	6.0	506.1	4.9	0.65	100.0
Z68		0.059	1.3	0.661	1.8	0.082	1.1	555.4	29.1	515.2	7.1	506.2	5.5	0.63	98.3
Z60R		0.058	1.5	0.659	2.0	0.082	1.4	547.3	32.2	514.3	8.1	506.9	6.6	0.67	98.6
Z27R		0.059	2.1	0.667	2.5	0.082	1.4	569.9	44.8	518.6	10.0	507.1	6.8	0.67	97.8
Z40		0.058	1.4	0.658	1.9	0.082	1.3	540.3	31.4	513.6	7.7	507.6	6.1	0.65	98.8
Z64		0.058	1.9	0.661	2.6	0.082	1.8	547.6	41.0	515.4	11.0	508.1	8.9	0.69	98.6
Z65		0.058	1.9	0.662	2.3	0.082	1.3	546.1	41.0	516.0	9.2	509.2	6.2	0.66	98.7

Z6	0.057	1.4	0.652	1.8	0.083	1.1	503.2	30.8	509.9	7.2	511.4	5.5	0.65	100.0
Z15	0.058	1.2	0.657	1.6	0.083	1.1	517.8	25.4	512.8	6.5	511.6	5.5	0.68	99.8
Z3	0.058	8.5	0.659	8.6	0.083	1.1	517.9	187	514.1	35	513.2	5.3	0.63	99.8
Z30B	0.058	1.2	0.662	1.6	0.083	1.0	527.2	25.4	516.0	6.3	513.4	5.1	0.65	99.5
Z18	0.057	1.3	0.65	1.7	0.083	1.0	486.1	29.5	508.8	6.7	513.8	4.9	0.58	101.0
Z51	0.058	1.5	0.659	1.8	0.083	1.0	513.4	32.5	514.0	7.3	514.1	5.1	0.55	100.0
Z37	0.059	1.7	0.672	2.3	0.083	1.6	553.7	36.9	522.2	9.4	515.1	7.8	0.68	98.6
Z45	0.059	2.3	0.678	2.9	0.083	1.7	564.9	51.0	525.5	12.0	516.5	8.4	0.69	98.3
Z24B	0.059	1.5	0.678	2.0	0.084	1.3	557.4	31.7	525.3	8.0	517.9	6.5	0.66	98.6
Z10	0.058	1.2	0.675	2.7	0.084	2.5	544.9	25.4	523.5	11.0	518.6	12.0	0.73	99.1
Z50	0.058	1.2	0.67	1.5	0.084	1.0	527.7	26.2	520.9	6.2	519.4	4.8	0.61	99.7
Z16	0.058	1.7	0.669	2.2	0.084	1.4	517.4	36.7	519.8	8.8	520.4	6.8	0.62	100.0
Z57	0.058	1.2	0.678	1.5	0.084	0.9	547.8	25.8	525.8	6.1	520.7	4.5	0.58	99.0
Z69	0.058	1.2	0.677	1.5	0.084	0.9	535.7	26.4	524.8	6.1	522.3	4.5	0.57	99.5
Z7	0.058	1.2	0.674	1.7	0.085	1.2	522.4	26.0	523.4	7.0	523.6	6.2	0.71	100.0
Z28R	0.059	1.1	0.689	1.4	0.085	0.8	566.9	24.3	531.9	5.8	523.8	4.2	0.57	98.5
Z22	0.058	1.1	0.681	1.4	0.085	0.8	541.0	24.1	527.6	5.7	524.5	4.1	0.57	99.4
Z39C	0.059	2.5	0.687	3.4	0.085	2.4	558.3	52.9	530.9	14	524.5	12	0.69	98.8
Z48	0.058	1.3	0.684	1.8	0.085	1.3	544.6	27.5	529.2	7.4	525.6	6.4	0.70	99.3
Z54	0.058	1.8	0.685	2.8	0.085	2.1	542.7	40.3	529.5	11.0	526.5	10.0	0.65	99.4
Z49	0.058	1.2	0.686	1.6	0.085	1.0	542.0	26.1	530.2	6.6	527.5	5.3	0.64	99.5

Geocronologia e isotopía do magmatismo paleozoico na zona de Diablillos, borda oriental da Puna austral (NW da Argentina): Evolução crustal do orôgeno paleozoico inferior na margem ocidental de Gondwana

Z55	0.059	2.0	0.693	3.0	0.085	2.3	563.9	43.9	534.4	13.0	527.6	12.0	0.75	98.7
Z23	0.058	1.3	0.685	1.7	0.085	1.1	538.1	28.5	530.0	7.0	528.1	5.5	0.62	99.6
Z52R	0.058	1.3	0.689	1.7	0.085	1.1	547.6	27.7	532.3	6.9	528.7	5.5	0.63	99.3
Z47	0.058	1.4	0.685	1.8	0.086	1.1	534.9	30.3	530.1	7.4	529.0	5.8	0.62	99.8
Z44	0.059	2.3	0.696	3.3	0.086	2.3	564.5	51.0	536.5	14.0	529.9	12.0	0.70	98.8
Z58	0.058	1.2	0.689	1.5	0.086	0.9	541.7	25.8	532.3	6.2	530.1	4.7	0.58	99.6
Z21R	0.059	2.7	0.696	2.9	0.086	0.9	561.4	59.2	536.2	12.0	530.3	4.7	0.60	98.9
Z21C	0.058	1.9	0.683	2.4	0.086	1.6	516.2	41.1	528.5	10.0	531.4	8.0	0.64	101.0
Z61	0.059	2.4	0.696	2.7	0.086	1.3	549.7	51.4	536.2	11.0	533.0	6.7	0.63	99.4
Z24	0.059	1.3	0.699	1.8	0.087	1.3	551.0	28.3	538.4	7.6	535.5	6.6	0.66	99.4
Z31	0.060	1.3	0.834	1.9	0.100	1.4	612.4	27.6	615.6	8.7	616.5	8.1	0.72	100.0
Z12C	0.064	1.3	0.94	2.1	0.107	1.7	734.7	28.0	672.7	10.0	654.3	10.0	0.78	97.3
Z67C	0.065	1.3	0.994	1.9	0.110	1.4	786.5	26.9	700.7	9.4	674.3	8.7	0.72	96.2
Z38	0.064	1.6	1.012	3.9	0.115	3.6	733.3	34.0	710.0	20.0	702.6	24.0	0.66	99.0
Z1R	0.070	1.1	1.417	1.6	0.147	1.1	926.1	22.8	896.0	9.4	883.9	9.2	0.69	98.6
Z1C	0.074	1.1	1.739	1.4	0.171	0.8	1035.0	22.0	1023.0	8.8	1018.0	7.7	0.57	98.4
Z5R	0.074	1.1	1.739	1.4	0.171	0.8	1035.0	22.0	1023.0	8.8	1018.0	7.7	0.57	98.4
Z27C	0.075	1.6	1.793	2.1	0.174	1.3	1056.0	32.8	1043.0	14.0	1037.0	13.0	0.62	98.2

Diorite D-13-40	Isotopic Ratios							Apparent Ages						
	Grain N°	$^{207}\text{Pb}/^{206}\text{Pb}$	1σ(%)	$^{207}\text{Pb}/^{235}\text{U}$	1σ(%)	$^{206}\text{Pb}/^{238}\text{U}$	1σ(%)	$^{207}\text{Pb}/^{206}\text{Pb}$	1σ(Ma)	$^{207}\text{Pb}/^{235}\text{U}$	1σ(Ma)	$^{206}\text{Pb}/^{238}\text{U}$	1σ(Ma)	Rho
Z22	0.058	2.0	0.632	2.4	0.079	1.4	540.9	43.3	497.2	9.6	487.8	6.6	0.57	98.1
Z37C	0.058	1.5	0.63	1.7	0.079	0.8	523.8	32.8	496.1	6.7	490.1	3.9	0.46	98.8
Z35	0.058	1.6	0.635	2.0	0.079	1.3	528.5	34.8	499.3	8.0	493.0	6.0	0.61	98.7
Z48	0.058	2.5	0.64	2.6	0.080	0.9	536.4	54.0	502.4	10.0	494.9	4.5	0.49	98.5
Z36R	0.058	1.5	0.646	1.7	0.080	0.9	541.6	32.0	505.8	6.9	498.0	4.5	0.52	98.4
Z51	0.058	1.6	0.647	2.2	0.081	1.5	535.8	35.4	506.6	8.8	500.1	7.2	0.67	98.7
Z40	0.058	1.4	0.648	1.6	0.081	0.9	516.0	29.8	507.0	6.6	505.1	4.5	0.46	99.6
Z56	0.058	1.4	0.65	1.5	0.082	0.7	518.8	29.8	508.7	6.2	506.5	3.6	0.45	99.6
Z38	0.058	1.5	0.663	1.8	0.083	1.1	540.6	31.9	516.6	7.4	511.2	5.4	0.58	99.0
Z12	0.058	1.4	0.669	1.8	0.083	1.1	547.8	31.5	520.1	7.3	513.9	5.2	0.57	98.8
Z44	0.058	1.6	0.662	1.8	0.083	0.9	523.3	34.1	516.1	7.2	514.5	4.3	0.5	99.7
Z46	0.058	1.6	0.668	1.9	0.083	1.1	539.9	34.3	519.7	7.8	515.1	5.4	0.56	99.1
Z34	0.059	1.8	0.673	2.0	0.083	0.8	555.9	39.5	522.7	8.1	515.2	4.0	0.47	98.6
Z21C	0.058	7.8	0.668	7.8	0.083	0.8	535.6	171.0	519.3	32.0	515.6	4.0	0.48	99.3
Z49	0.059	1.7	0.673	2.0	0.083	0.9	551.0	37.6	522.8	8.0	516.4	4.6	0.45	98.8
Z26	0.059	1.4	0.679	1.7	0.084	0.9	565.7	31.3	526.2	6.9	517.2	4.2	0.48	98.3
Z3	0.058	1.4	0.669	1.7	0.084	1.0	530.0	31.5	520.3	7.1	518.1	4.9	0.55	99.6
Z1	0.058	1.4	0.674	1.7	0.084	0.8	542.7	31.6	523.3	6.8	518.9	4.2	0.47	99.2

Geocronologia e isotopía do magmatismo paleozoico na zona de Diablillos, borda oriental da Puna austral (NW da Argentina): Evolução crustal do orôgeno paleozoico inferior na margem ocidental de Gondwana

Z45	0.059	2.2	0.683	3.0	0.084	2.0	567.1	48.6	528.6	12	519.7	9.8	0.66	98.3
Z11	0.058	1.6	0.673	1.9	0.084	1.1	531.6	34.3	522.8	7.7	520.8	5.3	0.54	99.6
Z30	0.059	1.5	0.690	1.8	0.085	1.1	573.6	31.7	532.8	7.7	523.4	5.7	0.57	98.2
Z32	0.058	1.8	0.680	2.6	0.086	1.9	518	39.5	527	11.0	529	9.7	0.72	100.0
Z52	0.059	1.6	0.703	2.4	0.086	1.8	581.6	34.9	540.3	10.0	530.6	9.1	0.74	98.2
Z9C	0.059	1.3	0.695	1.6	0.086	1.0	550.0	29.1	536	6.8	532.8	4.9	0.56	99.4
Z15	0.058	1.5	0.689	1.9	0.086	1.1	528.3	32.5	532.3	7.8	533.2	5.9	0.60	100.0
Z29	0.058	1.5	0.694	1.7	0.087	0.8	531.6	32.0	535.1	6.9	535.9	4.1	0.45	100.0
Z57	0.058	1.3	0.698	1.6	0.087	0.9	538.9	28.6	537.8	6.6	537.6	4.7	0.54	100.0
Z20	0.058	1.4	0.692	1.6	0.087	0.8	518.5	29.7	534	6.6	537.7	4.3	0.49	101.0
Z9R	0.057	4.3	0.828	5.8	0.106	3.8	477.3	94.7	612.2	26.0	649.3	24.0	0.67	106.0
Z14	0.077	4.7	1.598	4.9	0.151	1.3	1115.0	93.9	969.3	30.0	906.2	11.0	0.61	93.5

Granodiorite D-13-02	Isotopic Ratios							Apparent Ages						
	Grain N°	$^{207}\text{Pb}/^{206}\text{Pb}$	$2\sigma(\%)$	$^{207}\text{Pb}/^{235}\text{U}$	$2\sigma(\%)$	$^{206}\text{Pb}/^{238}\text{U}$	$2\sigma(\%)$	$^{207}\text{Pb}/^{206}\text{Pb}$	$2\sigma(\text{Ma})$	$^{207}\text{Pb}/^{235}\text{U}$	$2\sigma(\text{Ma})$	$^{206}\text{Pb}/^{238}\text{U}$	$2\sigma(\text{Ma})$	Rho
Z19	0.057	7.7	0.606	8.2	0.077	3.0	485.3	170.0	481.2	32.0	480.4	14.0	0.36	99.0
Z21	0.057	1.6	0.627	2.3	0.079	1.7	506.5	34.4	493.9	9.1	491.2	8.1	0.74	97.0
Z14C	0.058	0.9	0.659	2.2	0.083	2.0	524.6	20.2	514.1	8.9	511.8	9.9	0.91	97.6
Z39	0.058	1.2	0.668	2.0	0.084	1.7	528.3	26.1	519.4	8.3	517.4	8.3	0.81	97.9
Z66	0.058	2.5	0.674	4.7	0.084	4.1	538.0	53.7	523.2	19.0	519.8	20.0	0.86	96.6
Z11	0.058	1.1	0.675	4.1	0.084	3.9	530.9	24.8	523.6	17.0	521.9	20.0	0.96	98.3
Z9	0.058	1.0	0.682	2.3	0.085	2.1	541.6	21.4	527.9	9.5	524.7	11.0	0.91	96.9
Z4	0.058	1.3	0.681	4.0	0.085	3.8	524.1	27.9	527.5	16.0	528.3	19.0	0.95	101.0
Z24	0.058	1.1	0.745	4.5	0.094	4.3	518.1	24.5	565.6	19.0	577.5	24.0	0.97	111.0
Z10	0.06	1.3	0.782	3.0	0.094	2.7	608.6	28.5	586.8	14.0	581.2	15.0	0.9	95.5
Z2R	0.059	2.1	0.773	5.2	0.096	4.7	551.4	46.3	581.5	23.0	589.3	26.0	0.91	107.0
Z13	0.060	1.8	0.796	5.2	0.096	4.8	609.4	39.7	594.7	23.0	590.8	27.0	0.93	97.0
Z48R	0.058	1.4	0.778	4.9	0.097	4.7	532.9	30.0	584.3	22.0	597.7	27.0	0.96	112.0
Z7	0.060	1.9	0.884	7.9	0.107	7.7	605.7	40.8	643.2	38.0	653.9	48.0	0.97	108.0
Z8C	0.087	4.8	0.941	5.2	0.078	2.1	1364.0	89.8	673.5	25.0	486.1	9.7	0.4	35.6

Geocronologia e isotopía do magmatismo paleozoico na zona de Diablillos, borda oriental da Puna austral (NW da Argentina): Evolução crustal do orôgeno paleozoico inferior na margem ocidental de Gondwana

Table 3. Results of in situ Lu-Hf isotope analysis of zircon from rocks of the Diablillos Intrusive Complex, Eastern Magmatic Belt, Southern Puna. 2 sigma values refer to last digits of the isotope ratios. R: rim analysis. C: core analysis. Meas: measured.

Monzogranite D-13-01 Grain N°	T (Ma)	$^{176}\text{Lu}/^{177}\text{Hf}$	$\pm 2\sigma$	$(^{176}\text{Hf}/^{177}\text{Hf})_{\text{meas}}$	$\pm 2\sigma$	$(^{176}\text{Hf}/^{177}\text{Hf})_{\text{t}}$	$\pm 2\sigma$	Hf (T)	$\pm 1\sigma$	TDM (Ga)
Z3	513	0.002691	21	0.282417	22	0.28239	18	-2.61	0.10	1.482
Z49	527	0.003581	95	0.282455	35	0.282418	16	-1.30	0.06	1.422
Z47	529	0.002323	37	0.282489	31	0.282465	16	0.41	0.06	1.329
Z31	616	0.002455	50	0.282461	23	0.282432	16	1.17	0.02	1.359
Z12c	654	0.002836	77	0.282444	20	0.282408	13	1.20	0.05	1.389
Z38	703	0.001257	18	0.282308	83	0.282291	16	-1.88	0.01	1.599
Z1c	1035	0.000979	18	0.282351	21	0.282331	16	7.02	0.16	1.325
Z27c	1056	0.003054	81	0.282348	53	0.282285	16	5.86	0.17	1.463
<hr/>										
Diorite D-13-40 Grain N°										
Z48	495	0.001864	11	0.282552	59	0.282534	16	2.08	0.15	1.208
Z3	518	0.002691	21	0.282417	22	0.282390	16	-2.51	0.07	1.48
Z1	519	0.001951	15	0.282211	42	0.282192	16	-9.51	0.07	1.865
Z11	521	0.003496	22	0.282379	60	0.282343	16	-4.09	0.06	1.57
Z15	533	0.005571	68	0.282476	95	0.282418	16	-1.16	0.06	1.419
Z29	536	0.003236	30	0.282739	12	0.282706	16	9.07	0.12	0.854
Z8B	570	0.001505	23	0.282488	38	0.282471	16	1.53	0.04	1.301
Z14	1115	0.001075	88	0.282217	54	0.282194	16	3.98	0.19	1.616
<hr/>										
Granodiorite D-13-02 Grain N°										
Z5	484	0.001997	15	0.282440	22	0.282421	16	-2.17	0.08	1.433
Z25	490	0.002629	29	0.282561	23	0.282536	16	2.05	0.08	1.206
Z21	491	0.003171	29	0.282477	24	0.282447	16	-1.10	0.08	1.381
Z39	517	0.002394	11	0.282433	28	0.282409	16	-1.84	0.07	1.443
Z4	528	0.003207	10	0.282477	33	0.282444	16	-0.37	0.06	1.371
Z1c	538	0.000979	18	0.282351	21	0.282341	16	-3.80	0.06	1.568

Z7	654	0.004253	44	0.282548	49	0.282494	16	4.20	0.01	1.222
Z8c	1364	0.001668	12	0.282431	26	0.282386	16	16.40	0.30	1.125

Table 4. Microprobe analyses for zircon crystals from rocks of the Diablillos Intrusive Complex, Eastern Magmatic Belt, Southern Puna. Data in wt.%. Nd: not determined.

Grain N°/ Monzogranite D-13-01	Z5c	Z7	Z9	Z15	Z23	Z25	Z40	Z50	Z67r	Z67c
HfO ₂	1.556	1.423	1.592	1.596	1.72	1.541	1.66	1.525	1.632	1.48
SiO ₂	31.99	31.98	31.01	32.28	31.31	31.25	30.73	31.92	31.11	32.25
ZrO ₂	65.26	66.41	64.37	65.74	65.05	65.54	64.89	64.94	65.02	64.83
Total	98.81	99.81	96.97	99.61	98.07	98.33	97.28	98.39	97.76	98.56
Y ₂ O ₃	0.374	0.334	0.371	0.243	0.171	0.356	0.439	0.400	0.275	0.289
UO ₂	0.034	0.011	0.066	0.029	0.023	0.046	0.045	0.098	0.041	0.019
ThO ₂	0.007	0.023	0.009	nd	0.004	0.012	0.016	0.081	0.011	nd
Total	0.485	0.408	0.446	0.335	0.200	0.455	0.576	0.579	0.408	0.343
Th/U	0.206	2.091	0.136	nd	0.174	0.261	0.356	0.827	0.268	nd
Granodiorite D-13-02	Z1r	Z13	Z9c	Z8c	Z6	Z22r	Z26c	Z39	Z45c	Z63
HfO ₂	1.611	1.411	1.352	1.559	1.565	1.922	1.889	1.389	1.464	1.729
SiO ₂	32.64	34.12	33.17	32.94	32.32	33.46	32.20	34.28	31.62	32.49
ZrO ₂	64.33	63.55	62.16	65.84	64.86	64.58	64.51	64.28	63.92	64.61
Total	98.58	99.09	96.68	100.3	98.75	99.96	98.60	99.95	97.00	98.83
Y ₂ O ₃	0.208	0.103	1.181	0.103	0.193	0.136	0.426	0.041	0.254	0.278
UO ₂	0.042	0.051	0.187	0.001	0.018	0.039	0.048	0.039	0.045	0.017
ThO ₂	nd	0.007	0.224	nd	nd	nd	0.017	0.007	0.01	0.009
Total	0.25	0.161	1.592	0.194	0.224	0.175	0.605	0.163	0.319	0.365
Th/U	nd	0.137	1.198	nd	nd	nd	0.354	0.179	0.222	0.529
Diorite D-13-40	Z12	Z8A	Z30	Z34	Z36c	Z37c	Z38	Z49	Z51	Z43
HfO ₂	1.113	1.196	1.204	1.154	1.632	1.734	1.168	1.326	1.026	0.958
SiO ₂	32.72	31.87	32.83	32.39	34.2	32.89	31.65	32.28	34.28	32.89
ZrO ₂	64.46	65.57	66.72	64.93	61.06	67.19	65.41	65.59	65.79	65.80
Total	98.3	98.63	100.8	98.48	96.89	101.8	98.22	99.2	101.1	99.65
Y ₂ O ₃	0.817	0.237	nd	0.671	0.159	0.029	0.373	0.294	0.244	0.235
UO ₂	0.125	0.057	0.029	0.094	0.089	0.009	0.077	0.051	0.06	0.056
ThO ₂	0.206	0.05	0.015	0.195	0.007	0.007	0.085	0.083	0.086	0.054
Total	1.148	0.366	0.044	1.031	0.255	0.045	0.663	0.428	0.498	0.379
Th/U	1.648	0.877	0.517	2.074	0.079	0.778	1.104	1.627	1.433	0.964

Geocronologia e isotopia do magmatismo paleozoico na zona de Diablillos, borda oriental da Puna austral (NW da Argentina): Evolução crustal do orôgeno paleozoico inferior na margem ocidental de Gondwana

Table 5. Whole rock Sr and Nd isotope analyses on rocks of the CID and CEO, Eastern Magmatic Belt, Southern Puna. Elemental abundances of Rb and Sr are taken from whole-rock geochemical analyses (Table 1). Meas: measured.

Sample	Petrology	Age (Ma)	Rb (ppm)	Sr (ppm)	$^{87}\text{Rb}/^{86}\text{Sr}$	$(^{87}\text{Sr}/^{86}\text{Sr})_{\text{meas}}$	$(^{87}\text{Sr}/^{86}\text{Sr})_t$	Sm (ppm)	Nd (ppm)	$^{147}\text{Sm}/^{144}\text{Nd}$	$(^{143}\text{Nd}/^{144}\text{Nd})_{\text{meas}}$	$(^{143}\text{Nd}/^{144}\text{Nd})_t$	$e\text{Nd}_{(T)}$	$T_{\text{DM}} (\text{Ga})$
D-13-01	Monzogranite (CID)	518	173.8	110.9	4.551	0.74638 ± 2	0.71278	10.9	53.99	0.122	0.512250 ± -17	0.511833	-2.63	1.32
CB-13-05	Monzogranite (CEO)	518	168.5	89.5	5.470	0.75103 ± 2	0.71065	3.30	15.08	0.132	0.512196 ± -25	0.511745	-4.35	1.56
D-13-02	Granodiorite (CID)	518	145.7	116.3	3.635	0.73796 ± 1	0.71112	8.65	40.95	0.128	0.512229 ± -10	0.511794	-3.4	1.43
BA-13-07	Granodiorite (CEO)	518	126.8	201.5	1.824	0.72873 ± 3	0.71526	11.5	63.04	0.110	0.512096 ± -10	0.511722	-4.8	1.38
D-13-15	Tonalite (CID)	518	86.1	126.1	1.839	-	-	8.58	34.98	0.148	0.512365 ± -12	0.511860	-2.11	1.55
D-13-40	Diorite (CID)	518	74.5	141.1	1.529	0.71698 ± 3	0.70569	5.86	23.88	0.148	0.512447 ± -20	0.511942	-0.51	1.38
CB-13-04	Diorite basic dyke	518	9.0	104.4	0.249	0.70708 ± 2	0.70524	3.01	10.11	0.180	0.512700 ± -24	0.512088	2.34	-
CB-13-02	Diorite (CID)	518	47.7	155.6	0.887	0.71101 ± 2	0.70446	6.34	23.14	0.166	0.512625 ± -14	0.512061	1.82	-

Submission Confirmation

From: santosh@cugb.edu.cn

To: agustinortiz13@hotmail.com; agustinortiz13@gmail.com

Date: Fri, 13 May 2016 23:25:34 +0100

Subject: Submission Confirmation

Article Type: Research Paper

Dear Mr. Agustín Ortiz,

Your submission entitled "Zircon U-Pb ages and Hf isotopes for the Diablillos Intrusive Complex, Southern Puna, Argentina: crustal evolution of the Lower Paleozoic orogen, Southwestern Gondwana margin" has been received by Gondwana Research

You may check on the progress of your paper by logging on to the Elsevier Editorial System as an author. The URL is <http://ees.elsevier.com/gr/>.

Your manuscript will be given a reference number once an Editor has been assigned.

Thank you for submitting your work to this journal.

Kind regards,

Elsevier Editorial System
Gondwana Research